

Higher bottomonium zoo

Jun-Zhang Wang^{1,2,*}, Zhi-Feng Sun^{1,2,†}, Xiang Liu^{1,2,‡},§ and Takayuki Matsuki^{3,4,¶}

¹Research Center for Hadron and CSR Physics, Lanzhou University & Institute of Modern Physics of CAS, Lanzhou 730000, China

²School of Physical Science and Technology, Lanzhou University, Lanzhou 730000, China

³Tokyo Kasei University, 1-18-1 Kaga, Itabashi, Tokyo 173-8602, Japan

⁴Theoretical Research Division, Nishina Center, RIKEN, Wako, Saitama 351-0198, Japan

In this work, we study higher bottomonia up to the $nL = 8S, 6P, 5D, 4F, 3G$ multiplets using the modified Godfrey-Isgur (GI) model, which takes account of color screening effects. The calculated mass spectra of bottomonium states are in reasonable agreement with the present experimental data. Based on spectroscopy, partial widths of all allowed radiative transitions, annihilation decays, hadronic transitions, and open-bottom strong decays of each state are also evaluated by applying our numerical wave functions. Comparing our results with the former results, we point out difference among various models and derive new conclusions obtained in this paper. Notably, we find a significant difference between our model and the GI model when we study D, F , and G and $n \geq 4$ states. Our theoretical results are valuable to search for more bottomonia in experiments, such as LHCb, and forthcoming Belle II.

PACS numbers:

I. INTRODUCTION

Since the observation of J/ψ and $\Upsilon(1S)$ in 1974 and 1977, respectively [1–4], a heavy quarkonium has become a more and more concerned research field because its physical processes cover the whole energy range of QCD. This energy range provides us an excellent place to study the properties of perturbative and non-perturbative QCD [5], and an exhaustive and deep study of a heavy quarkonium can help people better understand the QCD characteristics. Since the bottomonium family are an important member of heavy quarkonia, people have made great progress in the experimental and theoretical study of a bottomonium in the past years. As early as thirty years ago, some higher excited bottomonia, including $\Upsilon(nS)$ with the radial quantum number n from 2 to 6 and P -wave spin-triplet states $\chi_{bJ}(1P)$ and $\chi_{bJ}(2P)$ with $J = 1, 2, 3$, have been experimentally observed in succession [3, 4, 6–11]. With the upgrade and improvement of two B -Factories BaBar and Belle together with LHC, some new breakthroughs in the experimental research have been achieved in recent years. First, the pseudoscalar partner $\eta_b(1S)$ and $\eta_b(2S)$ were identified by the BaBar Collaboration in 2008 and 2011, respectively [12, 13]. Subsequently, the follow-up research by the CLEO [14, 15] and Belle Collaborations [16] confirmed the existence of these two bottomonia, where Belle did the most accurate measurements of mass to date with values of $9402.4 \pm 1.5 \pm 1.8$ MeV and $9999.0 \pm 3.5^{+2.8}_{-1.9}$ MeV, respectively [16]. The $\chi_{b1}(3P)$ state is the new state discovered by LHC in the chain decay of $\chi_{b1}(3P) \rightarrow \gamma\Upsilon(1S)/\gamma\Upsilon(2S) \rightarrow \gamma\mu^+\mu^-$ [17]. This state has been confirmed by the DØ Collaboration [18]. BaBar discovered a possible signal of the P -wave spin-singlet $h_b(1P)$ state

in 2011 [19], and subsequently, Belle firstly and successfully confirmed observation of the $h_b(1P)$ in the process of $\Upsilon(5S) \rightarrow \pi^+\pi^-h_b(1P)$, where the first radial excited state $h_b(2P)$ has also been observed with mass value $10259.76 \pm 0.64^{+1.43}_{-1.03}$ MeV [20]. Thus, both the ground and first radial excited states of the P -wave bottomonium have been fully established experimentally. However, this is not enough to make people satisfied because many of experimental information is still incomplete, including the total width and the branching ratios of some significant decay channels, which still require both of experimental and theoretical efforts. In regard to search of D -wave bottomonium in the experiments also has some progress by the CLEO and BaBar Collaborations [21, 22], where spin-triplet $\Upsilon(1^3D_2)$ was observed with a 5.8σ significance while confirmation of $\Upsilon(1^3D_1)$ and $\Upsilon(1^3D_3)$ states are dubious on account of lower significance [22].

Such plentiful experimental achievements in the bottomonium family not only increase our confidence to search for more higher excited bottomonia in future experiments but also provide an excellent opportunity to test various theories and phenomenological models. To better understand the properties of bottomonium, both the progress of experimental measurements and the calculation of theoretical and phenomenological methods are necessary. The lattice QCD is usually considered to be the most promising solution to the non-perturbative difficulty in low energy regions. In principle, the spectrum of the heavy quarkonium is directly obtained from the lattice QCD, but actually it is quite troublesome compared with the calculation of that of the light quarkonium since an additional large-scale heavy quark mass m_Q needs a tremendous computational effort [23]. In spite of this, lattice QCD still has an advantage in the calculations of bottomonium [24, 25]. Before the lattice method becomes more comprehensive, the mass spectra of hadrons are usually treated by the phenomenological model, namely, potential model, which takes into account the non-perturbative effects of QCD in the interaction potential and can give results consistent with the experiments.

In the past decades, a variety of potential models have been

*Corresponding author

*Electronic address: wangjzh2012@lzu.edu.cn

†Electronic address: sunzhif09@lzu.edu.cn

‡Electronic address: xiangliu@lzu.edu.cn

¶Electronic address: matsuki@tokyo-kasei.ac.jp

used to study the bottomonium system [26–45], among which the most well-known model is the Godfrey-Isgur relativistic quark model, which is widely used in the study from light mesons to heavy mesons [26, 46]. Recently, Godfrey and Moats used the Godfrey-Isgur relativistic quark model for investigating the properties of the $b\bar{b}$ system systematically. This system contains a large number of higher excited states, and they gave the results of the production in e^+e^- and pp collisions to help future experiments look for and observe most promising new bottomonia [26]. However, this is similar to the case of other meson families with abundant experimental information, i.e., high-lying states are related to the higher mass values forecasted by the GI model. By comparison with the measured results of $b\bar{b}$ state, one of the most salient particles is the $\Upsilon(11020)$ or $\Upsilon(6S)$ whose theoretical mass values are about 100 MeV larger than experimental data. In Ref. [47], the authors proposed a modified GI model with color screening effects to investigate higher excited charm-strange mesons. Namely, they take into account the effect that the confinement potential may be softened by the influence of light quarks induced from the vacuum in the long-range region [49], and find that the addition of this effect can well describe the properties of higher charm-strange mesons. Hence the recent study of bottomonia by the GI model [26] motivates us to explore what different conclusions can be drawn after considering screening effects into the GI model. With this motivation, we will carry out a most comprehensive study on the property of the bottomonium family in the modified GI model with screening effects, primarily focusing on the properties of higher excited states.

In this work, we calculate the mass spectrum and decay behaviors of bottomonia using the modified GI model, including radiative transition, hadronic transition, annihilation process and OZI-allowed two-body strong decay, where the meson wave function also comes from the modified GI model. This model will be thoroughly introduced in the next section. After the χ^2 fit utilizing rich experimental information, we can give a fairly good description for the mass spectrum of bottomonia, where the mass of the high excited state has been greatly improved compared to the estimates of the GI model [26], at the same time, we also predict the masses of higher bottomonia which are valuable for the experiments such as BaBar, Belle and LHC to search for these still unobserved particles. On the basis of mass spectrum of $b\bar{b}$ states, we discuss bottomonia by dividing them into those below and above open-bottom thresholds.

For the states below the threshold, strong decay channels have not opened and radiative transition and annihilation decay are usually dominant. Dipion hadronic transition is, of course, also a major decay mode. By comparing calculated partial width of these modes with the results of GI model, we find our results are almost identical to those of the GI model for low-lying states but are different for the high excited states such as $1F$ or $1G$ states. It is shown that the screening effect has little influence on the low-lying state but it is very important for the higher states. For the states above the threshold, we calculate the strong decay using 3P_0 model, where we adopt a numerical meson wave function rather than the SHO

wave function with a corresponding effective β value. Because the states above threshold have relatively large masses so that an influence of the screening effect is more obvious in this region and our results that are so different from the GI estimate should give a better prediction for the higher excited states.

In addition, it is emphasized that the discussion and prediction on the higher bottomonia are the main points of our work derived from our calculations. We hope that the present investigation can not only reveal the inherent properties of observed bottomonia but also provide valuable clues to help experiment search for more missing $b\bar{b}$ states in the future.

This paper is organized as follows. In Sec. II, we will give a brief introduction to the modified GI model with the screening effect and compare the results of the GI model and modified GI model. With our mass spectrum, bottomonium spectroscopy will be analyzed in this section. Combining information of mass spectrum and decay behaviors, we will study properties of the states below the $B\bar{B}$ threshold and those above the threshold in Secs. III and IV, respectively, where plentiful predictions will be given. We make a summary in Sec. V. Finally, all the theoretical tools of various decay processes and physical quantities, like partial decay width, branching ratios, annihilation decay, radiative transition, hadronic transition, and total widths, will be presented in Appendix A.

II. SPECTRUM

A. Modified GI model with a screening effect

In this work, we use the modified Godfrey-Isgur model with a screening potential [47] to calculate bottomonium mass spectrum and wave function, which will be employed in the calculation of decay processes. The Godfrey-Isgur relativized quark model [46] is one of the most successful model in predicting mass spectra of mesons. Even though the GI model has achieved great success, for the higher orbital and radial excitations, the predicted masses are larger on the whole than the observed masses of newly discovered particles in recent decades. Coupled-channel effects usually play an important role for the higher excitations and a screening effect could partly substitute the coupled-channel effect [50]. In 1985, Godfrey and Isgur proposed a relativized quark model motivated by QCD [46]. Compared with other models, relativistic corrections and universal one-gluon-exchange interaction as well as linear confinement potential are the most important features of this model. In the following, before presenting our modified GI model, we will introduce the GI model one by one. The Hamiltonian of a meson system is composed of kinetic energy and interaction between quark and anti-quark, and kinetic energy adopts a relativistic form as

$$H_0 = \sqrt{p^2 + m_1^2} + \sqrt{p^2 + m_2^2}, \quad (1)$$

where m_1 and m_2 are constituent quark masses corresponding to quark and anti-quark, respectively. The interaction between quark and anti-quark includes short-range one-gluon-

exchange potential $G(r)$ and long-range confinement $S(r)$, spin-orbit interaction, color hyperfine interaction (contact and tensor term). $G(r)$ and $S(r)$ have the following forms as

$$G(r) = -\frac{4\alpha_s(r)}{3r} \quad (2)$$

and

$$S(r) = br + c, \quad (3)$$

where $\alpha_s(r)$ is a running coupling constant. Relativistic contributions are divided into two parts. Firstly, the model makes a smearing transformation of $G(r)$ and $S(r)$. To express it shortly, we use a general function symbol $V(r)$ instead of $G(r)$ and $S(r)$. A special operation follows as

$$\tilde{V}(r) = \int V(r')\rho(\mathbf{r}-\mathbf{r}')dr' \quad (4)$$

with

$$\rho(\mathbf{r}-\mathbf{r}') = \frac{\sigma^3}{\pi^{\frac{3}{2}}} e^{-\sigma^2(\mathbf{r}-\mathbf{r}')^2}, \quad (5)$$

where σ is a smearing parameter. Second, an important reflection of relativistic effects lies in the momentum dependence of interactions between quark and anti-quark. Therefore, a momentum-dependent factor is brought into the interactions. In this situations, a one-gluon-exchange potential $G(r)$ is modified as

$$\tilde{G}(r) \rightarrow \left(1 + \frac{p^2}{E_1 E_2}\right)^{1/2} \tilde{G}(r) \left(1 + \frac{p^2}{E_1 E_2}\right)^{1/2}. \quad (6)$$

Tensor, contact, scalar spin-orbit, and vector spin-scalar terms should be changed as

$$\frac{\tilde{V}(r)}{m_1 m_2} \rightarrow \left(\frac{m_1 m_2}{E_1 E_2}\right)^{1/2+\varepsilon_i} \frac{\tilde{V}_i(r)}{m_1 m_2} \left(\frac{m_1 m_2}{E_1 E_2}\right)^{1/2+\varepsilon_i}, \quad (7)$$

where E_1 and E_2 are the energies of quark and anti-quark and ε_i corresponds to i -th type of interactions (ε_c , ε_t , ε_{sov} , and ε_{sos}). We readily notice that in the non-relativistic limit the factors become unity, and particular values of ε_i can be obtained from Table I.

After simply looking back to the GI model, we will introduce a modified GI model with a screening potential. Our previous work [47] presented the modified GI model with a color screening effect and revisited the properties of charm-strange mesons, subsequently, charm mesons have been also studied in the framework of the modified GI model [48], where higher excitations have been greatly improved. A screening effect can be achieved by modifying a confinement potential as

$$br \rightarrow \frac{b(1 - e^{-\mu r})}{\mu}, \quad (8)$$

where μ is a parameter which expresses the strength of a screening effect. As described in the preceding paragraphs, the modified confinement potential Eq. (8) also needs relativistic corrections. Details of techniques can be seen in Ref.

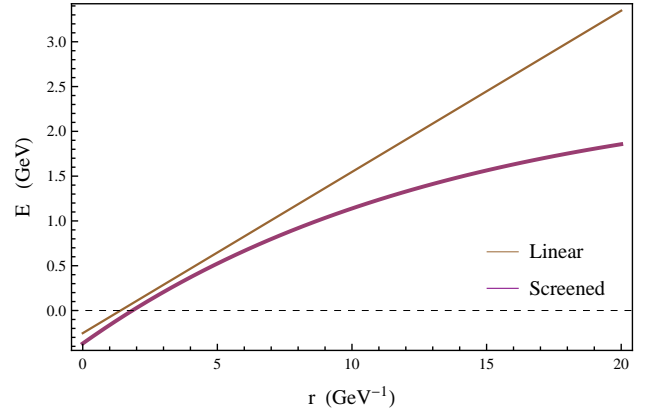


FIG. 1: Comparison of confinement potential curves of the modified GI model with screening effects and the GI model. Our screening effect parameter μ is 0.07426 GeV and other confinement parameters b and c are found in Table I.

[47]. It is worth mentioning that the modified GI model also employs simple harmonic oscillator (SHO) wave functions which can be considered as a complete basis set to expand exact meson wave functions. In the momentum space, an SHO wave function has the form

$$\Psi_{nLM_L}(\mathbf{p}) = R_{nL}(p, \beta) Y_{LM_L}(\Omega_p) \quad (9)$$

with

$$R_{nL}(p, \beta) = \frac{(-1)^{n-1}(-i)^L}{\beta^{3/2}} \sqrt{\frac{2(n-1)!}{\Gamma(n+L+1/2)}} \left(\frac{p}{\beta}\right)^L \times e^{\frac{-p^2}{2\beta^2}} L_{n-1}^{L+1/2}\left(\frac{p^2}{\beta^2}\right), \quad (10)$$

where $Y_{LM_L}(\Omega_p)$ is a spherical harmonic function, $L_{n-1}^{L+1/2}\left(\frac{p^2}{\beta^2}\right)$ is an associated Laguerre polynomial, and β is a parameter of an oscillator radial wave function. In the next subsection, we calculate our bottomonium mass spectra via the modified GI model, which helps us well understand the $b\bar{b}$ family and is also used for the subsequent decay processes.

B. Mass spectrum

Due to the introduction of a new parameter μ in our modified GI model, we need to combine experimental information to scale all available model parameters, at the same time, the richness of bottomonia in the experiment also provides us with an excellent opportunity to determine these model parameters, where the χ^2 fitting method is adopted. The χ^2 fitting method is to find the minimum χ^2 value, thereby, to obtain a set of corresponding fitting parameters in which the theoretical predictions of phenomenological model and experimental results are most consistent on the whole and χ^2 is defined as

$$\chi^2 = \sum_i \left(\frac{\mathcal{V}_{Exp}(i) - \mathcal{V}_{Th}(i)}{\mathcal{V}_{Er}(i)} \right)^2, \quad (11)$$

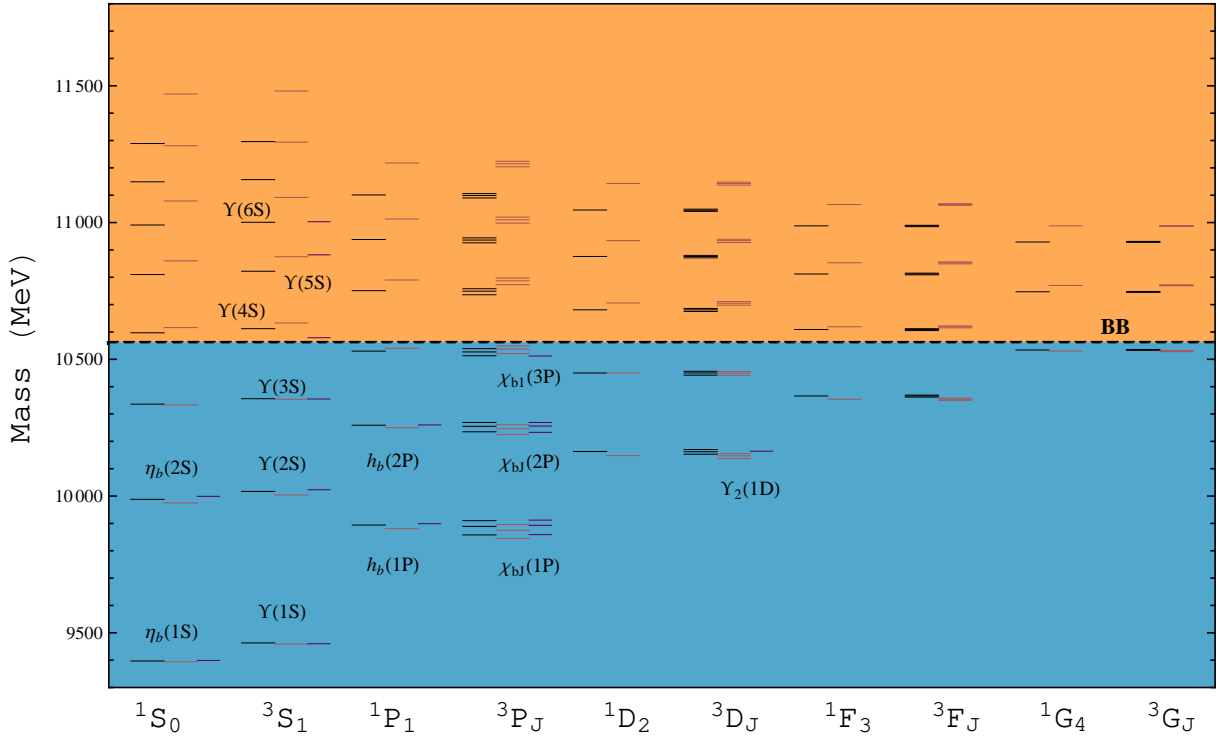


FIG. 2: Mass spectrum of bottomonium. Here, bottomonia are classified by the quantum number $^{2S+1}L_J$, from left to right successively in each category, black, pink, and purple lines stand for our results from the modified GI model, the predictions of the GI model [26, 46], and experimental values taken from PDG [51], respectively. The position of the open-bottom threshold is identified by the dashed line. In addition, the notation J means all the total angular momentum numbers of triplet states such as $J = 0, 1, 2$ for the P -wave states and $J = 1, 2, 3$ for the D -wave states and so on.

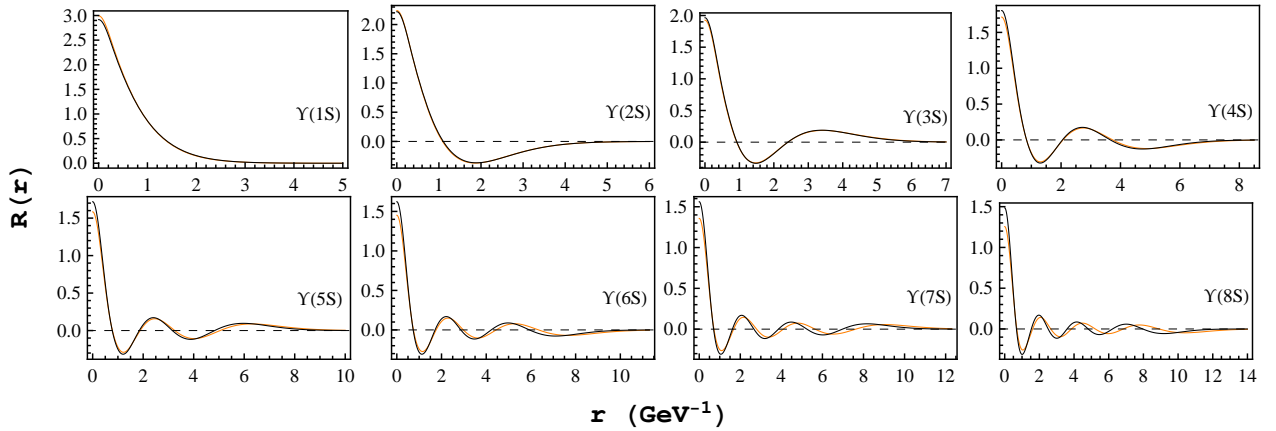


FIG. 3: The radial wave functions of the S -wave $Y(nS)$ state in the position space, which includes radial quantum number from one to eight. The orange and black curves represent the results from our modified GI model and GI model, respectively.

where the $\mathcal{V}_{Exp}(i)$, $\mathcal{V}_{Th}(i)$ and $\mathcal{V}_{Er}(i)$ are experimental value, theoretical value and error of i -th data, respectively. We select eighteen bottomonia to fit our model parameters as shown in Table II that have been established in the experiments. In this Table, all experimental masses are taken from PDG [51] and a uniform value of $\mathcal{V}_{Er}(i) = 5.0$ MeV is chosen as a fitting error for all the states, which is larger than the experimen-

tal uncertainty of all particles. The reason of this is that the experimental errors of these particles are relatively small and unevenly distributed. In other words, if the error of a particle is much smaller than the others, the mass of this particle will be too precise so that it is unfavorable to the overall fitting. The final fitting χ^2 value is given as 11.3 in conjunction with a uniform error and all corresponding fitting parameters of the

TABLE I: Parameters of the modified GI relativistic quark model with screening effects in bottomonium system.

Parameter	modified GI model	GI model [46]
ϵ_{sov}	-0.04098	-0.035
ϵ_c	-0.15384	-0.168
ϵ_t	0.02597	0.025
ϵ_{sos}	0.05777	0.055
m_b	5.027	4.977
b	0.21355	0.18
c	-0.36804	-0.253
μ	0.07426	-

TABLE II: Experimentally observed mass values of bottomonia which are used to calculate the minimum χ^2 and to obtain the model parameters listed in Table I. Experimental values and errors in the fitting are listed in the last two columns, respectively. The notation n in the χ^2/n is the number of selected particles here (= 18) and all mass values are in units of MeV.

States	$n^{2S+1}L_J$	This work	GI [46]	Experiment [51]	error
$\eta_b(1S)$	1^1S_0	9398	9394	9399 ± 2.3	5.0
$\eta_b(2S)$	2^1S_0	9989	9975	$9999 \pm 3.5_{-1.9}^{+2.8}$	5.0
$\Upsilon(1S)$	1^3S_1	9463	9459	9460.3 ± 0.26	5.0
$\Upsilon(2S)$	2^3S_1	10017	10004	10023.3 ± 0.31	5.0
$\Upsilon(3S)$	3^3S_1	10356	10354	10355.2 ± 0.5	5.0
$\Upsilon(4S)$	4^3S_1	10612	10633	10579.4 ± 1.2	5.0
$\Upsilon(10860)$	5^3S_1	10822	10875	$10881.8_{-1.1}^{+1.0} \pm 1.2$	5.0
$\Upsilon(11020)$	6^3S_1	11001	11092	$11003.0 \pm 1.1_{-1.0}^{+0.9}$	5.0
$h_b(1P)$	1^1P_1	9894	9881	9899.3 ± 0.8	5.0
$h_b(2P)$	2^1P_1	10259	10250	$10259.8 \pm 0.5 \pm 1.1$	5.0
$\chi_{b0}(1P)$	1^3P_0	9858	9845	$9859.4 \pm 0.42 \pm 0.31$	5.0
$\chi_{b0}(2P)$	2^3P_0	10235	10225	$10232.5 \pm 0.4 \pm 0.5$	5.0
$\chi_{b1}(1P)$	1^3P_1	9889	9875	$9892.8 \pm 0.26 \pm 0.31$	5.0
$\chi_{b1}(2P)$	2^3P_1	10255	10246	$10255.5 \pm 0.22 \pm 0.50$	5.0
$\chi_{b1}(3P)$	3^3P_1	10527	10537	$10512.1 \pm 2.1 \pm 0.9$	5.0
$\chi_{b2}(1P)$	1^3P_2	9910	9896	$9912.2 \pm 0.26 \pm 0.31$	5.0
$\chi_{b2}(2P)$	2^3P_2	10269	10261	$10268.7 \pm 0.22 \pm 0.50$	5.0
$\Upsilon(1D)$	1^3D_2	10162	10147	10163.7 ± 1.4	5.0
χ^2/n		11.3	31.4		

modified GI model are listed in Table I, where parameters of the GI model are also given for comparison.

In Table II, theoretical mass values of the GI model are also listed and the corresponding χ^2 value is 31.4 based on the same experimental center values and errors with the modified GI model. Comparing χ^2 values, one can easily see that the fitted modified GI model well improves the whole description

TABLE III: The mass spectrum of the predicted bottomonia. All mass values are in units of MeV.

States	This work	GI [46]	States	This work	GI [46]
$\eta_b(3^1S_0)$	10336	10333	$\Upsilon_1(4^3D_1)$	10871	10927
$\eta_b(4^1S_0)$	10597	10616	$\Upsilon_2(4^3D_2)$	10876	10934
$\eta_b(5^1S_0)$	10810	10860	$\Upsilon_3(4^3D_3)$	10880	10939
$\eta_b(6^1S_0)$	10991	11079	$\eta_{b2}(5^1D_2)$	11046	11143
$\eta_b(7^1S_0)$	11149	11281	$\Upsilon_1(5^3D_1)$	11041	11137
$\Upsilon(7^3S_1)$	11157	11294	$\Upsilon_2(5^3D_2)$	11045	11143
$\eta_b(8^1S_0)$	11289	11470	$\Upsilon_3(5^3D_3)$	11049	11148
$\Upsilon(8^3S_1)$	11296	11481	$h_{b3}(1^1F_3)$	10366	10354
$h_b(3^1P_1)$	10530	10540	$\chi_{b2}(1^3F_2)$	10362	10350
$\chi_{b0}(3^3P_0)$	10513	10521	$\chi_{b3}(1^3F_3)$	10366	10354
$\chi_{b2}(3^3P_2)$	10539	10549	$\chi_{b4}(1^3F_4)$	10369	10358
$h_b(4^1P_1)$	10751	10790	$h_{b3}(2^1F_3)$	10609	10619
$\chi_{b0}(4^3P_0)$	10736	10773	$\chi_{b2}(2^3F_2)$	10605	10615
$\chi_{b1}(4^3P_1)$	10749	10787	$\chi_{b3}(2^3F_3)$	10609	10619
$\chi_{b2}(4^3P_2)$	10758	10797	$\chi_{b4}(2^3F_4)$	10612	10622
$h_b(5^1P_1)$	10938	11013	$h_{b3}(3^1F_3)$	10812	10853
$\chi_{b0}(5^3P_0)$	10926	10998	$\chi_{b2}(3^3F_2)$	10809	10849
$\chi_{b1}(5^3P_1)$	10936	11010	$\chi_{b3}(3^3F_3)$	10812	10853
$\chi_{b2}(5^3P_2)$	10944	11020	$\chi_{b4}(3^3F_4)$	10815	10856
$h_b(6^1P_1)$	11101	11218	$h_{b3}(4^1F_3)$	10988	11066
$\chi_{b0}(6^3P_0)$	11090	11204	$\chi_{b2}(4^3F_2)$	10985	11063
$\chi_{b1}(6^3P_1)$	11099	11215	$\chi_{b3}(4^3F_3)$	10988	11066
$\chi_{b2}(6^3P_2)$	11106	11224	$\chi_{b4}(4^3F_4)$	10990	11069
$\eta_{b2}(1^1D_2)$	10163	10148	$\eta_{b4}(1^1G_4)$	10534	10530
$\Upsilon_1(1^3D_1)$	10153	10137	$\Upsilon_3(1^3G_3)$	10533	10528
$\Upsilon_3(1^3D_3)$	10170	10155	$\Upsilon_4(1^3G_4)$	10535	10530
$\eta_{b2}(2^1D_2)$	10450	10450	$\Upsilon_5(1^3G_5)$	10536	10532
$\Upsilon_1(2^3D_1)$	10442	10441	$\eta_{b4}(2^1G_4)$	10747	10770
$\Upsilon_2(2^3D_2)$	10450	10449	$\Upsilon_3(2^3G_3)$	10745	10769
$\Upsilon_3(2^3D_3)$	10456	10455	$\Upsilon_4(2^3G_4)$	10747	10770
$\eta_{b2}(3^1D_2)$	10681	10706	$\Upsilon_5(2^3G_5)$	10748	10772
$\Upsilon_1(3^3D_1)$	10675	10698	$\eta_{b4}(3^1G_4)$	10929	10988
$\Upsilon_2(3^3D_2)$	10681	10705	$\Upsilon_3(3^3G_3)$	10928	10986
$\Upsilon_3(3^3D_3)$	10686	10711	$\Upsilon_4(3^3G_4)$	10929	10988
$\eta_{b2}(4^1D_2)$	10876	10934	$\Upsilon_5(3^3G_5)$	10931	10989

of the bottomonium spectrum. Although the GI model was successful in investigating the bottomonium spectrum, comparing with the observed masses, there are two main shortcomings in the theoretical estimation of the GI model. The first one is that the theoretical mass values of low-lying states are universally 10-20 MeV smaller than the experimental values. The second is that the theoretical predictions for higher excited states become larger than the experiments. This is because the screening effect is not taken into account, especially for the $\Upsilon(6S)$ state whose mass difference is close to

100 MeV. It is worth mentioning that the experimental mass value of $\Upsilon(10860)$ or $\Upsilon(5S)$ state is overestimated. That is, the recent BaBar experiment tends to give a 30 MeV higher than the initial experimental value [51]. This means that the theoretical prediction of the modified GI model for this state will be inevitably small and this can also explain why the fitted χ^2 value can not be much smaller. In fact, including other studies of non-relativistic potential models that also consider a screening effect are also not very satisfactory for the description of this state, $\Upsilon(5S)$. Except for the $\Upsilon(10860)$, our results for the bottomonium spectrum are pretty good that can be seen from Table II. Our model not only solves the two above shortcomings of the GI model but also gives a fairly precise theoretical estimate, where the calculated mass values of many particles are almost the same as experimental results within the fitting errors. Based on our excellent description of the bottomonium spectrum with experimental information, we also predict mass values for those $b\bar{b}$ particles from S -wave to G -wave that have not yet been observed in Table III, which we hope to provide a meaningful help for the search of new bottomonium states in the future experiment. It is worth mentioning the spectrum position of higher S -wave Υ states including $\Upsilon(7S)$ and $\Upsilon(8S)$ with the expected masses, 11157 and 11296 MeV, respectively, which are significantly lower than the prediction of the GI model.

In order to facilitate the readers more intuitively and more conveniently to understand the bottomonia, the mass spectra are also shown in Fig. 2, which could also give an overall grasp of the spectroscopy and is convenient for the comparison among the results of two models and experiments. As seen from Fig. 2, after introducing the screening effect, the impact of a screening potential on the ground states and low-lying states is not so large, which is very obvious in the area below the open-bottom threshold in the figure. In contrast, the screening effect begins to be important in the part of higher excited states, especially in the particles with larger radial quantum numbers n and the greater the n value the more prominent this effect is because of the more and more obvious mass differences between the GI model and modified GI model. This feature can also be reflected from the wave function of bottomonia and we take the S -wave Υ family as an example, whose radial wave functions are shown in Fig. 3. Here the wave functions of the $\Upsilon(mS)$ with $m = 1, \dots, 4$ are almost undistinguishable but the higher radial excited states appear to be visibly different in the positions of nodes and radial distributions. Of course, to thoroughly understand the impact of the screening effect and the nature of the bottomonium family, we also need to analyze their decay behaviors, which is also the main task of the later sections.

III. ANALYSIS OF STATES BELOW OPEN-BOTTOM THRESHOLDS

A. The η_b states

The η_b family with a quantum number $1S_0$ is the partner of spin-triplet Υ states. The ground state $\eta_b(1S)$ and ra-

dial excited state $\eta_b(2S)$ have been established in the experiment, whose measured averaged mass values are 9399.0 ± 2.3 MeV and $9999 \pm 3.5^{+2.8}_{-1.9}$ MeV [51], respectively. Our theoretical mass values in Table II are in pretty good agreement with the experimental results. There is also a more interesting physical quantity, i.e., the hyperfine mass splitting between the spin-singlet and spin-triplet states $\Delta m(nS) = m[\Upsilon(nS)] - m[\eta_b(nS)]$, which reflects the spin-dependent interaction and can be used to test various theoretical models. For the $\eta_b(1S)$ state, the predicted mass splitting of the lattice regularized QCD is 60.3 ± 7.7 MeV [89] which is comparable with the measured averaged value 62.3 ± 3.2 MeV [51]. On the other hand, our theoretical result of hyperfine mass splitting is 65 MeV within the upper limit of error, which is well consistent with the experiment and the lattice calculation. Furthermore, it is worth mentioning that the predicted mass splittings from the GI model and our modified GI model are exactly the same, although there are some differences in the respective masses. The $\Delta m(2S)$ from our modified GI model is estimated as 28 MeV which is also equally well consistent with the measured value $24.3^{+4.0}_{-4.5}$ MeV [16] and the lattice computation $23.5 - 28.0$ MeV [89].

Together with the successful description of the mass of η_b family, we also need to explore their decay behaviors. We list the partial widths and branching ratios of electromagnetic decays, annihilation decay, and hadronic transitions for η_b states below the open-bottom thresholds from $\eta_b(1S)$ up to $\eta_b(4S)$ in Table VI. Here, the OZI-allowed two-body strong decay channels do not yet open so that the annihilation into the two gluons is dominant, whose corresponding branching ratio is almost 100%. From Table VI, we see that the decay widths from our modified GI model are not so different from those of the GI results. This is because screening effects are weak for the wave function of low-lying states as discussed in Section II, and the decay predictions of $\eta_b(1S)$ and $\eta_b(2S)$ are also consistent among three potential models, our work and Refs. [26, 27].

For the two unobserved $\eta_b(3S)$ and $\eta_b(4S)$ state, we predict the mass of 10336 and 10597 MeV and total width of

TABLE IV: The mass values of the bottom and bottom-strange mesons involved in the present calculation. Because of the tiny measured mass difference between B^\pm and B_0 , we use the experimental mass of B_0 as an input, i.e., $B(1^1S_0)$ meson.

State	$n^{2S+1}L_J$	input mass (MeV)
B	1^1S_0	5280 [51]
B^*	1^3S_1	5325 [51]
$B(1^3P_0)$	1^3P_0	5700
$B(1P_1)$	$\cos(\theta) 1^1P_1\rangle + \sin(\theta) 1^3P_1\rangle$	5717
$B(1P'_1)$	$-\sin(\theta) 1^1P_1\rangle + \cos(\theta) 1^3P_1\rangle$	5726 [51]
$B(1^3P_2)$	1^3P_2	5740 [51]
B_s	1^1S_0	5367 [51]
B_s^*	1^3S_1	5415 [51]

TABLE V: The calibration of the parameter γ in the 3P_0 model. $\Gamma_{Exp.}$ and $\Gamma_{Th.}$ denote the experimental and theoretical widths, respectively. Γ_{Error} represents fitting error. For $b\bar{b}$ system, we obtain $\gamma = 7.09$ with $\chi^2/n = 1.2229$ where $n = 3$. All width results are in units of MeV.

bottomonium	$\Gamma_{Exp.}$ [51]	$\Gamma_{Th.}$	Γ_{Error}
$\Upsilon(4S)$	20.5 ± 2.5	24.6747	2.5
$\Upsilon(10860)$	$48.5^{+1.9+2.0}_{-1.8-2.8}$	45.5839	3.33
$\Upsilon(11020)$	$39.3^{+1.7+1.3}_{-1.6-2.4}$	38.3302	2.88
γ	7.09		

5.52 and 4.07 MeV, respectively. The corresponding hyperfine mass splitting $\Delta m(3S)$ is 20 MeV while the result of non-relativistic constituent quark model [27] is 19 MeV, and our estimate for $\Delta m(4S)$ is 15 MeV. These predictions require further validation by the future experiment. In addition to the dominant two gluon annihilation decay, some other possible main decay channels of $\eta_b(3S)$ are $\eta_b(1S)\pi\pi$ and $h_b(2P)\gamma$, both of which have almost the same branching ratios. The decay mode $h_b(1P)\gamma$ is also estimated to be important in our calculation but the corresponding prediction of nonrelativistic constituent quark model [27] is two orders of magnitude smaller than our result. Similarly, the hadronic transition to $\eta_b(1S)\pi\pi$ and E1 radiative transition to $h_b(3P)\gamma$ are predicted to be important decay modes of $\eta_b(4S)$ with the branching ratios of (9.1×10^{-3}) and (3.7×10^{-4}) , respectively.

B. The Υ states

From Fig. 2, we can clearly see that $\Upsilon(4S)$ state is slightly above the open-bottom threshold. Hence, it can decay into the $B\bar{B}$ and the states below the thresholds are only $\Upsilon(1S)$, $\Upsilon(2S)$, and $\Upsilon(3S)$, which were first discovered bottomonia together in the E288 Collaboration at Fermilab by studying produced muon pairs in a regime of invariant masses larger than 5 GeV [3, 4]. At present, these three particles do not arose much controversy due to the high accuracy of the experimental measurements for their mass, which can be usually matched by the calculation of most of the potential models and the lattice QCD. The mass difference between our theoretical estimates and experimental center values for these three states are 3, 5 and 1 MeV, respectively, which also indicates the reliability of our modified GI quark model in the mass spectrum. The above mass difference can be seen in Table II, where the considerable improvement of the mass spectrum for $\Upsilon(2S)$ by our modified GI model compared with the original GI model can be also found. In addition, the BaBar collaboration [90] measured the level difference $m[\Upsilon(3S)] - m[\Upsilon(2S)]$ with $331.50 \pm 0.02 \pm 0.13$ MeV. Our corresponding theoretical result of 339 MeV is also in good agreement with this BaBar measurement.

The partial widths and branching ratios of electromagnetic decays, annihilation decay, and hadronic transitions and the

total width for $\Upsilon(1S)$, $\Upsilon(2S)$, and $\Upsilon(3S)$ are listed in Table VII. Compared with the S -wave spin-singlet η_b family, the experimental information of the spin-triplet Υ states is clearly much more abundant, which includes total widths and partial rates of most of the decay processes. Next, we firstly start from the analysis of the common decay properties of $\Upsilon(1S)$, $\Upsilon(2S)$, and $\Upsilon(3S)$. From Table VII, the annihilation decay to three gluons is dominant since each branching ratio is 89%, 63.8% and 58.7% from our model, respectively, and the contributions to the total width from other three annihilation decay modes $\ell^+\ell^-$, $\gamma\gamma\gamma$, and $\gamma\gamma\gamma$ are much smaller. Especially, the $\gamma\gamma\gamma$ decay is difficult to search for in the experiment due to the very small branching ratio, the $10^{-5} \sim 10^{-6}$ order of magnitude, and leptonic annihilation decay and $\gamma\gamma\gamma$ decay modes have almost the same predicted partial widths. All the experimental widths and branching ratios basically agree with our theoretical calculations although the errors in $\Upsilon(3S)$ state are large. Additionally, it needs to be emphasized that the experimental partial widths marked as b shown in Table VII are obtained by combining measured total widths and branching ratios of the PDG [51].

The M1 radiative transition $\Upsilon(1S) \rightarrow \eta_b(1S)\gamma$ is the unique electromagnetic decay of $\Upsilon(1S)$ state, which has no experimental information until now. The calculations of three models of Table VII give a consistent estimate, 0.01 keV, and the total width of $\Upsilon(1S)$ is also compatible with our theoretical result.

Numerous radiative decay modes are opened for $\Upsilon(2S)$ including the transition to $\chi_{bJ}(1P)$, all of which are measured by experiment. By comparison, we can see that the experimental data of radiative transition of $\Upsilon(2S)$ can be well reproduced by three theoretical models except for the decay channel $\eta_b(1S)\gamma$. It should be mentioned that the calculations of branching ratios by the nonrelativistic constituent quark model [27] adopt measured total widths, which is the reason why our theoretical results are smaller but the estimates of partial widths are close to the values of Ref. [27]. At last, the hadronic transition $\Upsilon(2S) \rightarrow \Upsilon(1^3S_1)\pi\pi$ has been used to fix the unknown model parameter C_1 in the QCD multipole expansion approach, Eq. (A11) in Appendix A.

There are some difficulties in the theoretical description of $\Upsilon(3S)$ as a whole. Our theoretical total width of $\Upsilon(3S)$ is 35.8 keV, which is larger than the PDG result of 20.32 ± 1.85 keV. The excess mainly comes from the annihilation mode of ggg and hadronic mode of $\Upsilon(1S)\pi\pi$. Considering the uncertainty of the phenomenological models, we make a comparison in other decay channels by using calculated experimental partial widths rather than directly measured branch ratios. Our predictions for $\chi_{bJ}(2P)\gamma$ are satisfactory and in spite of some deviations, the $\chi_{bJ}(1P)\gamma$ and $\eta_b(1S)\gamma$ modes can be ensured in the order of magnitude.

C. The P -wave χ_{bJ} and h_b states

The P -wave states $\chi_{bJ}(1P)$ and $\chi_{bJ}(2P)$ with $J = 1, 2, 3$ are the bottomonium particles discovered in 1982 in search for the radiative processes $\Upsilon(2S) \rightarrow \chi_{bJ}(1P)\gamma$ [10] and

TABLE VI: Partial widths and branching ratios of annihilation decay, radiative transition, and hadronic transition and total widths for the S -wave η_b below the open-bottom thresholds. Experimental results are taken from the PDG [51]. The theoretical results of the Godfrey-Isgur relativized quark model [26] and the nonrelativistic constituent quark model [27] are summarized in the rightmost columns. The width results are in units of keV.

state	channels	This work		Expt. [51]		GI [26]		Ref. [27]	
		Width	$\mathcal{B}(\%)$	Width	$\mathcal{B}(\%)$	Width	$\mathcal{B}(\%)$	Width	$\mathcal{B}(\%)$
$\eta_b(1S)$	gg	17.9 MeV	~ 100	16.6 MeV	~ 100	20.18 MeV	~ 100
	$\gamma\gamma$	1.05	5.87×10^{-3}	0.94	5.7×10^{-3}	0.69	3.42×10^{-3}
	Total	17.9 MeV	100	10^{+5}_{-4} MeV	...	16.6 MeV	100	20.18 MeV	100
$\eta_b(2S)$	gg	8.33 MeV	~ 100	7.2 MeV	~ 100	10.64 MeV	99.86
	$\gamma\gamma$	0.489	5.86×10^{-3}	0.41	5.7×10^{-3}	0.36	3.38×10^{-3}
	$h_b(1^1P_1)\gamma$	2.467	2.96×10^{-2}	2.48	3.4×10^{-2}	2.85	2.68×10^{-2}
	$\Upsilon(1^3S_1)\gamma$	0.0706	8.47×10^{-4}	0.068	9.4×10^{-4}	0.045	4.22×10^{-4}
	$\eta_b(1^1S_0)\pi\pi$	10.3	0.124	12.4	0.17	11.27	0.1058
	Total	8.34 MeV	100	<24 MeV	...	7.2 MeV	100	10.66 MeV	100
$\eta_b(3S)$	gg	5.51 MeV	~ 100	4.9 MeV	~ 100	7.94 MeV	99.93
	$\gamma\gamma$	0.323	5.85×10^{-3}	0.29	5.9×10^{-3}	0.27	3.4×10^{-3}
	$h_b(1^1P_1)\gamma$	1.12	2.03×10^{-2}	1.3	2.6×10^{-2}	0.0084	1.06×10^{-4}
	$h_b(2^1P_1)\gamma$	2.88	5.22×10^{-2}	2.96	6×10^{-2}	2.60	3.27×10^{-3}
	$\Upsilon(1^3S_1)\gamma$	0.0732	1.33×10^{-3}	0.074	1.5×10^{-3}	0.0051	6.42×10^{-4}
	$\Upsilon(2^3S_1)\gamma$	0.0111	2.01×10^{-4}	0.0091	1.8×10^{-4}	0.0092	1.16×10^{-4}
	$\eta_b(1^1S_0)\pi\pi$	3.18	5.76×10^{-2}	1.70 ± 0.22	3.5×10^{-2}	1.95	2.45×10^{-3}
	$\eta_b(2^1S_0)\pi\pi$	0.501	9.08×10^{-3}	1.16 ± 0.10	2.4×10^{-2}	0.34	4.28×10^{-3}
	Total	5.52 MeV	100	4.9 MeV	100	7.95 MeV	100
$\eta_b(4S)$	gg	4.03 MeV	99	3.4 MeV	~ 100
	$\gamma\gamma$	0.237	5.82×10^{-3}	0.20	5.9×10^{-3}
	$h_b(1^1P_1)\gamma$	0.688	1.69×10^{-2}
	$h_b(2^1P_1)\gamma$	0.732	1.8×10^{-2}
	$h_b(3^1P_1)\gamma$	1.50	3.69×10^{-2}	1.24	3.6×10^{-2}
	$\Upsilon(1^3S_1)\gamma$	0.0594	1.46×10^{-3}
	$\Upsilon(2^3S_1)\gamma$	0.0141	3.46×10^{-4}
	$\Upsilon(3^3S_1)\gamma$	0.00308	7.57×10^{-5}
	$\eta_b(1^1S_0)\pi^+\pi^-$	24.6	0.604	2.03 ± 0.29	6×10^{-2}
	$\eta_b(2^1S_0)\pi^+\pi^-$	0.183	4.5×10^{-3}	1.9 ± 0.36	5.6×10^{-2}
	Total	4.07 MeV	100	3.4 MeV	100

$\Upsilon(3S) \rightarrow \chi_{bJ}(2P)\gamma$ [11]. The corresponding spin-singlet partners $h_b(1P)$ and $h_b(2P)$ had been missing until 2012, which were firstly observed by the Belle collaboration at the same time [20]. In the same year, 2012, the Large Hadron Collider brought good news about the confirmation of first observed $3P$ bottomonium state $\chi_{b1}(3P)$ in the chain decay of the radiative transition to $\Upsilon(1S)\gamma$ and $\Upsilon(2S)\gamma$ and to $\Upsilon(1S, 2S) \rightarrow \mu^+\mu^-$. This experiment reported the measured mass of $10530 \pm 5 \pm 9$ MeV [17], whose central value is consistent with our theoretical prediction of 10527 MeV in Table II although statistical and systematic uncertainties are relatively large. Subsequent several measurements of LHCb give mass value about 15 MeV less than [17], which are incompatible with the cur-

rent predictions of most of the potential models. Therefore, further study on $\chi_{b1}(3P)$ in more experiments is necessary. Furthermore, the predicted mass of other $3P$ states are listed in Table III. Table II shows that our theoretical mass for all of $1P$ and $2P$ states are in remarkable agreement with the experiments with error of less than 5 MeV, which again proves the validity of the modified GI model with a screening effect.

The partial widths and branching ratios of radiative transition, annihilation decay, and hadronic transitions and the total width for $1P$ to $3P$ bottomonium states are successively given in Tables VIII-XI. Because there are currently no measured total widths and partial widths available for all observed $1P$ and $2P$ states, we will analyze the decay properties of P -

TABLE VII: Partial widths and branching ratios of annihilation decay, radiative transition, and hadronic transition and total widths for the S -wave Υ below the open-bottom thresholds. Experimental results are taken from the PDG [51]. The theoretical results of the GI model [26] and the nonrelativistic constituent quark model [27] are summarized in the rightmost columns. The width results are in units of keV.

state	channels	This work		Expt. [51]		GI [26]		Ref. [27]	
		Width	$\mathcal{B}(\%)$	Width	$\mathcal{B}(\%)$	Width	$\mathcal{B}(\%)$	Width	$\mathcal{B}(\%)$
$\Upsilon(1S)$	$\ell^+\ell^-$	1.65	2.89	1.340 ± 0.018	2.38 ± 0.11	1.44	2.71	0.71	1.31
	ggg	50.8	89	44.13 ± 1.09^b	81.7 ± 0.7	47.6	89.6	41.63	77.06
	γgg	1.32	2.31	1.19 ± 0.33^b	2.20 ± 0.60	1.2	2.3	0.79	1.46
	$\gamma\gamma\gamma$	1.94×10^{-5}	3.4×10^{-5}	1.7×10^{-5}	3.2×10^{-5}	3.44×10^{-6}	6.37×10^{-6}
	$\eta_b(1^1S_0)\gamma$	0.00952	1.67×10^{-2}	0.010	1.9×10^{-2}	0.00934	1.73×10^{-2}
	Total	57.1	100	54.02 ± 1.25	...	53.1	100	44.6 ^a	...
$\Upsilon(2S)$	$\ell^+\ell^-$	0.821	1.84	0.612 ± 0.011	1.91 ± 0.16	0.73	1.8	0.37	1.16
	ggg	28.4	63.8	18.80 ± 1.59^b	58.8 ± 1.2	26.3	65.4	24.25	75.83
	γgg	0.739	1.66	0.60 ± 0.10^b	1.87 ± 0.28	0.68	1.7	0.46	1.44
	$\gamma\gamma\gamma$	1.09×10^{-5}	2.45×10^{-5}	9.8×10^{-6}	2.4×10^{-5}	2.00×10^{-6}	6.25×10^{-6}
	$\chi_{b0}(1^3P_0)\gamma$	0.907	2.04	1.22 ± 0.16^b	3.8 ± 0.4	0.91	2.3	1.09	3.41
	$\chi_{b1}(1^3P_1)\gamma$	1.60	3.60	2.21 ± 0.22^b	6.9 ± 0.4	1.63	4.05	1.84	5.75
	$\chi_{b2}(1^3P_2)\gamma$	1.86	4.18	2.29 ± 0.22^b	7.15 ± 0.35	1.88	4.67	2.08	6.50
	$\eta_b(1^1S_0)\gamma$	0.0688	0.155	0.012 ± 0.005^b	$(3.9 \pm 1.5) \times 10^{-2}$	0.081	0.20	0.0565	0.18
	$\eta_b(2^1S_0)\gamma$	5.82×10^{-4}	1.31×10^{-3}	5.9×10^{-4}	1.5×10^{-3}	5.80×10^{-4}	1.81×10^{-3}
	$\Upsilon(1^3S_1)\pi\pi$	8.46	19	8.46 ± 0.71^b	26.45 ± 0.48	8.46	21.0	8.57	26.80
	Total	44.5	100	31.98 ± 2.63	...	40.2	100	39.5 ^a	...
$\Upsilon(3S)$	$\ell^+\ell^-$	0.569	1.59	0.443 ± 0.008	2.18 ± 0.21	0.53	1.8	0.27	1.33
	ggg	21.0	58.7	7.25 ± 0.85^b	35.7 ± 2.6	19.8	67.9	18.76	92.32
	γgg	0.547	1.53	0.20 ± 0.04^b	0.97 ± 0.18	0.52	1.8	0.36	1.77
	$\gamma\gamma\gamma$	8.04×10^{-6}	2.25×10^{-5}	7.6×10^{-6}	2.6×10^{-5}	1.55×10^{-6}	7.63×10^{-6}
	$\chi_{b0}(1^3P_0)\gamma$	0.0099	2.77×10^{-2}	0.055 ± 0.010^b	0.27 ± 0.04	0.01	0.03	0.15	0.74
	$\chi_{b1}(1^3P_1)\gamma$	0.0363	0.101	0.018 ± 0.010^b	$(9 \pm 5) \times 10^{-2}$	0.05	0.2	0.16	0.79
	$\chi_{b2}(1^3P_2)\gamma$	0.359	1.0	0.20 ± 0.03^b	0.99 ± 0.13	0.45	1.5	0.0827	0.41
	$\chi_{b0}(2^3P_0)\gamma$	1.06	2.96	1.20 ± 0.16^b	5.9 ± 0.6	1.03	3.54	1.21	5.96
	$\chi_{b1}(2^3P_1)\gamma$	1.96	5.47	2.56 ± 0.34^b	12.6 ± 1.2	1.91	6.56	2.13	10.48
	$\chi_{b2}(2^3P_2)\gamma$	2.37	6.62	2.66 ± 0.41^b	13.1 ± 1.6	2.30	7.90	2.56	12.60
	$\eta_b(1^1S_0)\gamma$	0.0604	0.169	0.010 ± 0.002^b	$(5.1 \pm 0.7) \times 10^{-2}$	0.060	0.20	0.057	0.28
	$\eta_b(2^1S_0)\gamma$	0.0118	3.3×10^{-2}	$< 0.014^b$	< 0.062 (90% C.L.)	0.19	0.65	0.011	5.41×10^{-2}
	$\eta_b(3^1S_0)\gamma$	3.37×10^{-4}	9.4×10^{-4}	2.5×10^{-4}	8.6×10^{-4}	6.58×10^{-4}	3.24×10^{-3}
	$\Upsilon(1^3S_1)\pi\pi$	6.17	17.2	1.34 ± 0.13^b	6.57 ± 0.15	1.34	4.60	1.77	8.71
	$\Upsilon(2^3S_1)\pi\pi$	0.479	1.34	0.95 ± 0.10^b	4.67 ± 0.23	0.95	3.3	0.42	2.07
	Total	35.8	100	20.32 ± 1.85	...	29.1	100	28.5 ^a	...

^aFrom the summation of partial widths of Ref. [27].

^bFrom the calculation of combining experimental total widths and branching ratios of the PDG [51].

wave bottomonium states directly from the branching ratios. For $1P$ states, there are actually not many open decay channels and the annihilation processes of multi-gluon or hybrid $q\bar{q}g$ final state have dominant contributions to the total width. As for radiative transitions, the CLEO collaboration released the most accurate measurement on electromagnetic process of

$\chi_{bJ}(1P) \rightarrow \Upsilon(1S)\gamma$ with $J = 1, 2, 3$, whose branching ratios are $1.76 \pm 0.30 \pm 0.78\%$, $33.1 \pm 1.8 \pm 1.7\%$, and $18.6 \pm 1.1 \pm 0.9\%$ [91], respectively.

In the past few years, the Belle collaboration has studied the decay mode of $h_b(1P) \rightarrow \eta_b(1S)\gamma$, whose branching ratio is $49.2 \pm 5.7^{+5.6}_{-3.3}\%$ in 2012 [16] and $56 \pm 8 \pm 4\%$ in 2015

TABLE VIII: Partial widths and branching ratios of annihilation decay and radiative transition and total widths for the $1P$ bottomonium states. Experimental results are taken from the PDG [51]. The theoretical results of the GI model [26] and the nonrelativistic constituent quark model [27] are summarized in the rightmost columns. The width results are in units of keV.

state	channels	This work		Expt. [51]		GI [26]		Ref. [27]	
		Width	$\mathcal{B}(\%)$	Width	$\mathcal{B}(\%)$	Width	$\mathcal{B}(\%)$	Width	$\mathcal{B}(\%)$
$h_b(1^1P_1)$	ggg	44.7	56.5	37	51	35.26	44.68
	$\eta_b(1^1S_0)\gamma$	34.4	43.5	...	52_{-5}^{+6}	35.7	49	43.66	55.32
	$\chi_{b0}(1^3P_0)\gamma$	9.01×10^{-4}	1.14×10^{-3}	8.9×10^{-4}	1.2×10^{-5}	8.61×10^{-4}	1.09×10^{-3}
	$\chi_{b1}(1^3P_1)\gamma$	9.23×10^{-6}	1.17×10^{-5}	1.0×10^{-5}	1.4×10^{-5}	1.15×10^{-5}	1.46×10^{-5}
	Total	79.1	100	73	100	78.92	100
$\chi_{b0}(1^3P_0)$	$\gamma\gamma$	0.199	5.87×10^{-3}	0.15	5.8×10^{-3}	0.12	5.91×10^{-3}
	gg	3.37 MeV	99.4	2.6 MeV	~ 100	2.00 MeV	98.61
	$\Upsilon(1^3S_1)\gamma$	22.8	0.673	...	1.76 ± 0.35	23.8	0.92	28.07	1.38
	Total	3.39 MeV	100	2.6 MeV	100	2.03 MeV	100
$\chi_{b1}(1^3P_1)$	$q\bar{q}g$	81.7	74.3	67	70	71.53	66.73
	$\Upsilon(1^3S_1)\gamma$	28.3	25.7	...	33.9 ± 2.2	29.5	31	35.66	33.27
	Total	110	100	96	100	107.19	100
$\chi_{b2}(1^3P_2)$	$\gamma\gamma$	0.0106	5.41×10^{-3}	9.3×10^{-3}	5.2×10^{-3}	3.08×10^{-3}	2.51×10^{-3}
	gg	165	84.2	147	81.7	83.69	68.13
	$\Upsilon(1^3S_1)\gamma$	31.4	16.0	...	19.1 ± 1.2	32.8	18.2	39.15	31.87
	$h_b(1^1P_1)\gamma$	9.37×10^{-5}	4.78×10^{-5}	9.6×10^{-5}	5.3×10^{-5}	8.88×10^{-5}	7.23×10^{-5}
	Total	196	100	180	100	122.84	100

[92]. Combining the results mentioned above with the PDG averaged ratios [51], we can see that the theoretical estimates shown in Table VIII are also generally supported by experimental data.

Different from the case of $1P$ states, experimental measurements for the $E1$ radiative decays $\chi_{bJ}(2P) \rightarrow \Upsilon(1S, 2S)\gamma$ with $J = 1, 2, 3$ and $h_b(2P) \rightarrow \eta_b(1S, 2S)\gamma$ are much larger than theoretical results as shown in Table IX. It may be due to an overestimation of annihilation decay calculation or due to the experimental measurement error. After all, the uncertainties of some experimental data are quite large.

In addition, it is worth noting that our results of critical hadronic decay channel of $\chi_{bJ}(2P) \rightarrow \chi_{bJ}(1P)\pi\pi$ with non-flip J and $h_b(2P) \rightarrow h_b(1P)\pi\pi$ calculated by the QCD multipole expansion approach are roughly consistent with the GI's one. However, our results for the process of $\chi_{bJ}(2P) \rightarrow \chi_{bJ'}(1P)\pi\pi$ with $J \neq J'$ is incompatible with the GI model where our estimates are quite suppressed similar to the calculation of nonrelativistic constituent quark model [27]. The analogous situation also exists in the $3P$ and D -wave bottomonium states, which needs to be identified by the future experimental measurements.

Although the first $3P$ state has been experimentally observed, the experimental information of decay behaviors is still lacking. Our predictions for various decay channels of 3^1P_1 , 3^3P_0 and 3^3P_1 , 3^3P_2 states are listed in Tables X and XI, respectively. In addition to annihilation decay ggg , the decay

modes $\eta_b(1S, 2S, 3S)\gamma$ and $h_b(1P)\pi\pi$ are also important for $h_b(3P)$ states. Especially, the process of $h_b(3P) \rightarrow \eta_b(3S)\gamma$ has a predicted branching ratio of 10.4%. If $h_b(3P)$ is confirmed in the future, we suggest that experiment can search for the missing $\eta_b(3S)$ state by studying this radiative process of $h_b(3P)$. Likewise, compared to other radiative transition processes, the decay process to the S -wave Υ state is very significant for $\chi_{bJ}(3P)$ state. It should be noted that the $\chi_{b1}(3P)$ state is just found in the chain decay of the radiative transition to $\Upsilon(1S, 2S)\gamma$ and to $\Upsilon \rightarrow \mu^+\mu^-$. It should be also emphasized that our prediction in the partial width of hadronic transition of $\chi_{b0}(3P) \rightarrow \chi_{b0}(1P)\pi\pi$ gives an opportunity to observe $\chi_{b0}(3P)$ in this channel.

Finally, we discuss the predicted total widths of P -wave bottomonia below the open-bottom threshold, where all of $\Gamma_{total}[h_b(nP)]$ with $n=1,2,3$ are about 80-90 keV. The total widths of $\Gamma_{total}[\chi_{b1}(nP), \chi_{b2}(nP)]$ with $n = 1, 2, 3$ are around 110-145 keV and 196-264 keV, respectively. However, the total widths of $\chi_{b0}(nP)$ states with $n=1,2,3$ are around 3.13-3.54 MeV, whose differences could possibly distinguish P -wave spin-triplet χ_{bJ} states from each other in experiments.

D. The $1D$ and $2D$ states

The ground state and first radial excitations of the D -wave bottomonia with orbital angular momentum $L = 2$ were usu-

TABLE IX: Partial widths and branching ratios of annihilation decay, radiative transition, and hadronic transition and total widths for the $2P$ bottomonium states. Experimental results are taken from the PDG [51]. The theoretical results of the GI model [26] and the nonrelativistic constituent quark model [27] are summarized in the rightmost columns. The width results are in units of keV.

state	channels	This work		Expt. [51]		GI [26]		Ref. [27]	
		Width	$\mathcal{B}(\%)$	Width	$\mathcal{B}(\%)$	Width	$\mathcal{B}(\%)$	Width	$\mathcal{B}(\%)$
$h_b(2^1P_1)$	ggg	64.6	69.6	54	64	52.70	57.82
	$\eta_b(1^1S_0)\gamma$	10.8	11.6	...	22 ± 5	13.0	15	14.90	16.35
	$\eta_b(2^1S_0)\gamma$	15.0	16.2	...	48 ± 13	14.1	17	17.60	19.31
	$\eta_{b2}(1^1D_2)\gamma$	1.81	1.95	1.7	2.0	5.36	5.88
	$\chi_{b0}(1^3P_0)\gamma$	0.00556	5.99×10^{-3}	3.2×10^{-4}	3.8×10^{-4}	0.0364	3.99×10^{-2}
	$\chi_{b1}(1^3P_1)\gamma$	0.00130	1.40×10^{-3}	0.0011	1.3×10^{-3}	0.00128	1.41×10^{-3}
	$\chi_{b2}(1^3P_2)\gamma$	9.92×10^{-4}	1.07×10^{-3}	0.0022	2.6×10^{-3}	6.91×10^{-6}	7.58×10^{-6}
	$\chi_{b0}(2^3P_0)\gamma$	2.76×10^{-4}	2.97×10^{-4}
	$\chi_{b1}(2^3P_1)\gamma$	2.74×10^{-6}	2.95×10^{-6}
	$h_b(1^1P_1)\pi\pi$	0.624	0.672	0.94	1.1	0.54	0.59
	Total	92.8	100	84	100	91.14	100
$\chi_{b0}(2^3P_0)$	$\gamma\gamma$	0.205	5.79×10^{-3}	0.15	5.7×10^{-3}	0.14	5.85×10^{-3}
	gg	3.52 MeV	99.4	2.6 MeV	~ 100	2.37 MeV	99.17
	$\Upsilon(1^3S_1)\gamma$	2.31	6.53×10^{-2}	...	0.9 ± 0.6	2.5	9.6×10^{-2}	5.44	0.23
	$\Upsilon(2^3S_1)\gamma$	11.1	0.314	...	4.6 ± 2.1	10.9	0.42	12.80	0.54
	$\Upsilon_1(1^3D_1)\gamma$	1.05	2.97×10^{-2}	1.0	3.8×10^{-2}	0.74	3.09×10^{-2}
	$h_b(1^1P_1)\gamma$	0.00521	1.47×10^{-4}	0.0097	3.7×10^{-4}	0.00239	9.99×10^{-5}
	$\chi_{b0}(1^3P_0)\pi\pi$	0.809	2.29×10^{-2}	0.44	1.7×10^{-2}	0.72	3.01×10^{-2}
	$\chi_{b1}(1^3P_1)\pi\pi$	0	0
	$\chi_{b2}(1^3P_2)\pi\pi$	5.19×10^{-5}	1.47×10^{-6}	0.5	2×10^{-2}	4.08×10^{-5}	1.71×10^{-6}
	Total	3.54 MeV	100	2.6 MeV	100	2.39 MeV	100
$\chi_{b1}(2^3P_1)$	$q\bar{q}g$	117	84.8	96	82	106.14	79.57
	$\Upsilon(1^3S_1)\gamma$	5.09	3.69	...	9.2 ± 0.8	5.5	4.7	9.13	6.84
	$\Upsilon(2^3S_1)\gamma$	13.7	9.93	...	19.9 ± 1.9	13.3	11.3	15.89	11.91
	$\Upsilon_1(1^3D_1)\gamma$	0.511	0.37	0.5	0.4	0.41	0.31
	$\Upsilon_2(1^3D_2)\gamma$	1.25	0.906	1.2	1.0	1.26	0.95
	$h_b(1^1P_1)\gamma$	3.90×10^{-9}	2.83×10^{-9}	0.0022	1.9×10^{-3}	1.67×10^{-4}	1.25×10^{-4}
	$\chi_{b0}(1^3P_0)\pi\pi$	0	0
	$\chi_{b1}(1^3P_1)\pi\pi$	0.651	0.472	...	0.91 ± 0.13	0.57 ± 0.09	0.48	0.57	0.43
	$\chi_{b2}(1^3P_2)\pi\pi$	2.40×10^{-4}	1.74×10^{-4}	0.38	0.32	1.94×10^{-4}	1.45×10^{-4}
	Total	138	100	117	100	133.40	100
$\chi_{b2}(2^3P_2)$	$\gamma\gamma$	0.0133	5.43×10^{-3}	0.012	5.2×10^{-3}	0.00384	2.82×10^{-3}
	gg	220	89.8	207	89.0	104.26	76.62
	$\Upsilon(1^3S_1)\gamma$	7.86	3.21	...	7.0 ± 0.7	8.4	3.6	11.38	8.36
	$\Upsilon(2^3S_1)\gamma$	14.6	5.96	...	10.6 ± 2.6	14.3	6.15	17.50	12.86
	$\Upsilon_1(1^3D_1)\gamma$	0.0267	1.09×10^{-2}	0.03	1.0×10^{-2}	0.0209	1.54×10^{-2}
	$\Upsilon_2(1^3D_2)\gamma$	0.339	0.138	0.3	0.1	0.35	0.26
	$\Upsilon_3(1^3D_3)\gamma$	1.61	0.657	1.5	0.65	2.06	1.51
	$h_b(1^1P_1)\gamma$	0.00386	1.58×10^{-3}	2.4×10^{-4}	1.0×10^{-4}	0.00178	1.31×10^{-3}
	$h_b(2^1P_1)\gamma$	3.11×10^{-5}	1.27×10^{-5}	2.8×10^{-5}	1.2×10^{-5}	2.86×10^{-5}	2.10×10^{-5}
	$\chi_{b0}(1^3P_0)\pi\pi$	8.60×10^{-4}	3.51×10^{-4}	0.10	4.3×10^{-2}	8.49×10^{-6}	6.24×10^{-6}
	$\chi_{b1}(1^3P_1)\pi\pi$	6.39×10^{-4}	2.61×10^{-4}	0.23	0.10	6.06×10^{-4}	4.45×10^{-4}
	$\chi_{b2}(1^3P_2)\pi\pi$	0.576	0.235	...	0.51 ± 0.09	0.62 ± 0.12	0.27	0.49	0.36
	Total	245	100	232.5	100	136.07	100

TABLE X: Partial widths and branching ratios of annihilation decay, radiative transition, and hadronic transition and total widths for 3^1P_1 and 3^3P_0 bottomonium states. The width results are in units of keV.

state	channels	Width	$\mathcal{B}(\%)$
$h_b(3^1P_1)$	ggg	71.1	74.6
	$\eta_b(1^1S_0)\gamma$	3.91	4.10
	$\eta_b(2^1S_0)\gamma$	4.60	4.83
	$\eta_b(3^1S_0)\gamma$	9.94	10.4
	$\eta_{b2}(1^1D_2)\gamma$	0.0585	6.14×10^{-2}
	$\eta_{b2}(2^1D_2)\gamma$	1.44	1.51
	$\chi_{b0}(1^3P_0)\gamma$	0.00510	5.35×10^{-3}
	$\chi_{b1}(1^3P_1)\gamma$	0.00101	1.06×10^{-3}
	$\chi_{b2}(1^3P_2)\gamma$	0.00148	1.55×10^{-3}
	$\chi_{b0}(2^3P_0)\gamma$	0.00216	2.27×10^{-3}
	$\chi_{b1}(2^3P_1)\gamma$	5.59×10^{-4}	5.87×10^{-4}
	$\chi_{b2}(2^3P_2)\gamma$	4.07×10^{-4}	4.27×10^{-4}
	$\chi_{b0}(3^3P_0)\gamma$	6.89×10^{-5}	7.23×10^{-5}
	$\chi_{b1}(3^3P_1)\gamma$	1.15×10^{-6}	1.21×10^{-6}
	$h_b(1^1P_1)\pi\pi$	4.21	4.42
	Total	95.3	100
$\chi_{b0}(3^3P_0)$	$\gamma\gamma$	0.180	5.75×10^{-3}
	gg	3.10 MeV	99
	$\Upsilon(1^3S_1)\gamma$	0.427	1.36×10^{-2}
	$\Upsilon(2^3S_1)\gamma$	1.26	4.03×10^{-2}
	$\Upsilon(3^3S_1)\gamma$	7.15	0.228
	$\Upsilon_1(1^3D_1)\gamma$	0.189	6.04×10^{-3}
	$\Upsilon_1(2^3D_1)\gamma$	0.966	3.09×10^{-2}
	$h_b(1^1P_1)\gamma$	0.00623	1.99×10^{-4}
	$h_b(2^1P_1)\gamma$	0.00205	6.55×10^{-5}
	$\chi_{b0}(1^3P_0)\pi\pi$	17.9	0.572
	$\chi_{b1}(1^3P_1)\pi\pi$	0	
	$\chi_{b2}(1^3P_2)\pi\pi$	0.174	5.56×10^{-3}
	Total	3.13 MeV	100

ally estimated as 10120-10150 MeV and 10420-10450 MeV, respectively by most of the quark potential models. Here the predicted mass values are below the $B\bar{B}$ thresholds and compared with S, P -wave states, the annihilation decays to three-gluon or two-gluon are generally suppressed. Therefore, all of the $1D$ and $2D$ states of $b\bar{b}$ mesons are expected to be narrow states. In 2010, the BaBar Collaboration observed D -wave spin-triplet $\Upsilon(1^3D_J)$ states through decays into $\Upsilon(1S)\pi^+\pi^-$ [22] and the member of $J = 2$ was confirmed with a significance of 5.8σ , although other two states $\Upsilon_1(1^3D_1)$ and $\Upsilon_3(1^3D_3)$ have lower significances of standard deviations 1.8 and 1.6, respectively. In general, the experimental stud-

TABLE XI: Partial widths and branching ratios of annihilation decay, radiative transition, and hadronic transition and total widths for 3^3P_1 and 3^3P_2 bottomonium states. The width results are in units of keV.

state	channels	Width	$\mathcal{B}(\%)$
$\chi_{b1}(3^3P_1)$	$q\bar{q}g$	126	86.9
	$\Upsilon(1^3S_1)\gamma$	1.62	1.12
	$\Upsilon(2^3S_1)\gamma$	2.49	1.72
	$\Upsilon(3^3S_1)\gamma$	8.36	5.77
	$\Upsilon_1(1^3D_1)\gamma$	0.00418	2.88×10^{-3}
	$\Upsilon_2(1^3D_2)\gamma$	0.0615	4.24×10^{-2}
	$\Upsilon_1(2^3D_1)\gamma$	0.425	0.293
	$\Upsilon_2(2^3D_2)\gamma$	0.950	0.655
	$h_b(1^1P_1)\gamma$	3.19×10^{-5}	2.20×10^{-5}
	$h_b(2^1P_1)\gamma$	9.80×10^{-7}	6.76×10^{-7}
	$\chi_{b0}(1^3P_0)\pi\pi$	0	
	$\chi_{b1}(1^3P_1)\pi\pi$	5.23	3.61
	$\chi_{b2}(1^3P_2)\pi\pi$	0.0330	2.28×10^{-2}
	Total	145	100
$\chi_{b2}(3^3P_2)$	$\gamma\gamma$	0.0141	5.34×10^{-3}
	gg	243	92
	$\Upsilon(1^3S_1)\gamma$	3.17	1.20
	$\Upsilon(2^3S_1)\gamma$	3.66	1.39
	$\Upsilon(3^3S_1)\gamma$	9.30	3.52
	$\Upsilon_1(1^3D_1)\gamma$	1.15×10^{-4}	4.36×10^{-5}
	$\Upsilon_2(1^3D_2)\gamma$	3.11×10^{-4}	1.18×10^{-4}
	$\Upsilon_3(1^3D_3)\gamma$	0.0288	1.09×10^{-4}
	$\Upsilon_1(2^3D_1)\gamma$	0.0248	9.39×10^{-3}
	$\Upsilon_2(2^3D_2)\gamma$	0.295	0.112
	$\Upsilon_3(2^3D_3)\gamma$	1.37	0.519
	$h_b(1^1P_1)\gamma$	0.00353	1.34×10^{-3}
	$h_b(2^1P_1)\gamma$	0.00174	6.59×10^{-4}
	$h_b(3^1P_1)\gamma$	3.11×10^{-5}	1.18×10^{-5}
	$\chi_{b0}(1^3P_0)\pi\pi$	5.80×10^{-4}	2.20×10^{-4}
	$\chi_{b1}(1^3P_1)\pi\pi$	0.00319	1.21×10^{-3}
	$\chi_{b2}(1^3P_2)\pi\pi$	2.82	1.07
	Total	264	100

ies on the D -wave bottomonia are presently not enough with regard to total width and the branching ratio of typical decay channels. For the $\Upsilon_2(1^3D_2)$ state, the predicted mass calculated by the GI model [26] and the nonrelativistic constituent quark model [27] are 10147 and 10122 MeV, respectively, which are much lower than the measured mass values 10163.7 ± 1.4 MeV [51]. Our theoretical mass is 10162

TABLE XII: Partial widths and branching ratios of annihilation decay, and radiative transition and total widths for the $1D$ bottomonium states. Experimental results are taken from the PDG [51]. The theoretical results of the GI model [26] and the nonrelativistic constituent quark model [27] are summarized in the rightmost columns. The width results are in units of keV.

state	channels	This work		Expt. [51]		GI [26]		Ref. [27]	
		Width	$\mathcal{B}(\%)$	Width	$\mathcal{B}(\%)$	Width	$\mathcal{B}(\%)$	Width	$\mathcal{B}(\%)$
$\eta_{b2}(1^1D_2)$	gg	0.657	2.6	1.8	6.6	0.37	2.07
	$h_b(1^1P_1)\gamma$	24.3	96	24.9	91.5	17.23	96.58
	$\Upsilon_1(1^3D_1)\gamma$	2.56×10^{-5}	1.01×10^{-4}
	$\Upsilon_2(1^3D_2)\gamma$	4.28×10^{-8}	1.69×10^{-7}
	$\eta_b(1^1S_0)\pi^+\pi^-$	0.241	0.953	0.35	1.3	0.16	0.9
	Total	25.3	100	27.2	100	17.84	100
$\Upsilon_1(1^3D_1)$	$\ell^+\ell^-$	0.00188	5.08×10^{-3}	0.00138	3.93×10^{-3}	0.00140	3.17×10^{-3}
	ggg	10.4	28.1	8.11	23.1	9.97	22.57
	$\chi_{b0}(1^3P_0)\gamma$	16.3	44.1	16.5	47.1	20.98	47.49
	$\chi_{b1}(1^3P_1)\gamma$	9.51	25.7	9.7	28	12.29	27.82
	$\chi_{b2}(1^3P_2)\gamma$	0.550	1.49	0.56	1.6	0.65	1.47
	$\Upsilon(1^3S_1)\pi^+\pi^-$	0.146	0.395	...	$0.42^{+0.27}_{-0.23} \pm 0.10$ [22]	0.140	0.399	0.193	0.44
	Total	37.0	100	35.1	100	44.18	100
$\Upsilon_2(1^3D_2)$	ggg	0.821	3.23	0.69	2.7	0.62	2.13
	$\chi_{b1}(1^3P_1)\gamma$	18.8	74	19.2	74.7	21.95	75.46
	$\chi_{b2}(1^3P_2)\gamma$	5.49	21.6	5.6	22	6.23	21.42
	$\Upsilon(1^3S_1)\pi^+\pi^-$	0.167	0.656	...	$0.66^{+0.15}_{-0.14} \pm 0.06$	0.169 ± 0.045	0.658	0.193	0.667
	Total	25.4	100	25.7	100	29.09	100
$\Upsilon_3(1^3D_3)$	ggg	2.19	8.30	2.07	7.75	0.22	0.87
	$\chi_{b2}(1^3P_2)\gamma$	23.9	90.5	24.3	91	24.74	97.98
	$\eta_{b2}(1^1D_2)\gamma$	1.47×10^{-5}	5.57×10^{-5}	1.5×10^{-5}	5.6×10^{-5}
	$\Upsilon(1^3S_1)\pi^+\pi^-$	0.187	0.707	...	$0.29^{+0.22}_{-0.18} \pm 0.06$ [22]	0.197	0.738	0.193	0.767
	Total	26.4	100	26.7	100	25.25	100

MeV which is exactly within the range of experimental error. This again shows an excellent description of bottomonium mass spectrum in this work. Furthermore, we also predict the mass splittings $m[\Upsilon_3(1^3D_3)] - m[\Upsilon_2(1^3D_2)] = 8$ MeV and $m[\Upsilon_2(1^3D_2)] - m[\Upsilon_1(1^3D_1)] = 9$ MeV. The predicted mass values of $2D$ bottomonia are presented in Table III. Ignoring delicate differences of hyperfine spin splittings, mass of the $2D$ bottomonium is estimated to be about 10450 MeV, which we hope is verified in the prospective search of $2D$ bottomonium states.

The decay properties of D -wave states are different from those of S, P -wave states below the $B\bar{B}$ thresholds since the annihilation decays of D -wave bottomonia no longer play leading roles in most cases. The radiative transitions of $1D \rightarrow 1P$ and $2D \rightarrow 2P$ usually become the dominant decay mode. Partial widths and branching ratios of annihilation decay, radiative transition, and hadronic transition and the total widths for the $1D$ and $2D$ bottomonia are shown in Table XII and Tables XIII-XIV, respectively. For the $1D$ bottomonium states, we focus on the only experimental information of the branching ratios of $\Upsilon(1^3D_J) \rightarrow \Upsilon(1S)\pi^+\pi^-$ since the

spin triplet states of $1D$ bottomonium were finally observed in this hadronic decay process. We notice that the process $\Upsilon_2(1^3D_2) \rightarrow \Upsilon(1S)\pi^+\pi^-$ can determine the constant C_2 of Eq. (A11) and the calculated branching ratios of the identical hadronic processes for other two members with $J = 1, 3$ are also consistent with different theoretical models shown in Table XII. The radiative transition of $\eta_{b2}(1D) \rightarrow h_b(1P)\gamma$ may be an optimal channel to detect $\eta_{b2}(1D)$ on account of our estimate of the branching ratio 96%. Accordingly, the radiative process of $\Upsilon(1^3D_J) \rightarrow \chi_{bJ'}(1^3P_{J'})\gamma$ with $J = J' + 1$ is the dominant decay mode for spin-triplet states of $1D$ bottomonium, which has the estimated branching ratios of 44.1 %, 74 % and 90.5 % for $J = 1, 2, 3$, respectively. Surely, the non-forbidden radiative decay to P -wave χ_{bJ} states is also significant for $\Upsilon(1^3D_J)$ state. There are similar decay behaviors in $2D$ bottomonium states, where the radiative transitions to P -wave bottomonium states are still dominant except for the $\Upsilon_1(2^3D_1)$ state, whose half of the total width is contributed by the annihilation mode ggg . The analysis of other decay channels of $2D$ bottomonium states from Tables XIII and XIV can be summarized as follows:

TABLE XIII: Partial widths and branching ratios of annihilation decay, radiative transition, and hadronic transition and total widths for 2^1D_2 and 2^3D_1 bottomonium states. The width results are in units of keV.

state	channels	Width	$\mathcal{B}(\%)$
$\eta_{b2}(2^1D_2)$	gg	1.22	5.33
	$h_b(1^1P_1)\gamma$	3.36	14.7
	$h_b(2^1P_1)\gamma$	16.8	73.4
	$h_{b3}(1^1F_3)\gamma$	1.35	5.90
	$\Upsilon_1(1^3D_1)\gamma$	0.00102	4.46×10^{-3}
	$\Upsilon_2(1^3D_2)\gamma$	2.57×10^{-4}	1.12×10^{-3}
	$\Upsilon_3(1^3D_3)\gamma$	4.69×10^{-5}	2.05×10^{-4}
	$\Upsilon_1(2^3D_1)\gamma$	1.31×10^{-5}	5.73×10^{-5}
	$\eta_b(1^1S_0)\pi\pi$	0.118	0.516
	$\eta_b(2^1S_0)\pi\pi$	0.0210	9.18×10^{-2}
	$\eta_{b2}(1^1D_2)\pi\pi$	0.00263	1.15×10^{-2}
	Total	22.9	100
$\Upsilon_1(2^3D_1)$	$\ell^+\ell^-$	0.00281	6.46×10^{-3}
	ggg	20.1	46.2
	$\chi_{b0}(1^3P_0)\gamma$	2.99	6.88
	$\chi_{b1}(1^3P_1)\gamma$	1.03	2.37
	$\chi_{b2}(1^3P_2)\gamma$	0.0300	6.90×10^{-2}
	$\chi_{b0}(2^3P_0)\gamma$	11.0	25.3
	$\chi_{b1}(2^3P_1)\gamma$	6.71	15.4
	$\chi_{b2}(2^3P_2)\gamma$	0.400	0.920
	$\chi_{b2}(1^3F_2)\gamma$	1.18	2.71
	$\eta_{b2}(1^1D_2)\gamma$	2.21×10^{-4}	5.08×10^{-4}
	$\Upsilon(1^3S_1)\pi\pi$	0.00267	6.14×10^{-3}
	$\Upsilon(2^3S_1)\pi\pi$	0.0115	2.65×10^{-2}
	$\Upsilon_1(1^3D_1)\pi\pi$	0.00502	1.15×10^{-2}
	$\Upsilon_2(1^3D_2)\pi\pi$	2.52×10^{-10}	5.79739×10^{-10}
	$\Upsilon_3(1^3D_3)\pi\pi$	1.87×10^{-8}	4.30203×10^{-8}
	Total	43.5	100

TABLE XIV: Partial widths and branching ratios of annihilation decay, radiative transition, and hadronic transition and total widths for 2^3D_2 and 2^3D_3 bottomonium states. The width results are in units of keV.

state	channels	Width	$\mathcal{B}(\%)$
$\Upsilon_2(2^3D_2)$	ggg	1.65	7.05
	$\chi_{b1}(1^3P_1)\gamma$	2.81	12.0
	$\chi_{b2}(1^3P_2)\gamma$	0.489	2.09
	$\chi_{b1}(2^3P_1)\gamma$	13.1	55.9
	$\chi_{b2}(2^3P_2)\gamma$	3.96	16.9
	$\chi_{b2}(1^3F_2)\gamma$	0.164	0.700
	$\chi_{b3}(1^3F_3)\gamma$	1.21	5.17
	$\eta_{b2}(1^1D_2)\gamma$	7.41×10^{-5}	3.16×10^{-4}
	$\Upsilon(1^3S_1)\pi\pi$	0.0175	7.47×10^{-2}
	$\Upsilon(2^3S_1)\pi\pi$	0.0141	6.02×10^{-2}
	$\Upsilon_1(1^3D_1)\pi\pi$	4.57×10^{-7}	1.95×10^{-6}
	$\Upsilon_2(1^3D_2)\pi\pi$	0.00384	1.64×10^{-2}
	$\Upsilon_3(1^3D_3)\pi\pi$	1.80×10^{-10}	7.69×10^{-10}
$\Upsilon_3(2^3D_3)$	Total	23.4	100
	ggg	4.56	17.6
	$\chi_{b2}(1^3P_2)\gamma$	2.99	11.5
	$\chi_{b2}(2^3P_2)\gamma$	16.8	64.8
	$\chi_{b2}(1^3F_2)\gamma$	0.00384	1.48×10^{-2}
	$\chi_{b3}(1^3F_3)\gamma$	0.125	0.482
	$\chi_{b4}(1^3F_4)\gamma$	1.37	5.29
	$\eta_{b2}(1^1D_2)\gamma$	9.78×10^{-4}	3.77×10^{-3}
	$\eta_{b2}(2^1D_2)\gamma$	9.23×10^{-6}	3.56×10^{-5}
	$\Upsilon(1^3S_1)\pi\pi$	0.0458	0.177
	$\Upsilon(2^3S_1)\pi\pi$	0.0159	6.14×10^{-2}
	$\Upsilon_1(1^3D_1)\pi\pi$	1.40×10^{-7}	5.40×10^{-7}
	$\Upsilon_2(1^3D_2)\pi\pi$	1.57×10^{-7}	6.06×10^{-7}
	$\Upsilon_3(1^3D_3)\pi\pi$	0.00173	6.68×10^{-3}
	Total	25.9	100

1. The branching ratios of $M1$ radiative transitions of $2D \rightarrow 1D$ and $2D \rightarrow 2D$ with spin-flip are about $10^{-5} \sim 10^{-7}$, which also indicates that it is difficult to observe these decay modes in experiments.
2. The $E1$ spin non-flip radiative transition of $2D \rightarrow 1F$ with $J_i = J_f - 1$ with the total angular momentum of initial (final) state $J_{i(f)}$ can be used to study first F -wave bottomonium, due to the predicted partial width of $0.16 \sim 1.4$ keV and branching ratio of $0.7\% \sim 6\%$.
3. Compared to radiative transitions, the contributions of the $\pi\pi$ hadronic decays are much smaller, where the de-

cays to S -wave η_b or Υ states and D -wave η_{b2} or Υ_J states occupy about $10^{-3} \sim 10^{-1}\%$ and $10^{-10} \sim 10^{-2}\%$, respectively.

4. It is easy to see that the width of leptonic annihilation decay of D -wave Υ state is much smaller than S -wave Υ states with three orders of magnitude by comparing Table VII with Tables XII-XIII, which can be used to distinguish two kinds of Υ states with the same $J^{PC} = 1^{--}$ in experiment.

TABLE XV: Partial widths and branching ratios of annihilation decay, radiative transition, and hadronic transition and total widths for the $1F$ bottomonium states. The widths are in units of keV.

state	channels	Width	$\mathcal{B}(\%)$
$h_{b3}(1^1F_3)$	$\eta_{b2}(1^1D_2)\gamma$	22.0	~ 100
	$\chi_{b2}(1^3F_2)\gamma$	1.95×10^{-6}	8.86×10^{-6}
	$h_b(1^1P_1)\pi\pi$	0.0412	0.187
	Total	22.0	100
$\chi_{b2}(1^3F_2)$	gg	0.834	3.53
	$\Upsilon_1(1^3D_1)\gamma$	19.4	82.1
	$\Upsilon_2(1^3D_2)\gamma$	3.26	13.8
	$\Upsilon_3(1^3D_3)\gamma$	0.0852	0.360
	$\chi_{b0}(1^3P_0)\pi\pi$	0.0351	0.149
	$\chi_{b1}(1^3P_1)\pi\pi$	0.0192	8.12×10^{-2}
	$\chi_{b2}(1^3P_2)\pi\pi$	0.00191	8.08×10^{-3}
	Total	23.6	100
$\chi_{b3}(1^3F_3)$	gg	0.0672	0.305
	$\Upsilon_2(1^3D_2)\gamma$	19.7	89.4
	$\Upsilon_3(1^3D_3)\gamma$	2.26	10.3
	$\chi_{b1}(1^3P_1)\pi\pi$	0.00107	4.86×10^{-3}
	$\chi_{b2}(1^3P_2)\pi\pi$	0.00311	1.41×10^{-2}
	Total	22.0	100
$\chi_{b4}(1^3F_4)$	gg	0.05	0.235
	$\Upsilon_3(1^3D_3)\gamma$	21.2	99.5
	$h_{b3}(1^1F_3)\gamma$	1.15×10^{-6}	5.40×10^{-6}
	$\chi_{b2}(1^3P_2)\pi\pi$	0.0354	0.166
	Total	21.3	100

E. The $1F$ and $1G$ states

As the high spin states, the F -wave and G -wave bottomonia have no experimental signals at present. If these states can be experimentally observed, it could be a good confirmation for the theoretical calculation of the potential model. The predicted decay properties of $1F$ and $1G$ bottomonia for partial widths and branching ratios of annihilation decay, electromagnetic transition, and hadronic transition and the total widths are listed in Tables XV and XVI, respectively, where one can find a very interesting common decay feature. That is, the dominant decay modes of eight particles are all sorts of the radiative transition of $1F_{(J)} \rightarrow 1D_{(J-1)}\gamma$ or $1G_{(J)} \rightarrow 1F_{(J-1)}\gamma$ with almost more than 90% branching ratios where subindices $J / J - 1$ represent the total angular momentum of a particle. This also indicates that experiments are likely to observe the first F -wave bottomonia via these radiative processes of $h_{b3}(1^1F_3) \rightarrow \eta_{b2}(1^1D_2)\gamma$ and $\chi_{bJ}(1^3F_J) \rightarrow \Upsilon_{J-1}(1^3D_{J-1})\gamma$ once all the ground states of D -wave bottomonium are experimentally established. In the same way, search for the first

TABLE XVI: Partial widths and branching ratios of annihilation decay, radiative transition, and hadronic transition and total widths for the $1G$ bottomonium states. The widths are in units of keV.

state	channels	Width	$\mathcal{B}(\%)$
$\eta_{b4}(1^1G_4)$	gg	6.61×10^{-4}	3.13×10^{-3}
	$h_{b3}(1^1F_3)\gamma$	21.1	~ 100
	$\Upsilon_3(1^3G_3)\gamma$	3.33×10^{-8}	1.58×10^{-7}
	$\eta_{b2}(1^1D_2)\pi\pi$	0.00580	2.75×10^{-2}
	Total	21.1	100
$\Upsilon_3(1^3G_3)$	$\chi_{b2}(1^3F_2)\gamma$	20.1	92.2
	$\chi_{b3}(1^3F_3)\gamma$	1.67	7.66
	$\chi_{b4}(1^3F_4)\gamma$	0.0256	0.117
	$\Upsilon_1(1^3D_1)\pi\pi$	0.00634	2.91×10^{-2}
	$\Upsilon_2(1^3D_2)\pi\pi$	0.00123	5.64×10^{-3}
$\Upsilon_4(1^3G_4)$	$\Upsilon_3(1^3D_3)\pi\pi$	5.74×10^{-5}	2.63×10^{-4}
	Total	21.8	100
$\Upsilon_5(1^3G_5)$	$\chi_{b3}(1^3F_3)\gamma$	20.1	93.9
	$\chi_{b4}(1^3F_4)\gamma$	1.30	6.07
	$\eta_{b4}(1^1G_4)\gamma$	4.28×10^{-8}	2.0×10^{-7}
	$\Upsilon_2(1^3D_2)\pi\pi$	0.00530	2.48×10^{-2}
	$\Upsilon_3(1^3D_3)\pi\pi$	7.50×10^{-4}	3.50×10^{-3}
$\Upsilon_5(1^3G_5)$	Total	21.4	100
	$\chi_{b4}(1^3F_4)\gamma$	21.1	~ 100
	$\eta_{b4}(1^1G_4)\gamma$	3.42×10^{-7}	1.62×10^{-6}
	$\Upsilon_3(1^3D_3)\pi\pi$	0.00476	2.26×10^{-2}
	Total	21.1	100

G -wave bottomonia also requires the confirmation of the F -wave states in experiment. This forms a chain-like relationship, which means that search for these high spin states is probably achieved step by step. Our predicted mass values of $1F$ and $1G$ states are shown in Table III, where the average mass values of the spin triplet states for $1F$ and $1G$ are estimated as 10366 MeV and 10535 MeV, respectively. These are almost the same as those of the spin singlet states. We hope that these predicted results will be helpful for the future experimental studies on high spin F and G -wave states. In addition, it can be seen from Tables XV-XVI that the $1F$ ($1G$) states could also transit to the specific P (D)-wave states by emitting two light mesons $\pi\pi$. However, partial widths of these hadronic decay processes are calculated to be relatively small. Predicted total widths of the ground states of F and G -wave bottomonia are all about 20 keV, which are consistent with the estimates of the GI model [26].

IV. ANALYSIS AND PREDICTIONS OF HIGHER BOTTOMONIA

A. higher η_b radial excitations

As the pseudoscalar partner of the S -wave Υ family, the η_b states are not like Υ as many of the radial excitations of Υ have been found in experiment. Based on this fact, we need to predict some theoretical results and simultaneously make a systematic study on the higher excited states of η_b family that will not only provide meaningful clues to experimentally search for these η_b particles above thresholds but also further reveal their inner nature. Different from the states below thresholds, the $b\bar{b}$ states above thresholds can usually decay into a pair of positive and negative bottom mesons or bottom-strange mesons. Here, the strong decay channel of $B\bar{B}$ is prohibited as a result of parity conservation for the η_b . Therefore, it should be noted that the mass summation of pseudoscalar meson B and vector meson B^* is generally used as the strong decay threshold of η_b .

In this subsection, higher η_b radial excitations up to $\eta_b(8S)$ are systematically studied, whose mass values are predicted in Table III. Their corresponding decay properties including total widths and partial widths and branching ratios of OZI-allowed strong decay, annihilation decay and radiative transition are listed in Tables XIX-XXI. The mass of $\eta_b(5S)$ state is calculated as 10810 MeV by the modified GI model. We give another estimated mass value of $\eta_b(5S)$ to 10870 MeV utilizing the results of theoretical mass splitting and measured mass of $\Upsilon(10860)$. At the same time, this estimated mass value is also used as the model parameter of strong decay calculations. In Table XIX, one can see that the total width of $\eta_b(5S)$ is predicted to be 28.4 MeV, which can mainly decay into the BB^* , gg , $B_s^*B_s^*$, $B_sB_s^*$, and B^*B^* and the corresponding branching ratios are 71.5 %, 11.5 %, 10.2 %, 3.91 %, and 2.71 %, respectively. The dominant radiative decay mode is $h_b(4^1P_1)\gamma$ with the partial width of 33.5 keV. We should notice that the notation BB^* refers to $B\bar{B}^*+B^*\bar{B}$, B^*B^* to $B^*\bar{B}^*$, and so on. The predicted mass of $\eta_b(6S)$ state is 10991 MeV, which should be also similarly improved compared with the estimates of 11079 MeV by the GI model. The total width of $\eta_b(6S)$ is estimated to be 20.4 MeV, which is about the same as the total width of $\eta_b(5S)$. The dominant decay channel of $\eta_b(6S)$ is still BB^* with a branching ratio of 73 % and other decay modes gg , $BB(1^3P_0)$, $B_sB_s^*$, and B^*B^* also have large contributions to the total width. In general, our decay results indicate that the $\eta_b(5S)$ and $\eta_b(6S)$ are most likely to be detected in the BB^* mode.

It is very difficult to experimentally detect $\eta_b(7S)$ and $\eta_b(8S)$ at present because of too high energy levels. They are the partners of $\Upsilon(7S, 8S)$, which are likely to become a new research area for bottomonium physics in the future since the corresponding lower radial excited states have all been observed by experiment. Furthermore, to compare with $\Upsilon(7S, 8S)$ research, we also make a comprehensive study on $\eta_b(7S, 8S)$ in this paper. We predict their mass as 11149\11289 MeV for the $\eta_b(7S)\backslash\eta_b(8S)$, respectively, whose hyperfine mass splittings $\Delta m(7S)\backslash\Delta m(8S)$ are

8\7 MeV, respectively. There is obviously large difference between the predicted mass by the GI model and modified GI model, which can be seen in Table III. From Tables XX and XXI, the predicted total widths of $\eta_b(7S)$ and $\eta_b(8S)$ are 94.8 MeV and 64.4 MeV, respectively, which indicates $\eta_b(7S)$ is possibly a broad state. Our calculation shows that the dominant decay channels of $\eta_b(7S)$ are BB^* , $B^*B(1^3P_2)$, $B^*B(1P_1)$, $B^*B(1P_1')$ and B^*B^* . The corresponding partial widths are 27.7, 17.9, 15.0, 13.9 and 11.1 MeV, respectively. The decay channels BB^* , B^*B^* and $BB(1^3P_2)$ for $\eta_b(8S)$ have pivotal partial widths of 29.5, 19.0 and 7.61 MeV, respectively. From here, we can see the latent importance of P -wave bottom mesons in the OZI-allowed open-flavor strong decay processes of these extremely high bottomonium radial excitations. In addition, since the contributions of radiative transition and strong decay of bottom-strange mesons are small for the total widths of these two bottomonium particles, we suggest future experiments to find them with generated final states of bottom mesons.

B. higher Υ radial excitations

The S -wave Υ states with $J^{PC} = 1^{--}$ have always been the significant research field of bottomonium physics. Up to now, it is also the unique place to experimentally study some interesting effects above open-bottom thresholds, which includes $\Upsilon(4S)$, $\Upsilon(10860)$, and $\Upsilon(11020)$. Therefore, further theoretical exploration for higher Υ bottomonia is necessary. Additionally, the strong decay into two bottom mesons or bottom-strange mesons will be dominant for the three Υ 's mentioned above. Hence, their experimental information will determine the model parameter γ of the strong decay calculation in the QPC model.

There is no controversy in experimental measurements of the $\Upsilon(4S)$ state, whose total width was first measured as 25 ± 2.5 MeV and $20 \pm 2 \pm 4$ MeV by the CUSB [7] and CLEO [6] collaborations, respectively. On the other hand, BaBar's measurements in 2005 gave the similar resonance state parameters [93] and the current average total width of PDG is 20.5 ± 2.5 MeV [51].

For the $\Upsilon(5S)$ and $\Upsilon(6S)$, however, the situation is not so optimistic since the early measured data and the recent experimental results of mass values and the total widths are incompatible with each other. In short, after 2010, the Belle collaboration released consistent mass values of $\Upsilon(10860)$ by the different production cross sections of $e^+e^- \rightarrow \Upsilon(nS)\pi^+\pi^-$ with $n=1,2,3$ and $e^+e^- \rightarrow b\bar{b}$, as well as $e^+e^- \rightarrow h_b(nP)\pi^+\pi^-$ with $n=1,2$ [94–96]. Their values are larger than the theoretical calculation and early experimental values and Belle's results of the total width also disagreed with the previous experimental conclusion of a broad state of $\Upsilon(10860)$ [6, 7]. Although there are a few experimental results of $\Upsilon(11020)$, the center mass values of BaBar [97] and the recent Belle collaboration [95, 96] are consistently about 20 MeV smaller than the earlier experimental results [6, 7]. It can be seen clearly from the PDG [51] that the total width of $\Upsilon(11020)$ is measured about 30-60 MeV by integrating the present ex-

TABLE XVII: Partial widths and branching ratios of the OZI-allowed strong decay, annihilation decay, and radiative transition and the total width for $\Upsilon(4S)$. Experimental results are taken from the PDG [51]. The theoretical results of the GI model [26] and the nonrelativistic constituent quark model [27] are summarized in the rightmost columns. The width results are in units of keV.

state	channels	This work		Expt. [51]		GI [26]		Ref. [27]	
		Width	$\mathcal{B}(\%)$	Width	$\mathcal{B}(\%)$	Width	$\mathcal{B}(\%)$	Width	$\mathcal{B}(\%)$
$\Upsilon(4S)$	$\ell^+\ell^-$	0.431	1.74×10^{-3}	0.272 ± 0.029	$(1.57 \pm 0.08) \times 10^{-3}$	0.39	1.8×10^{-3}	0.21	1.02×10^{-3}
	ggg	16.7	6.76×10^{-2}	15.1	6.86×10^{-2}	15.58	7.60×10^{-2}
	γgg	0.433	1.75×10^{-3}	0.40	1.8×10^{-3}	0.30	1.46×10^{-3}
	$\gamma\gamma\gamma$	6.36×10^{-6}	2.57×10^{-8}	6.0×10^{-6}	2.7×10^{-8}	1.29×10^{-6}	6.29×10^{-9}
	$\chi_{b0}(1^3P_0)\gamma$	5.12×10^{-4}	2.07×10^{-6}	0.0588	2.87×10^{-4}
	$\chi_{b1}(1^3P_1)\gamma$	0.0507	2.05×10^{-4}	0.0474	2.31×10^{-4}
	$\chi_{b2}(1^3P_2)\gamma$	0.219	8.87×10^{-4}	0.0120	5.85×10^{-5}
	$\chi_{b0}(2^3P_0)\gamma$	0.0137	5.55×10^{-5}	0.17	8.29×10^{-4}
	$\chi_{b1}(2^3P_1)\gamma$	0.0138	5.59×10^{-5}	0.18	8.78×10^{-4}
	$\chi_{b2}(2^3P_2)\gamma$	0.226	9.15×10^{-4}	0.11	5.37×10^{-4}
	$\chi_{b0}(3^3P_0)\gamma$	0.587	2.38×10^{-3}	0.48	2.2×10^{-3}	0.61	2.98×10^{-3}
	$\chi_{b1}(3^3P_1)\gamma$	1.14	4.62×10^{-3}	0.84	3.8×10^{-3}	1.17	5.71×10^{-3}
	$\chi_{b2}(3^3P_2)\gamma$	1.16	4.70×10^{-3}	0.82	3.7×10^{-3}	1.45	7.07×10^{-3}
	$\eta_b(1^1S_0)\gamma$	0.0572	2.32×10^{-4}	0.0498	2.43×10^{-4}
	BB	24.7 MeV	~ 100	...	>96	22 MeV	~ 100	20.59 MeV	100
	Total	24.7 MeV	100	20.5 ± 2.5 MeV	...	22 MeV	100	20.59 MeV	100

perimental information. At the same time, because the amount of data is not sufficient, the measurements of these two resonances by the analysis of the R value in the previous experiments are probably unconvincing to a great extent, where $R = \sigma(e^+e^- \rightarrow \text{hadrons})/\sigma(e^+e^- \rightarrow \mu^+\mu^-)$. Therefore, we hope to see the more accurate experimental results for the $\Upsilon(10860)$ and $\Upsilon(11020)$ in the forthcoming Belle II experiment. It is worth mentioning that in Belle's measurements of processes $e^+e^- \rightarrow \Upsilon(nS)\pi^+\pi^-$ and $e^+e^- \rightarrow b\bar{b}$ [95], the measured resonance parameters of $R_{\Upsilon(nS)\pi\pi}$ and R_b are completely consistent within the error range [95] although the application of a flat continuum in the R_b fit brings some inconsistencies between the fitted amplitudes for $R_{\Upsilon(nS)\pi\pi}$ and R_b . Furthermore, the measured mass values and total widths of $R_{\Upsilon(nS)\pi\pi}$ have too large statistical and systematic errors. So in the calibration of parameter γ , we select the latest Belle's measurement of the process $e^+e^- \rightarrow b\bar{b}$, which gives the resonance parameters for $\Upsilon(10860)$ and $\Upsilon(11020)$ as $M[\Upsilon(10860)] = 10881.8^{+1.0}_{-1.1} \pm 1.2$ MeV, $\Gamma[\Upsilon(10860)] = 48.5^{+1.9+2.0}_{-1.8-2.8}$ MeV and $M[\Upsilon(11020)] = 11003.0 \pm 1.1^{+0.9}_{-1.0}$ MeV, $\Gamma[\Upsilon(11020)] = 39.3^{+1.7+1.3}_{-1.6-2.4}$ MeV [95], respectively.

Based on the above consideration, in the following, the systematical study will be performed on the $\Upsilon(nS)$ states above the thresholds in the framework of the modified GI model and various decay models. Higher bottomonia $\Upsilon(7S)$ and $\Upsilon(8S)$ states are also discussed in this subsection.

1. $\Upsilon(4S)$, $\Upsilon(10860)$, and $\Upsilon(11020)$

Partial widths and branching ratios of the OZI-allowed strong decays, annihilation decay, and radiative transition and the total widths for $\Upsilon(4S)$ and $\Upsilon(10860)$, and $\Upsilon(11020)$ bottomonia shown in Tables XVII and XVIII, respectively. $\Upsilon(4S)$ is slightly (about 20 MeV) higher than the $B\bar{B}$ threshold. Hence, its unique dominant decay channel is $B\bar{B}$ and the corresponding experimental branching ratio is larger than 96%. Contrary to us, a 100% theoretical estimate for this channel is given by several potential models in Table XVII. Another measured decay channel of $\Upsilon(4S)$ is leptonic annihilation decay $\ell^+\ell^-$. Our branching ratio is 1.74×10^{-5} , which is well consistent with the PDG's result $(1.57 \pm 0.08) \times 10^{-5}$ [51].

The total widths of the $\Upsilon(10860)$ and $\Upsilon(11020)$ are estimated to be 45.6 MeV and 38.3 MeV in our modified GI model, which coincide well with Belle's results of $48.5^{+1.9+2.0}_{-1.8-2.8}$ and $39.3^{+1.7+1.3}_{-1.6-2.4}$ MeV [95], respectively. Hence, these two particles can be used to determine γ values in this paper. Additionally, other theoretical predictions for the total widths of the $\Upsilon(10860)$ and $\Upsilon(11020)$ are not unified [26, 27, 31]. One can see that the total widths of the GI model and non-relativistic constituent quark (NRCQ) model for the $\Upsilon(10860)$ state in Table XVIII are about 27 MeV, which is smaller than the recent Belle's result [95]. For the $\Upsilon(11020)$ state, the total width of 34 MeV and 79 MeV is predicted by the GI and NRCQ models, respectively. Here, one should notice that there is a large

TABLE XVIII: Partial widths and branching ratios of the OZI-allowed strong decay, annihilation decay, and radiative transition and the total widths for $\Upsilon(10860)$ and $\Upsilon(11020)$. Experimental results are taken from the PDG [51]. The theoretical results of the GI model [26] and the nonrelativistic constituent quark model [27] are summarized in the rightmost columns. The width results are in units of keV.

state	channels	This work		Expt. [51]		GI [26]		Ref. [27]	
		Width	$\mathcal{B}(\%)$	Width	$\mathcal{B}(\%)$	Width	$\mathcal{B}(\%)$	Width	$\mathcal{B}(\%)$
$\Upsilon(10860)$	$\ell^+ \ell^-$	0.348	7.63×10^{-4}	0.31 ± 0.07	$(5.7^{+1.5}_{-1.5}) \times 10^{-4}$	0.33	1.2×10^{-3}	0.18	3.27×10^{-4}
	ggg	14.2	3.11×10^{-2}	13.1	4.78×10^{-2}	13.33	2.42×10^{-2}
	γgg	0.370	8.11×10^{-4}	0.25	4.55×10^{-4}
	$\gamma\gamma\gamma$	5.43×10^{-6}	1.19×10^{-8}	1.10×10^{-6}	2.00×10^{-9}
	$\chi_{b0}(2^3P_0)\gamma$	2.69×10^{-4}	5.90×10^{-7}	0.22	4.00×10^{-4}
	$\chi_{b1}(2^3P_1)\gamma$	0.0532	1.17×10^{-4}	0.26	4.73×10^{-4}
	$\chi_{b2}(2^3P_2)\gamma$	0.341	7.48×10^{-4}	0.18	3.27×10^{-4}
	$\chi_{b0}(3^3P_0)\gamma$	0.0418	9.17×10^{-5}	0.15	5.5×10^{-4}	0.80	1.45×10^{-3}
	$\chi_{b1}(3^3P_1)\gamma$	0.0154	3.38×10^{-5}	6.2×10^{-5}	2.3×10^{-7}	1.35	2.45×10^{-3}
	$\chi_{b2}(3^3P_2)\gamma$	0.467	1.02×10^{-3}	0.42	1.5×10^{-3}	1.42	2.58×10^{-3}
	$\chi_{b0}(4^3P_0)\gamma$	5.38	1.18×10^{-2}	1.5	5.5×10^{-3}
	$\chi_{b1}(4^3P_1)\gamma$	13.9	3.05×10^{-2}	3.4	1.2×10^{-2}
	$\chi_{b2}(4^3P_2)\gamma$	20.6	4.52×10^{-2}	4.3	1.6×10^{-2}
	$\eta_b(1^1S_0)\gamma$	0.0692	1.52×10^{-4}	0.0597	1.09×10^{-4}
	BB	13.7 MeV	30.0	...	5.5 ± 1.0	5.35 MeV	19.5	6.22 MeV	22.29
	BB^*	26.5 MeV	58.1	...	13.7 ± 1.6	16.6 MeV	60.6	11.83 MeV	42.41
	B^*B^*	2.58 MeV	5.66	...	38.1 ± 3.4	2.42 MeV	8.83	0.09 MeV	0.32
	$B_s B_s$	0.484 MeV	1.06	...	0.5 ± 0.5	0.157 MeV	0.573	0.96 MeV	3.45
	$B_s B_s^*$	1.49 MeV	3.28	...	1.35 ± 0.32	0.833 MeV	3.04	1.15 MeV	4.11
	$B_s^* B_s^*$	0.872 MeV	1.91	...	17.6 ± 2.7	2.00 MeV	7.30	7.65 MeV	27.42
	Total	45.6 MeV	100	$48.5^{+1.9+2.0}_{-1.8-2.8}$ MeV [95]	...	27.4 MeV	100	27.89 MeV	100
$\Upsilon(11020)$	$\ell^+ \ell^-$	0.286	7.47×10^{-4}	0.130 ± 0.03	$(2.1^{+1.1}_{-0.6}) \times 10^{-4}$	0.27	8.0×10^{-4}	0.15	1.90×10^{-4}
	ggg	12.0	3.13×10^{-2}	11.0	3.24×10^{-2}	11.57	1.46×10^{-2}
	γgg	0.311	8.12×10^{-4}	0.22	2.78×10^{-4}
	$\gamma\gamma\gamma$	4.57×10^{-6}	1.19×10^{-8}	9.56×10^{-7}	1.21×10^{-9}
	$\chi_{b0}(3^3P_0)\gamma$	0.00498	1.30×10^{-5}	0.21	6.2×10^{-4}	0.26	3.29×10^{-4}
	$\chi_{b1}(3^3P_1)\gamma$	0.0256	6.68×10^{-5}	0.43	1.3×10^{-3}	0.35	4.43×10^{-4}
	$\chi_{b2}(3^3P_2)\gamma$	0.253	6.61×10^{-4}	0.53	1.6×10^{-3}	0.27	3.42×10^{-4}
	$\chi_{b0}(4^3P_0)\gamma$	0.0325	8.49×10^{-5}	0.1	3.0×10^{-4}
	$\chi_{b1}(4^3P_1)\gamma$	0.00133	3.47×10^{-6}	0.012	3.5×10^{-5}
	$\chi_{b2}(4^3P_2)\gamma$	0.173	4.52×10^{-4}	0.085	2.5×10^{-4}
	$\chi_{b0}(5^3P_0)\gamma$	1.14	2.98×10^{-3}	0.0064	1.9×10^{-5}
	$\chi_{b1}(5^3P_1)\gamma$	2.56	6.68×10^{-3}	8.3×10^{-4}	2.4×10^{-6}
	$\chi_{b2}(5^3P_2)\gamma$	3.19	8.33×10^{-3}
	$\eta_b(1^1S_0)\gamma$	0.0570	1.49×10^{-4}	0.0508	6.43×10^{-5}
	BB	7.81 MeV	20.4	1.32 MeV	3.89	4.18 MeV	5.28
	BB^*	16.5 MeV	43.0	7.59 MeV	22.4	15.49 MeV	19.57
	$BB(1P_1)$	8.27 MeV	21.6	7.81 MeV	23.0	40.08 MeV	50.64
	$BB(1P_1')$	Below threshold	10.8 MeV	31.8	3.95 MeV	4.98
	B^*B^*	4.43 MeV	11.5	5.89 MeV	17.4	11.87 MeV	14.99
	$B_s B_s$	0.101 MeV	0.263	1.31	3.86×10^{-3}	0.07 MeV	0.09
	$B_s B_s^*$	0.780 MeV	2.04	0.136 MeV	0.401	1.50 MeV	1.89
	$B_s^* B_s^*$	0.448 MeV	1.17	0.310 MeV	0.914	2.02 MeV	2.56
	Total	38.3 MeV	100	$39.3^{+1.7+1.3}_{-1.6-2.4}$ MeV [95]	...	33.9 MeV	100	79.16 MeV	100

TABLE XIX: Partial widths and branching ratios of the OZI-allowed strong decay, annihilation decay, and radiative transition and the total widths for 5^1S_0 and 6^1S_0 bottomonium states. The width results are in units of keV.

state	channels	Width	$\mathcal{B}(\%)$
$\eta_b(5^1S_0)$	gg	3.26 MeV	11.5
	$\gamma\gamma$	0.192	6.76×10^{-4}
	$h_b(1^1P_1)\gamma$	0.322	1.13×10^{-3}
	$h_b(2^1P_1)\gamma$	1.00	3.52×10^{-3}
	$h_b(3^1P_1)\gamma$	1.63	5.74×10^{-3}
	$h_b(4^1P_1)\gamma$	33.5	0.118
	$\Upsilon(1^3S_1)\gamma$	0.0642	2.26×10^{-4}
	BB^*	20.3 MeV	71.5
	B^*B^*	0.771 MeV	2.71
	$B_sB_s^*$	1.11 MeV	3.91
	$B_s^*B_s^*$	2.91 MeV	10.2
	Total	28.4 MeV	100
$\eta_b(6^1S_0)$	gg	2.59 MeV	12.7
	$\gamma\gamma$	0.152	7.45×10^{-4}
	$h_b(1^1P_1)\gamma$	0.274	1.34×10^{-3}
	$h_b(2^1P_1)\gamma$	0.364	1.78×10^{-3}
	$h_b(3^1P_1)\gamma$	0.681	3.34×10^{-3}
	$h_b(4^1P_1)\gamma$	0.596	2.92×10^{-3}
	$h_b(5^1P_1)\gamma$	4.75	2.33×10^{-2}
	$\Upsilon(1^3S_1)\gamma$	0.0492	2.41×10^{-4}
	BB^*	14.9 MeV	73.0
	$BB(1^3P_0)$	1.39 MeV	6.81
	B^*B^*	0.253 MeV	1.24
	$B_sB_s^*$	1.15 MeV	5.64
	$B_s^*B_s^*$	0.143 MeV	0.70
	Total	20.4 MeV	100

difference between these two predictions, nearly 50 MeV. Experiments have released the branching ratios of leptonic annihilation decays in the 10^{-6} orders of magnitude both for $\Upsilon(5S)$ and $\Upsilon(6S)$ [51]. This is in accord with our theoretical predictions. Branching ratios of all six kinematically-allowed open bottom decay modes BB , BB^* , B^*B^* , B_sB_s , $B_sB_s^*$, and $B_s^*B_s^*$ of $\Upsilon(5S)$ have been experimentally measured as $5.5 \pm 1.0\%$, $13.7 \pm 1.6\%$, $38.1 \pm 3.4\%$, $0.5 \pm 0.5\%$, $1.35 \pm 0.32\%$, and $17.6 \pm 2.7\%$ in PDG [51], respectively. One can see from these data that B^*B^* is the leading decay channel and the following $B_s^*B_s^*$ and BB^* are next-to-leading decay modes. This is not only contradictory with our calculations but most of other theoretical estimates of potential models cannot explain these current experimental results [26, 27, 31]. The possible reasons are the following: firstly, as mentioned before, ex-

TABLE XX: Partial widths and branching ratios of the OZI-allowed strong decay, annihilation decay, and radiative transition and the total widths for the $7S$ bottomonium states. The width results are in units of keV.

state	channels	Width	$\mathcal{B}(\%)$
$\eta_b(7^1S_0)$	gg	2.21 MeV	2.33
	$\gamma\gamma$	0.130	1.37×10^{-4}
	$h_b(1^1P_1)\gamma$	0.291	3.07×10^{-4}
	$h_b(2^1P_1)\gamma$	0.404	4.26×10^{-4}
	$h_b(3^1P_1)\gamma$	0.444	4.68×10^{-4}
	$h_b(4^1P_1)\gamma$	0.607	6.40×10^{-4}
	$h_b(5^1P_1)\gamma$	0.388	4.09×10^{-4}
	$h_b(6^1P_1)\gamma$	4.22	4.45×10^{-3}
	$\Upsilon(1^3S_1)\gamma$	0.0433	4.57×10^{-5}
	BB^*	27.7 MeV	29.2
	$BB(1^3P_0)$	0.974 MeV	1.03
	$BB(1^3P_2)$	4.76 MeV	5.02
	B^*B^*	11.1 MeV	11.7
	$B^*B(1P_1)$	15.0 MeV	15.8
$\Upsilon(7^3S_1)$	$B^*B(1P_1')$	13.9 MeV	14.7
	$B^*B(1^3P_2)$	17.9 MeV	18.9
	$B_sB_s^*$	0.475 MeV	0.501
	$B_s^*B_s^*$	0.741 MeV	0.782
	Total	94.8 MeV	100
	$\ell^+\ell^-$	0.243	2.40×10^{-4}
	ggg	10.4	1.03×10^{-2}
	$\gamma g g$	0.271	2.67×10^{-4}
	$\gamma\gamma\gamma$	3.99×10^{-6}	3.93×10^{-9}
	$\chi_{b0}(3^3P_0)\gamma$	0.00207	2.04×10^{-6}
	$\chi_{b1}(3^3P_1)\gamma$	0.0213	2.10×10^{-5}
	$\chi_{b2}(3^3P_2)\gamma$	0.163	1.61×10^{-4}
	$\chi_{b0}(4^3P_0)\gamma$	4.66×10^{-4}	4.60×10^{-7}
	$\chi_{b1}(4^3P_1)\gamma$	0.0269	2.65×10^{-5}
	$\chi_{b2}(4^3P_2)\gamma$	0.206	2.03×10^{-4}
$\eta_b(1^1S_0)\gamma$	$\chi_{b0}(5^3P_0)\gamma$	0.0363	3.58×10^{-5}
	$\chi_{b1}(5^3P_1)\gamma$	1.97×10^{-4}	1.94×10^{-7}
	$\chi_{b2}(5^3P_2)\gamma$	0.109	1.07×10^{-4}
	$\chi_{b0}(6^3P_0)\gamma$	1.02	1.01×10^{-3}
	$\chi_{b1}(6^3P_1)\gamma$	2.23	2.20×10^{-3}
	$\chi_{b2}(6^3P_2)\gamma$	2.76	2.72×10^{-3}
	BB	6.79 MeV	6.69
	BB^*	22.0 MeV	21.7
	$BB(1P_1)$	1.09 MeV	1.07
	$BB(1P_1')$	0.0879 MeV	8.67×10^{-2}
	$BB(1^3P_2)$	0.647 MeV	0.638
	B^*B^*	20.4 MeV	20.1
	$B^*B(1^3P_0)$	3.16 MeV	3.11
	$B^*B(1P_1)$	9.03 MeV	8.90
	$B^*B(1P_1')$	9.26 MeV	9.13
	$B^*B(1^3P_2)$	28.1 MeV	27.7
Total	B_sB_s	3.11×10^{-4} MeV	3.06×10^{-4}
	$B_sB_s^*$	0.181 MeV	0.178
	$B_s^*B_s^*$	0.770 MeV	0.759
	Total	101.4 MeV	100

TABLE XXI: Partial widths and branching ratios of the OZI-allowed strong decay, annihilation decay, and radiative transition and the total widths for the $8S$ bottomonium states. The width results are in units of keV.

state	channels	Width	$\mathcal{B}(\%)$
$\eta_b(8^1S_0)$	gg	1.81 MeV	2.81
	$\gamma\gamma$	0.106	1.65×10^{-4}
	$h_b(1^1P_1)\gamma$	0.211	3.28×10^{-4}
	$h_b(2^1P_1)\gamma$	0.257	3.99×10^{-4}
	$h_b(3^1P_1)\gamma$	0.336	5.22×10^{-4}
	$h_b(4^1P_1)\gamma$	0.246	3.82×10^{-4}
	$h_b(5^1P_1)\gamma$	0.410	6.37×10^{-4}
	$h_b(6^1P_1)\gamma$	0.286	4.44×10^{-4}
	$\Upsilon(1^3S_1)\gamma$	0.0348	5.40×10^{-5}
	BB^*	29.5 MeV	45.8
	$BB(1^3P_0)$	0.0349 MeV	5.42×10^{-2}
	$BB(1^3P_2)$	7.61 MeV	11.8
	B^*B^*	19.0 MeV	29.5
	$B^*B(1P_1)$	3.41 MeV	5.30
	$B^*B(1P_1')$	2.58 MeV	4.01
	$B^*B(1^3P_2)$	0.0128 MeV	1.99×10^{-2}
	$B_sB_s^*$	0.0348 MeV	5.40×10^{-2}
	$B_s^*B_s^*$	0.324 MeV	0.503
	Total	64.4 MeV	100
$\Upsilon(8^3S_1)$	$\ell^+\ell^-$	0.203	3.05×10^{-4}
	ggg	8.94	1.34×10^{-2}
	γgg	0.232	3.48×10^{-4}
	$\gamma\gamma\gamma$	3.42×10^{-6}	5.14×10^{-9}
	$\chi_{b0}(3^3P_0)\gamma$	7.37×10^{-5}	1.11×10^{-7}
	$\chi_{b1}(3^3P_1)\gamma$	0.0212	3.18×10^{-5}
	$\chi_{b2}(3^3P_2)\gamma$	0.149	2.24×10^{-4}
	$\chi_{b0}(4^3P_0)\gamma$	0.0219	3.29×10^{-5}
	$\chi_{b1}(4^3P_1)\gamma$	0.00249	3.74×10^{-6}
	$\chi_{b2}(4^3P_2)\gamma$	0.136	2.04×10^{-4}
	$\chi_{b0}(5^3P_0)\gamma$	0.00722	1.08×10^{-5}
	$\chi_{b1}(5^3P_1)\gamma$	0.00733	1.10×10^{-5}
	$\chi_{b2}(5^3P_2)\gamma$	0.136	2.04×10^{-4}
	$\chi_{b0}(6^3P_0)\gamma$	0.0329	4.94×10^{-5}
	$\chi_{b1}(6^3P_1)\gamma$	3.35×10^{-4}	5.03×10^{-7}
	$\chi_{b2}(6^3P_2)\gamma$	0.0944	1.42×10^{-4}
	$\eta_b(1^1S_0)\gamma$	0.0508	7.63×10^{-5}
	BB	5.20 MeV	7.82
	BB^*	20.7 MeV	31.0
	$BB(1P_1)$	0.181 MeV	0.271
	$BB(1P_1')$	4.35 MeV	6.54
	$BB(1^3P_2)$	4.71 MeV	7.08
	B^*B^*	27.2 MeV	40.9
	$B^*B(1^3P_0)$	0.00123 MeV	1.84×10^{-3}
	$B^*B(1P_1)$	0.174 MeV	0.262
	$B^*B(1P_1')$	2.53 MeV	3.80
	$B^*B(1^3P_2)$	1.26 MeV	1.90
	B_sB_s	0.0394 MeV	5.92×10^{-2}
	$B_sB_s^*$	7.23×10^{-5} MeV	1.09×10^{-4}
	$B_s^*B_s^*$	0.226 MeV	0.339
	Total	66.6 MeV	100

TABLE XXII: Partial widths and branching ratios of the OZI-allowed strong decay, annihilation decay, and radiative transition and the total widths for the $4P$ bottomonium states. The width results are in units of keV.

state	channels	Width	$\mathcal{B}(\%)$
$h_b(4^1P_1)$	ggg	73.2	0.152
	$\eta_b(1^1S_0)\gamma$	2.68	5.57×10^{-3}
	$\eta_b(2^1S_0)\gamma$	1.83	3.80×10^{-3}
	$\eta_b(3^1S_0)\gamma$	3.69	7.67×10^{-3}
	$\eta_b(4^1S_0)\gamma$	18.4	3.83×10^{-2}
	$\eta_{b2}(3^1D_2)\gamma$	3.17	6.59×10^{-3}
	$\chi_{b0}(1^3P_0)\gamma$	0.00556	1.16×10^{-5}
	$\chi_{b1}(1^3P_1)\gamma$	0.00110	2.29×10^{-6}
	$\chi_{b2}(1^3P_2)\gamma$	0.00169	3.51×10^{-6}
	BB^*	4.56 MeV	9.50
$\chi_{b0}(4^3P_0)$	B^*B^*	43.5 MeV	90.5
	Total	48.1 MeV	100
	$\gamma\gamma$	0.157	1.40×10^{-4}
	gg	2.73 MeV	2.44
	$\Upsilon(1^3S_1)\gamma$	0.241	2.15×10^{-4}
	$\Upsilon(2^3S_1)\gamma$	0.362	3.23×10^{-4}
	$\Upsilon(3^3S_1)\gamma$	1.11	9.90×10^{-4}
	$\Upsilon(4^3S_1)\gamma$	15.6	1.39×10^{-2}
	$\Upsilon_1(3^3D_1)\gamma$	2.20	1.96×10^{-3}
	$h_b(1^1P_1)\gamma$	0.00615	5.49×10^{-6}
$\chi_{b1}(4^3P_1)$	BB	1.19 MeV	1.06
	B^*B^*	104 MeV	92.8
	B_sB_s	4.53 MeV	4.04
	Total	112.1 MeV	100
	$q\bar{q}g$	128	0.318
	$\Upsilon(1^3S_1)\gamma$	1.08	2.68×10^{-3}
	$\Upsilon(2^3S_1)\gamma$	1.06	2.63×10^{-3}
	$\Upsilon(3^3S_1)\gamma$	2.14	5.31×10^{-3}
	$\Upsilon(4^3S_1)\gamma$	17.4	4.32×10^{-2}
	$\Upsilon_1(3^3D_1)\gamma$	0.889	2.21×10^{-3}
$\chi_{b2}(4^3P_2)$	$\Upsilon_2(3^3D_2)\gamma$	2.21	5.48×10^{-3}
	$h_b(1^1P_1)\gamma$	2.69×10^{-5}	6.67×10^{-8}
	BB^*	6.71 MeV	16.7
	B^*B^*	33.5 MeV	83.1
	Total	40.3 MeV	100
	$\gamma\gamma$	0.0142	2.15×10^{-5}
	gg	251	0.380
	$\Upsilon(1^3S_1)\gamma$	2.27	3.44×10^{-3}
	$\Upsilon(2^3S_1)\gamma$	1.85	2.80×10^{-3}
	$\Upsilon(3^3S_1)\gamma$	3.07	4.65×10^{-3}
$h_b(1^1P_1)$	$\Upsilon(4^3S_1)\gamma$	18.0	2.73×10^{-2}
	$\Upsilon_1(3^3D_1)\gamma$	0.0456	6.91×10^{-5}
	$\Upsilon_2(3^3D_2)\gamma$	0.588	8.91×10^{-4}
	$\Upsilon_3(3^3D_3)\gamma$	2.87	4.35×10^{-3}
	$h_b(1^1P_1)\gamma$	0.00378	5.73×10^{-6}
	BB	11.6 MeV	17.6
	BB^*	6.19 MeV	9.38
	B^*B^*	47.5 MeV	72.0
	B_sB_s	0.444 MeV	0.673
	Total	66.0 MeV	100

TABLE XXIII: Partial widths and branching ratios of the OZI-allowed strong decay, annihilation decay, and radiative transition and the total widths for 5^1P_1 and 5^3P_0 bottomonium states. The width results are in units of keV.

state	channels	Width	$\mathcal{B}(\%)$
$h_b(5^1P_1)$	ggg	76.2	0.154
	$\eta_b(1^1S_0)\gamma$	2.28	4.62×10^{-3}
	$\eta_b(2^1S_0)\gamma$	1.85	3.74×10^{-3}
	$\eta_b(3^1S_0)\gamma$	1.72	3.48×10^{-3}
	$\eta_b(4^1S_0)\gamma$	4.14	8.38×10^{-3}
	$\eta_b(5^1S_0)\gamma$	1.34	2.71×10^{-3}
	$\eta_{b2}(4^1D_2)\gamma$	3.37	6.82×10^{-3}
	$\chi_{b0}(1^3P_0)\gamma$	0.00499	1.01×10^{-5}
	$\chi_{b1}(1^3P_1)\gamma$	9.04×10^{-4}	1.83×10^{-6}
	$\chi_{b2}(1^3P_2)\gamma$	0.00173	3.50×10^{-6}
	BB^*	37.4 MeV	75.7
	B^*B^*	10.4 MeV	21.1
	$B_sB_s^*$	1.25 MeV	2.53
	$B_s^*B_s^*$	0.242 MeV	0.490
	Total	49.4 MeV	100
$\chi_{b0}(5^3P_0)$	$\gamma\gamma$	0.146	3.95×10^{-4}
	gg	2.54 MeV	6.86
	$\Upsilon(1^3S_1)\gamma$	0.133	3.59×10^{-4}
	$\Upsilon(2^3S_1)\gamma$	0.230	6.22×10^{-4}
	$\Upsilon(3^3S_1)\gamma$	0.300	8.11×10^{-4}
	$\Upsilon(4^3S_1)\gamma$	1.24	3.35×10^{-3}
	$\Upsilon(5^3S_1)\gamma$	0.515	1.39×10^{-3}
	$\Upsilon_1(4^3D_1)\gamma$	2.47	6.68×10^{-3}
	$h_b(1^1P_1)\gamma$	0.00585	1.58×10^{-5}
	BB	28.1 MeV	75.9
	B^*B^*	5.71 MeV	15.4
	B_sB_s	0.533 MeV	1.44
	$B_s^*B_s^*$	0.112 MeV	0.303
	Total	37 MeV	100

perimental measurement is not enough and one cannot rule out the latent error in experiment; secondly, the calculated partial width of strong decay is dependent on particle's real mass and a more accurate mass value may reduce the possible deviation from the phenomenological decay model. Finally, there may be some other physical effects and mechanisms in the strong decay process of $\Upsilon(10860)$. In Ref. [98], authors just discussed the application of the Franck-Condon principle, which is common in molecular physics on the anomalous high branching ratios of $B_s^*B_s^*$ versus $B_sB_s^*$.

For the $\Upsilon(11020)$ state, there are presently no experimental

TABLE XXIV: Partial widths and branching ratios of OZI-allowed strong decay, annihilation decay, and radiative transition and the total widths for 5^3P_1 and 5^3P_2 bottomonium states. The width results are in units of keV.

state	channels	Width	$\mathcal{B}(\%)$
$\chi_{b1}(5^3P_1)$	$q\bar{q}g$	132	0.283
	$\Upsilon(1^3S_1)\gamma$	0.743	1.59×10^{-3}
	$\Upsilon(2^3S_1)\gamma$	0.741	1.59×10^{-3}
	$\Upsilon(3^3S_1)\gamma$	0.824	1.77×10^{-3}
	$\Upsilon(4^3S_1)\gamma$	2.32	4.98×10^{-3}
	$\Upsilon(5^3S_1)\gamma$	0.835	1.79×10^{-3}
	$\Upsilon_1(4^3D_1)\gamma$	0.921	1.98×10^{-3}
	$\Upsilon_2(4^3D_2)\gamma$	2.32	4.98×10^{-3}
	$h_b(1^1P_1)\gamma$	4.90×10^{-5}	1.05×10^{-7}
	BB^*	33.3 MeV	71.5
	B^*B^*	11.8 MeV	25.3
	$B_sB_s^*$	1.08 MeV	2.32
	$B_s^*B_s^*$	0.292 MeV	0.627
	Total	46.6 MeV	100
$\chi_{b2}(5^3P_2)$	$\gamma\gamma$	0.0143	2.71×10^{-5}
	gg	258	0.490
	$\Upsilon(1^3S_1)\gamma$	1.68	3.19×10^{-3}
	$\Upsilon(2^3S_1)\gamma$	1.38	2.62×10^{-3}
	$\Upsilon(3^3S_1)\gamma$	1.41	2.68×10^{-3}
	$\Upsilon(4^3S_1)\gamma$	3.31	6.28×10^{-3}
	$\Upsilon(5^3S_1)\gamma$	1.12	2.13×10^{-3}
	$\Upsilon_1(4^3D_1)\gamma$	0.0475	9.01×10^{-5}
	$\Upsilon_2(4^3D_2)\gamma$	0.619	1.17×10^{-3}
	$\Upsilon_3(4^3D_3)\gamma$	3.08	5.84×10^{-3}
	$h_b(1^1P_1)\gamma$	0.00332	6.30×10^{-6}
	BB	9.72 MeV	18.4
	BB^*	25.8 MeV	49.0
	B^*B^*	15.7 MeV	29.8
	B_sB_s	0.0566 MeV	0.107
	$B_sB_s^*$	0.775 MeV	1.47
	$B_s^*B_s^*$	0.324 MeV	0.615
	Total	52.7 MeV	100

data in the open-bottom decay channel. We predict that the dominant modes of $\Upsilon(6S)$ are BB^* , $BB(1P_1)$, BB , B^*B^* with the corresponding branching ratios as 43 %, 21.6 %, 20.4 % and 11.5 %, respectively, which are expected to be tested by the forthcoming Belle II in the future. It is worth noting that these partial widths are quite different from predictions by the GI model [26] due to the reflection of a screening effect al-

TABLE XXV: Partial widths and branching ratios of OZI-allowed strong decay, annihilation decay, and radiative transition and the total widths for 6^1P_1 and 6^3P_0 bottomonium states. The width results are in units of keV.

state	channels	Width	$\mathcal{B}(\%)$
$h_b(6^1P_1)$	ggg	74.1	6.01×10^{-2}
	$\eta_b(1^1S_0)\gamma$	1.98	1.61×10^{-3}
	$\eta_b(2^1S_0)\gamma$	1.55	1.26×10^{-3}
	$\eta_b(3^1S_0)\gamma$	1.51	1.22×10^{-3}
	$\eta_b(4^1S_0)\gamma$	1.17	0.949×10^{-3}
	$\eta_b(5^1S_0)\gamma$	1.25	1.01×10^{-3}
	$\eta_b(6^1S_0)\gamma$	7.50	6.08×10^{-3}
	$\eta_{b2}(5^1D_2)\gamma$	3.30	2.68×10^{-3}
	$\chi_{b0}(1^3P_0)\gamma$	0.00456	3.70×10^{-6}
	$\chi_{b1}(1^3P_1)\gamma$	8.04×10^{-4}	6.52×10^{-7}
	$\chi_{b2}(1^3P_2)\gamma$	0.00168	1.36×10^{-6}
	BB^*	40.5 MeV	32.8
	$BB(1^3P_0)$	0.0327 MeV	2.65×10^{-2}
	$BB(1P_1)$	6.10×10^{-7} MeV	4.95×10^{-7}
	$BB(1P'_1)$	2.72×10^{-5} MeV	2.21×10^{-5}
	$BB(1^3P_2)$	9.38 MeV	7.61
	B^*B^*	28.0 MeV	22.7
	$B^*B(1^3P_0)$	2.41×10^{-4} MeV	1.96×10^{-4}
	$B^*B(1P_1)$	18.5 MeV	15.1
	$B^*B(1P'_1)$	5.69 MeV	4.62
	$B^*B(1^3P_2)$	20.4 MeV	16.5
	$B_sB_s^*$	0.143 MeV	0.116
	$B_s^*B_s^*$	0.614 MeV	0.498
	Total	123.3 MeV	100
$\chi_{b0}(6^3P_0)$	$\gamma\gamma$	0.128	1.06×10^{-4}
	gg	2.24 MeV	1.86
	$\Upsilon(1^3S_1)\gamma$	0.0563	4.68×10^{-5}
	$\Upsilon(2^3S_1)\gamma$	0.0784	6.51×10^{-5}
	$\Upsilon(3^3S_1)\gamma$	0.215	1.79×10^{-4}
	$\Upsilon(4^3S_1)\gamma$	0.266	2.21×10^{-4}
	$\Upsilon(5^3S_1)\gamma$	0.364	3.02×10^{-4}
	$\Upsilon(6^3S_1)\gamma$	5.47	4.54×10^{-3}
	$\Upsilon_1(5^3D_1)\gamma$	2.45	2.03×10^{-3}
	$h_b(1^1P_1)\gamma$	0.00523	4.34×10^{-6}
	BB	29.5 MeV	24.5
	$BB(1P_1)$	2.97 MeV	2.47
	$BB(1P'_1)$	14.5 MeV	12.0
	B^*B^*	31.0 MeV	25.7
	$B^*B(1^3P_0)$	2.81 MeV	2.33
	$B^*B(1P_1)$	1.51 MeV	1.25
	$B^*B(1P'_1)$	0.0403 MeV	3.35×10^{-2}
	$B^*B(1^3P_2)$	34.7 MeV	28.8
	B_sB_s	1.05×10^{-4} MeV	8.72×10^{-5}
	$B_s^*B_s^*$	1.13 MeV	0.939
	Total	120.4 MeV	100

TABLE XXVI: Partial widths and branching ratios of OZI-allowed strong decay, annihilation decay, and radiative transition and the total widths for 6^3P_1 and 6^3P_2 bottomonium states. The width results are in units of keV.

state	channels	Width	$\mathcal{B}(\%)$
$\chi_{b1}(6^3P_1)$	$q\bar{q}g$	128	9.13×10^{-2}
	$\Upsilon(1^3S_1)\gamma$	0.478	3.41×10^{-4}
	$\Upsilon(2^3S_1)\gamma$	0.394	2.81×10^{-4}
	$\Upsilon(3^3S_1)\gamma$	0.616	4.39×10^{-4}
	$\Upsilon(4^3S_1)\gamma$	0.741	5.29×10^{-4}
	$\Upsilon(5^3S_1)\gamma$	0.706	5.04×10^{-4}
	$\Upsilon(6^3S_1)\gamma$	6.45	4.60×10^{-3}
	$\Upsilon_1(5^3D_1)\gamma$	0.921	6.57×10^{-4}
	$\Upsilon_2(5^3D_2)\gamma$	2.37	1.69×10^{-3}
	$h_b(1^1P_1)\gamma$	5.02×10^{-5}	3.58×10^{-8}
	BB^*	43.7 MeV	31.2
	$BB(1^3P_0)$	1.27×10^{-4} MeV	9.08×10^{-5}
	$BB(1P_1)$	1.14 MeV	0.815
	$BB(1P'_1)$	1.90 MeV	1.35
	$BB(1^3P_2)$	10.3 MeV	7.36
	B^*B^*	27.3 MeV	19.5
	$B^*B(1^3P_0)$	2.90 MeV	2.07
	$B^*B(1P_1)$	4.49 MeV	3.20
	$B^*B(1P'_1)$	12.0 MeV	8.59
	$B^*B(1^3P_2)$	35.5 MeV	25.3
	$B_sB_s^*$	0.200 MeV	0.143
	$B_s^*B_s^*$	0.661 MeV	0.472
	Total	140.2 MeV	100
$\chi_{b2}(6^3P_2)$	$\gamma\gamma$	0.0139	1.30×10^{-5}
	gg	255	0.238
	$\Upsilon(1^3S_1)\gamma$	1.21	1.13×10^{-3}
	$\Upsilon(2^3S_1)\gamma$	0.852	7.96×10^{-4}
	$\Upsilon(3^3S_1)\gamma$	1.09	1.02×10^{-3}
	$\Upsilon(4^3S_1)\gamma$	1.27	1.19×10^{-3}
	$\Upsilon(5^3S_1)\gamma$	1.03	9.62×10^{-4}
	$\Upsilon(6^3S_1)\gamma$	7.04	6.57×10^{-3}
	$\Upsilon_1(5^3D_1)\gamma$	0.0472	4.41×10^{-5}
	$\Upsilon_2(5^3D_2)\gamma$	0.628	5.86×10^{-4}
	$\Upsilon_3(5^3D_3)\gamma$	3.05	2.85×10^{-3}
	$h_b(1^1P_1)\gamma$	0.00299	2.79×10^{-6}
	BB	5.63 MeV	5.27
	BB^*	21.4 MeV	20.0
	$BB(1P_1)$	0.469 MeV	0.439
	$BB(1P'_1)$	0.527 MeV	0.493
	$BB(1^3P_2)$	1.66 MeV	1.55
	B^*B^*	37.5 MeV	35.1
	$B^*B(1^3P_0)$	2.35 MeV	2.20
	$B^*B(1P_1)$	5.62 MeV	5.26
	$B^*B(1P'_1)$	13.3 MeV	12.4
	$B^*B(1^3P_2)$	17.7 MeV	16.6
	B_sB_s	0.0384 MeV	3.59×10^{-2}
	$B_sB_s^*$	0.0289 MeV	2.70×10^{-2}
	$B_s^*B_s^*$	0.653 MeV	0.611
	Total	107.1 MeV	100

though both of the predicted total widths are contiguous.

C. P -wave states

2. $\Upsilon(7S)$ and $\Upsilon(8S)$

In Ref. [26], authors did not study the properties of $\Upsilon(7S)$ and $\Upsilon(8S)$ in the framework of the GI model. Considering the importance of a screening effect for higher bottomonia, we employ the modified GI model with a screening effect to study the nature of the two particles in this subsection. In Table III, we predict the mass of $\Upsilon(7S)$ and $\Upsilon(8S)$ as 11157 MeV and 11296 MeV, which are raised by 154 and 293 MeV, respectively, compared with the mass value of $\Upsilon(11020)$ from Belle's measurement [95]. We suggest that future experiments will be able to search for these two bottomonia in the vicinity of their corresponding energies mentioned above. The decay information of partial widths and branching ratios of strong decay, annihilation decay, and radiative transition and the total widths for the $\Upsilon(7S)$ and $\Upsilon(8S)$ is shown in Tables XX and XXI, respectively. The total width of $\Upsilon(7S)$ is estimated to be 101.4 MeV, which means a broad state. There are thirteen open-bottom modes, among which the important decay channels are $B^*B(1^3P_2)$, BB^* , B^*B^* , $B^*B(1P_1')$, $B^*B(1P_1)$, and BB with the corresponding partial widths, 28.1, 22.0, 20.4, 9.26, 9.03, and 6.79 MeV, respectively. From Table XX, we find that the combination of a vector meson B^* and a P -wave bottom meson accounts for a large portion of the total width of $\Upsilon(7S)$. Contributions of the $B + B(1P)$ and bottom-strange meson modes can be almost ignored. Some typical ratios of partial widths are given by

$$\begin{aligned}
 \frac{\Gamma[\Upsilon(7^3S_1) \rightarrow BB^*]}{\Gamma[\Upsilon(7^3S_1) \rightarrow BB]} &= 3.24, \\
 \frac{\Gamma[\Upsilon(7^3S_1) \rightarrow B^*B^*]}{\Gamma[\Upsilon(7^3S_1) \rightarrow BB]} &= 3.00, \\
 \frac{\Gamma[\Upsilon(7^3S_1) \rightarrow B^*B(1^3P_2)]}{\Gamma[\Upsilon(7^3S_1) \rightarrow BB]} &= 4.14, \\
 \frac{\Gamma[\Upsilon(7^3S_1) \rightarrow B^*B(1P_1')]}{\Gamma[\Upsilon(7^3S_1) \rightarrow BB]} &= 1.36, \\
 \frac{\Gamma[\Upsilon(7^3S_1) \rightarrow B^*B(1P_1)]}{\Gamma[\Upsilon(7^3S_1) \rightarrow BB]} &= 1.33,
 \end{aligned} \tag{12}$$

which can be tested by future experiments.

In Table XXI, the total width of $\Upsilon(8S)$ is predicted to be 66.6 MeV and the dominant decay channels are B^*B^* and BB^* with branching ratios 40.9 % and 31.0 %, respectively. The B^*B^* and BB^* modes are excellent decay channels to detect the $\Upsilon(8S)$ bottomonium state in the future experiments. All the decay modes BB , $BB(1P_1')$, and $BB(1^3P_2)$ have a consistent partial width of about 4–5 MeV, which almost occupies the remaining contribution to the total width. It is difficult to experimentally observe the configuration of bottom-strange mesons in the $\Upsilon(8S)$ decay.

From Fig. 2, the first above-threshold P -wave bottomonia are $4P$ states, which include spin-singlet $h_b(4P)$ and spin-triplet $\chi_{bJ}(4P)$ with $J = 0, 1, 2$ and exceed the $B\bar{B}$ threshold by about 200 MeV according to our estimates. These above-threshold particles have not yet been found by experiments although their mass of about 10750 MeV is not too large. In Table III, the mass values of higher radial P -wave bottomonia $5P$ and $6P$ states are estimated to be about 10940 and 11100 MeV, respectively, which are reduced by about 70 and 110 MeV compared to GI's predictions, respectively. These predictions of mass values could be tested in future experiments. In this subsection, we will give a theoretical analysis of their decay properties including higher radial P -wave bottomonia $5P$ and $6P$ states in the framework of the modified GI model. We hope provides useful information for the search for these bottomonia in future experiments.

The decay behaviors of $4P$, $5P$, and $6P$ bottomonia are given in Tables XXII-XXVI in succession. As we have already discussed before, for high bottomonium states, the mass and wave function that can reflect internal structures of a particle will have a greater change when considering the screening potential. So in the $4P$ bottomonium states and even higher bottomonia with higher radial quantum number or higher orbital angular momentum, the screening effect begins to manifestly show its power in the description of corresponding decay properties since the theoretical calculations of various decay processes are usually and directly dependent on the mass value and wave function of a corresponding particle. Therefore, in the following discussion, including the subsequent higher D , F , and G -wave states, we will perform a detailed comparison of the predicted decay properties with and without a screening effect. In Ref. [26], authors studied the P -wave bottomonium only up to $5P$ states by using the GI model. So, we focus only on the comparison of $4P$ and $5P$ bottomonia and our predicted decay properties of $6P$ bottomonia will be illustrated at the end.

According to the numerical results in Tables XXII-XXIV and Ref. [26], we conclude the followings.

1. Compared with the predicted partial widths of the GI model, our values of radiative transitions $4P \rightarrow 3D$ and $5P \rightarrow 4D$ are 1.5~2 times smaller. Our calculated partial widths of the dominant radiative decays $4P \rightarrow (4, 3)S$ and $5P \rightarrow (5, 4)S$ are much smaller. Ours of the $5P$ states have an order of magnitude difference. In addition, the predictions of $4P \rightarrow 2S$ and $5P \rightarrow 3S$ from the GI model are almost negligible compared with other radiative transition processes due to corresponding partial widths of $10^{-1} \sim 10^{-4}$ keV on the whole. However, our calculations indicate that there have consistent numerical results of partial widths between $4P$ or $5P$ states transition to the S -wave ground state and the S -wave low-excited states.
2. For the $4P$ and $5P$ bottomonium states, open-bottom strong decay still is dominated and because predicted mass of GI model is higher than that of us, so in their

calculations some higher modes of bottom or bottom-strange configuration are included. From the perspective of the total width, the most obvious difference is from the $\chi_{b0}(4P)$ state, whose predicted total width is estimated to be 112.1 and 34.5 MeV by the modified GI model and GI model, respectively and for the other $4P$ states, the predictions of GI model are less than about 10 ~ 20 MeV compared that of modified GI model. After that, the predicted total widths of GI model in the $5P$ bottomonium states are overall higher than about 5 ~ 20 MeV except for the $h_b(5P)$ state since the contribution of P -wave bottom meson. Although the difference in total width is not conspicuous for most of the $4P$ and $5P$ states, but the predicted dominant decay modes of $4P$ and $5P$ states from two different models are almost all opposite, which also illustrates that the influences of the screening effect on the higher bottomonia is quite significant, hence the present work should be of great value for revealing nature of bottomonium.

3. The total width of the $h_b(4P)$ state is predicted to be 48.1 MeV and the dominant decay mode is B^*B^* with branching ratio 90.5 %. The total widths of spin-triplet $\chi_{bj}(4P)$ state are estimated to be 112.1, 40.3 and 66.0 MeV corresponding to $J = 1, 2, 3$, respectively, which show the $\chi_{b0}(4P)$ is a broad state and other two states are relatively narrow so that the triplet state of $4P$ bottomonium should be easily distinguished in the experiment. In addition, the dominant decay mode of three $\chi_{bj}(4P)$ state are all B^*B^* with branching ratio 92.8 %, 83.1 % and 72.0 %, respectively, so we also suggest the future experiments to detect $4P$ bottomonium states by the B^*B^* mode.
4. The total width of the $h_b(5P)$ state is predicted to be 49.4 MeV and is identical with that of the $h_b(4P)$ state. The dominant decay channels of the $h_b(5P)$ state are BB^* and B^*B^* , and corresponding branching ratios are 75.7 % and 21.1 % respectively. One predict that the total width of $\chi_{bj}(5P)$ is about 40 ~ 50 MeV, and decay mode BB and B^*B^* are critical for the $\chi_{b0}(5P)$ state and the dominant decay channels of $\chi_{b1}(5P)$ are BB^* and B^*B^* , furthermore, for the $\chi_{b2}(5P)$ state, there are three important decay modes BB^* , B^*B^* and BB which all have a great contribution for its total width. The above conclusions could be examined by experiment in the future.

The predicted averaged mass of $6P$ bottomonium states by modified GI model is 11099 MeV, which is about 80 ~ 100 MeV above the experimental value of observed $\Upsilon(11020)$ state with the highest mass until now. Hence, more strong decay channels of $6P$ states is opened. From Table XXV and XXVI, Our results indicate that the $h_b(6P)$ and $\chi_{bj}(6P)$ all are broad bottomonium mesons because of the predicted total width of about 107 ~ 140 MeV. Additionally, BB^* , B^*B^* , and $B^*B(1^3P_2)$ just simultaneously are the main decay channels for spin-singlet $h_b(6P)$ and triplet $\chi_{bj}(6P)$ with $J = 1, 2$, and the sum of their contributions all are more than 70 % to the

total decay width, and the decay modes $B^*B(1^3P_2)$, B^*B^* and BB are dominant for the $\chi_{b0}(6P)$ state with branching ratios of 28.8 %, 25.7 % and 24.5 %, respectively. A common decay feature of $6P$ bottomonium states can clearly be seen that is the role of mode B^*B^* and $B^*B(1^3P_2)$ are quite considerable.

D. D -wave states

In this subsection, we will discuss features of D -wave bottomonia. Among them, the D -wave vector bottomonium with $J^{PC} = 1^{--}$ is quite interesting because unlike charmonium system, there is no clear signal to show the existence of D -wave vector states although many S -wave vector bottomonia have been discovered by experiments. Hence it is clearly helpful for understanding this puzzle and further understanding the behaviors of bottomonia that we study the intrinsic properties of these still missing $\Upsilon_1(n^3D_1)$ states. There are only $1D$ and $2D$ bottomonia below the $B\bar{B}$ threshold. The mass of $3D$ states is located at around 10680 MeV according to our estimates, which is 120 MeV larger than the threshold. We also predict that the mass of $4D$ and $5D$ bottomonia are about 10880 and 11050 MeV, respectively, in Table III. In the same Table, we can notice that the predicted mass of $\Upsilon_1(4^3D_1)$ is 10871 MeV, which is very close to the measured value of the $\Upsilon(10860)$ state from the BaBar collaboration [95]. However, by the following analysis of its decay behaviors, the possibility of a such candidate for $\Upsilon(10860)$ can be basically excluded. Next, we discuss the decay properties of D -wave bottomonia up to $5D$ in detail and make a comparison with the prediction of the GI model, which has studied up to $4D$ [26].

In Tables XXVII-XXX, we list the numerical results of $3D$ and $4D$ bottomonium decays. Comparing ours with the calculation of Ref. [26], we can conclude

1. Compared with the GI model [26], almost all of our estimated partial widths of radiative transition for $3D$ and $4D$ bottomonia become smaller except for the electromagnetic processes of $3D \rightarrow 1P$ and $4D \rightarrow 2P$, which become larger from 20 % to 300 % range.
2. Similar to the situation of $\chi_{b0}(4P)$, our prediction of the total width for the $\Upsilon_1(3D)$ is 54.1 MeV, which is largely different from an estimate of 103.6 MeV by the GI model. Overall, the $3D$ bottomonia are broad resonances where the predicted total widths of other three particles $\eta_{b2}(3D)$, $\Upsilon_2(3D)$ and $\Upsilon_3(3D)$ are 143.0, 96.3, and 223.8 MeV, respectively. Our results of $3D$ and $4D$ states on the partial widths and branching ratios of strong decay channels are still quite different from those of the GI model. The strong decay modes of $\eta_{b2}(3D)$ are only B^*B^* and BB^* with close predicted ratios, which accounts for almost all the contributions to the total width. For the $\Upsilon_1(3D)$, the dominant decay mode is B^*B^* with a branching ratio 61.8 %. The mode BB with 10.1 % may not be the best process to experimentally search for $\Upsilon_1(3D)$. Additionally, the branching ratio of annihilating to the leptonic pair $\ell^+\ell^-$ is three orders of magnitude smaller than $\Upsilon(4S)$ state. Hence, it is hard

TABLE XXIX: Partial widths and branching ratios of OZI-allowed strong decay, annihilation decay, and radiative transition and total widths for 4^1D_2 and 4^3D_1 bottomonium states. The width results are in units of keV.

state	channels	Width	$\mathcal{B}(\%)$
$\eta_{b2}(4^1D_2)$	gg	1.86	2.27×10^{-3}
	$h_b(1^1P_1)\gamma$	0.697	8.49×10^{-4}
	$h_b(2^1P_1)\gamma$	1.10	1.34×10^{-3}
	$h_b(3^1P_1)\gamma$	2.88	3.51×10^{-3}
	$h_b(4^1P_1)\gamma$	11.4	1.39×10^{-2}
	$h_{b3}(1^1F_3)\gamma$	0.0131	1.60×10^{-5}
	$h_{b3}(2^1F_3)\gamma$	0.0125	1.52×10^{-5}
	$h_{b3}(3^1F_3)\gamma$	2.43	2.96×10^{-3}
	$\Upsilon_1(1^3D_1)\gamma$	8.76×10^{-4}	1.07×10^{-6}
	$\Upsilon_2(1^3D_2)\gamma$	1.42×10^{-4}	1.73×10^{-7}
	$\Upsilon_3(1^3D_3)\gamma$	1.65×10^{-4}	2.01×10^{-7}
	BB^*	51.9 MeV	63.2
	B^*B^*	27.4 MeV	33.4
	$B_sB_s^*$	1.63 MeV	1.98
	$B_s^*B_s^*$	1.16 MeV	1.41
	Total	82.1 MeV	100
$\Upsilon_1(4^3D_1)$	$\ell^+\ell^-$	0.003	3.44×10^{-6}
	ggg	30.4	3.49×10^{-2}
	$\chi_{b0}(1^3P_0)\gamma$	0.752	8.62×10^{-4}
	$\chi_{b1}(1^3P_1)\gamma$	0.166	1.90×10^{-4}
	$\chi_{b2}(1^3P_2)\gamma$	0.00114	1.31×10^{-6}
	$\chi_{b0}(2^3P_0)\gamma$	0.928	1.06×10^{-3}
	$\chi_{b1}(2^3P_1)\gamma$	0.296	3.39×10^{-4}
	$\chi_{b2}(2^3P_2)\gamma$	0.00625	7.17×10^{-6}
	$\chi_{b0}(3^3P_0)\gamma$	2.18	2.50×10^{-3}
	$\chi_{b1}(3^3P_1)\gamma$	0.948	1.09×10^{-3}
	$\chi_{b2}(3^3P_2)\gamma$	0.0329	3.77×10^{-5}
	$\chi_{b0}(4^3P_0)\gamma$	7.13	8.18×10^{-3}
	$\chi_{b1}(4^3P_1)\gamma$	4.62	5.30×10^{-3}
	$\chi_{b2}(4^3P_2)\gamma$	0.274	3.14×10^{-4}
	$\chi_{b2}(2^3F_2)\gamma$	0.0313	3.59×10^{-5}
	$\chi_{b2}(3^3F_2)\gamma$	2.25	2.58×10^{-3}
	$\eta_{b2}(1^1D_2)\gamma$	4.08×10^{-4}	4.68×10^{-7}
	BB	27.4 MeV	31.4
	BB^*	15.1 MeV	17.3
	B^*B^*	42.1 MeV	48.3
	B_sB_s	0.560 MeV	0.642
	$B_sB_s^*$	0.360 MeV	0.412
	$B_s^*B_s^*$	1.66 MeV	1.91
	Total	87.2 MeV	100

and the mode BB has also about 10 % contributions to the total width.

4. Compared with the S -wave Υ 's, the D -wave bottomonia behave more like quite broad states and the leptonic annihilation widths are too small as mentioned before. Hence, this can also explain why the S -wave Υ 's are experimentally found in succession but the D -wave Υ_1 's always have no movement in experiments.

The detailed decay information of $5D$ bottomonium states are presented in Table XXXI and XXXII. Our results indicate that the spin-singlet $\eta_{b2}(5D)$ and triplet $\Upsilon_J(5D)$ with $J = 1, 2, 3$ are all broad states, whose predicted total widths are 110.7, 121.7, 101.6, and 86.0 MeV, respectively. We also notice that all the dominant decay channels of $\eta_{b2}(5^1D_1)$, $\Upsilon_2(5^3D_2)$ and $\Upsilon_3(5^3D_3)$ are B^*B^* and BB^* and other relatively important decay modes are provided by the strong decay channels containing P -wave bottom mesons. It is very interesting to study the properties of $\Upsilon_1(5^3D_1)$ because the mass of $\Upsilon_1(5D)$ is only 40 MeV larger than that of $\Upsilon(6S)$ according to our prediction in Table III, which is nearly 100 MeV smaller than that of the GI model. Hence, this particle with $J^{PC} = 1^{--}$ is likely to be observed in the forthcoming Belle II experiment. Our numerical results show that the $\Upsilon_1(5^3D_1)$ is a broad state, for which there are ten open-bottom decay modes. Furthermore, its main decay channels are B^*B^* , BB , BB^* , $BB(1P_1')$ and $BB(1^3P_2)$, and the corresponding branching ratios are 38.7 %, 16.4 %, 15.8 %, 14.8 %, and 7.59 %, respectively. The contributions of bottom-strange mesons are too low to exceed 1 %. Finally, we hope that these results can provide valuable clues for future experiments to search for these particles.

TABLE XXX: Partial widths and branching ratios of the OZI-allowed strong decay, annihilation decay, and radiative transition and total widths for 4^3D_2 and 4^3D_3 bottomonium states. The width results are in units of keV.

state	channels	Width	$\mathcal{B}(\%)$
$\Upsilon_2(4^3D_2)$	ggg	2.75	3.12×10^{-3}
	$\chi_{b1}(1^3P_1)\gamma$	0.616	6.98×10^{-4}
	$\chi_{b2}(1^3P_2)\gamma$	0.0537	6.09×10^{-5}
	$\chi_{b1}(2^3P_1)\gamma$	0.927	1.05×10^{-3}
	$\chi_{b2}(2^3P_2)\gamma$	0.139	1.58×10^{-4}
	$\chi_{b1}(3^3P_1)\gamma$	2.344	2.66×10^{-3}
	$\chi_{b2}(3^3P_2)\gamma$	0.467	5.29×10^{-4}
	$\chi_{b1}(4^3P_1)\gamma$	8.77	9.94×10^{-3}
	$\chi_{b2}(4^3P_2)\gamma$	2.65	3.00×10^{-3}
	$\chi_{b2}(3^3F_2)\gamma$	0.297	3.37×10^{-4}
	$\chi_{b3}(3^3F_3)\gamma$	2.17	2.46×10^{-3}
	$\eta_{b2}(3^1D_2)\gamma$	6.39×10^{-5}	7.24×10^{-8}
	BB^*	52.2 MeV	59.2
	B^*B^*	33.1 MeV	37.6
	$B_sB_s^*$	1.55 MeV	1.76
	$B_s^*B_s^*$	1.33 MeV	1.51
	Total	88.2 MeV	100
$\Upsilon_3(4^3D_3)$	ggg	8.38	1.27×10^{-2}
	$\chi_{b2}(1^3P_2)\gamma$	0.522	7.91×10^{-4}
	$\chi_{b2}(2^3P_2)\gamma$	1.00	1.52×10^{-3}
	$\chi_{b2}(3^3P_2)\gamma$	2.59	3.92×10^{-3}
	$\chi_{b2}(4^3P_2)\gamma$	11.1	1.68×10^{-2}
	$\chi_{b2}(3^3F_2)\gamma$	0.00678	1.03×10^{-5}
	$\chi_{b3}(3^3F_3)\gamma$	0.220	3.33×10^{-4}
	$\chi_{b4}(3^3F_4)\gamma$	2.32	3.52×10^{-3}
	$\eta_{b2}(1^1D_2)\gamma$	7.40×10^{-4}	1.12×10^{-6}
	$\eta_{b2}(2^1D_2)\gamma$	8.72×10^{-4}	1.32×10^{-6}
	BB	6.82 MeV	10.3
	BB^*	28.5 MeV	43.1
	B^*B^*	28.9 MeV	43.8
	B_sB_s	0.00593 MeV	8.97×10^{-3}
	$B_sB_s^*$	0.892 MeV	1.35
	$B_s^*B_s^*$	0.945 MeV	1.43
	Total	66.0 MeV	100

TABLE XXXI: Partial widths and branching ratios of OZI-allowed strong decay, annihilation decay, and radiative transition and total widths for 5^1D_2 and 5^3D_1 bottomonium states. The width results are in units of keV.

state	channels	Width	$\mathcal{B}(\%)$
$\eta_{b2}(5^1D_2)$	gg	2.13	1.92×10^{-3}
	$h_b(1^1P_1)\gamma$	0.373	3.37×10^{-4}
	$h_b(2^1P_1)\gamma$	0.682	6.16×10^{-4}
	$h_b(3^1P_1)\gamma$	1.13	1.02×10^{-3}
	$h_b(4^1P_1)\gamma$	2.23	2.01×10^{-3}
	$h_b(5^1P_1)\gamma$	10.2	9.21×10^{-3}
	$h_{b3}(2^1F_3)\gamma$	0.0202	1.82×10^{-5}
	$h_{b3}(3^1F_3)\gamma$	0.00901	8.14×10^{-6}
	$h_{b3}(4^1F_3)\gamma$	2.72	2.46×10^{-3}
	$\Upsilon_1(1^3D_1)\gamma$	7.38×10^{-4}	6.67×10^{-7}
	$\Upsilon_2(1^3D_2)\gamma$	1.02×10^{-4}	9.21×10^{-8}
	$\Upsilon_3(1^3D_3)\gamma$	1.84×10^{-4}	1.66×10^{-7}
	BB^*	39.4 MeV	35.6
	$BB(1^3P_0)$	0.216 MeV	0.195
	$BB(1P_1)$	0.00109 MeV	9.87×10^{-4}
	$BB(1P'_1)$	0.00107 MeV	9.64×10^{-4}
	$BB(1^3P_2)$	14.7 MeV	13.3
	B^*B^*	37.2 MeV	33.6
	$B^*B(1^3P_0)$	0.00218 MeV	1.97×10^{-3}
	$B^*B(1P_1)$	18.5 MeV	16.7
$\Upsilon_1(5^3D_1)$	$B_sB_s^*$	0.0762 MeV	6.88×10^{-2}
	$B_s^*B_s^*$	0.590 MeV	0.533
	Total	110.7 MeV	100
	$\ell^+\ell^-$	0.00302	2.48×10^{-6}
	ggg	34.7	2.85×10^{-2}
	$\chi_{b0}(1^3P_0)\gamma$	0.508	4.17×10^{-4}
	$\chi_{b1}(1^3P_1)\gamma$	0.0757	6.22×10^{-5}
	$\chi_{b0}(2^3P_0)\gamma$	0.755	6.20×10^{-4}
	$\chi_{b1}(2^3P_1)\gamma$	0.178	1.46×10^{-4}
	$\chi_{b0}(3^3P_0)\gamma$	0.979	8.04×10^{-4}
	$\chi_{b1}(3^3P_1)\gamma$	0.324	2.66×10^{-4}
	$\chi_{b0}(4^3P_0)\gamma$	1.72	1.41×10^{-3}
	$\chi_{b1}(4^3P_1)\gamma$	0.739	6.07×10^{-4}
	$\chi_{b0}(5^3P_0)\gamma$	6.11	5.02×10^{-3}
	$\chi_{b1}(5^3P_1)\gamma$	4.07	3.34×10^{-3}
	$\chi_{b2}(5^3P_2)\gamma$	0.240	1.97×10^{-4}
	$\chi_{b2}(2^3F_2)\gamma$	0.0328	2.70×10^{-5}
	$\chi_{b2}(3^3F_2)\gamma$	0.0272	2.24×10^{-5}
	$\chi_{b2}(4^3F_2)\gamma$	2.49	2.05×10^{-3}
	$\eta_{b2}(1^1D_2)\gamma$	4.08×10^{-4}	3.35×10^{-7}
$\Upsilon_1(5^3D_1)$	BB	20.0 MeV	16.4
	BB^*	19.3 MeV	15.8
	$BB(1P_1)$	4.08 MeV	3.35
	$BB(1P'_1)$	18.1 MeV	14.8
	$BB(1^3P_2)$	9.23 MeV	7.59
	B^*B^*	47.1 MeV	38.7
	$B^*B(1^3P_0)$	3.02 MeV	2.48
	B_sB_s	0.0235 MeV	1.93×10^{-2}
	$B_sB_s^*$	0.103 MeV	8.44×10^{-2}
	$B_s^*B_s^*$	0.798 MeV	0.656
	Total	121.7 MeV	100

TABLE XXXII: Partial widths and branching ratios of the OZI-allowed strong decay, annihilation decay, and radiative transition and total widths for 5^3D_2 and 5^3D_3 bottomonium states. The width results are in units of keV.

state	channels	Width	$\mathcal{B}(\%)$
$\Upsilon_2(5^3D_2)$	ggg	3.23	3.18×10^{-3}
	$\chi_{b1}(1^3P_1)\gamma$	0.343	3.38×10^{-4}
	$\chi_{b2}(1^3P_2)\gamma$	0.0195	1.92×10^{-5}
	$\chi_{b1}(2^3P_1)\gamma$	0.604	5.94×10^{-4}
	$\chi_{b2}(2^3P_2)\gamma$	0.0574	5.65×10^{-5}
	$\chi_{b1}(3^3P_1)\gamma$	0.951	9.36×10^{-4}
	$\chi_{b2}(3^3P_2)\gamma$	0.142	1.40×10^{-4}
	$\chi_{b1}(4^3P_1)\gamma$	1.79	1.76×10^{-3}
	$\chi_{b2}(4^3P_2)\gamma$	0.363	3.57×10^{-4}
	$\chi_{b1}(5^3P_1)\gamma$	7.65	7.53×10^{-3}
	$\chi_{b2}(5^3P_2)\gamma$	2.30	2.26×10^{-3}
	$\chi_{b2}(4^3F_2)\gamma$	0.320	3.15×10^{-4}
	$\chi_{b3}(4^3F_3)\gamma$	2.30	2.26×10^{-3}
	$\eta_{b2}(4^1D_2)\gamma$	5.11×10^{-5}	5.03×10^{-8}
	BB^*	45.6 MeV	44.9
	$BB(1^3P_0)$	2.50×10^{-7} MeV	2.46×10^{-7}
	$BB(1P_1)$	2.61 MeV	2.57
	$BB(1P'_1)$	6.36 MeV	6.26
	$BB(1^3P_2)$	6.43 MeV	6.33
	B^*B^*	35.9 MeV	35.3
	$B^*B(1^3P_0)$	3.70 MeV	3.65
	$B^*B(1P_1)$	0.307 MeV	0.302
	$B_sB_s^*$	0.125 MeV	0.123
	$B_s^*B_s^*$	0.531 MeV	0.523
	Total	101.6 MeV	100
$\Upsilon_3(5^3D_3)$	ggg	10.1	1.17×10^{-2}
	$\chi_{b2}(1^3P_2)\gamma$	0.262	3.05×10^{-4}
	$\chi_{b2}(2^3P_2)\gamma$	0.510	5.93×10^{-4}
	$\chi_{b2}(3^3P_2)\gamma$	0.974	1.13×10^{-3}
	$\chi_{b2}(4^3P_2)\gamma$	1.99	2.31×10^{-3}
	$\chi_{b2}(5^3P_2)\gamma$	9.69	1.13×10^{-2}
	$\chi_{b2}(4^3F_2)\gamma$	0.00747	8.69×10^{-6}
	$\chi_{b3}(4^3F_3)\gamma$	0.238	2.77×10^{-4}
	$\chi_{b4}(4^3F_4)\gamma$	2.61	3.03×10^{-3}
	$\eta_{b2}(1^1D_2)\gamma$	6.08×10^{-4}	7.07×10^{-7}
	$\eta_{b2}(2^1D_2)\gamma$	8.06×10^{-4}	9.37×10^{-7}
	BB	2.20 MeV	2.56
	BB^*	14.1 MeV	16.5
	$BB(1P_1)$	2.19 MeV	2.54
	$BB(1P'_1)$	5.91 MeV	6.87
	$BB(1^3P_2)$	6.65 MeV	7.73
	B^*B^*	48.5 MeV	56.4
	$B^*B(1^3P_0)$	3.96 MeV	4.61
	$B^*B(1P_1)$	1.55 MeV	1.81
	B_sB_s	0.126 MeV	0.147
	$B_sB_s^*$	0.00506 MeV	5.88×10^{-3}
	$B_s^*B_s^*$	0.769 MeV	0.895
	Total	86.0 MeV	100

TABLE XXXIII: Partial widths and branching ratios of the OZI-allowed strong decay, annihilation decay, and radiative transition and total widths for the $2F$ bottomonium states. The width results are in units of keV.

state	channels	Width	$\mathcal{B}(\%)$
$h_{b3}(2^1F_3)$	$\eta_{b2}(1^1D_2)\gamma$	1.99	0.482
	$\eta_{b2}(2^1D_2)\gamma$	17.4	4.21
	$\eta_{b4}(1^1G_4)\gamma$	1.06	0.257
	$\chi_{b2}(1^3F_2)\gamma$	3.70×10^{-4}	8.96×10^{-5}
	$\chi_{b3}(1^3F_3)\gamma$	1.16×10^{-4}	2.81×10^{-5}
	BB^*	0.393 MeV	95.2
	Total	0.413 MeV	100
$\chi_{b2}(2^3F_2)$	gg	2.04	4.93×10^{-3}
	$\Upsilon_1(1^3D_1)\gamma$	1.95	4.71×10^{-3}
	$\Upsilon_2(1^3D_2)\gamma$	0.224	5.41×10^{-4}
	$\Upsilon_3(1^3D_3)\gamma$	0.00367	8.86×10^{-6}
	$\Upsilon_1(2^3D_1)\gamma$	15.1	3.65×10^{-2}
	$\Upsilon_2(2^3D_2)\gamma$	2.55	6.16×10^{-3}
	$\Upsilon_3(2^3D_3)\gamma$	0.0681	1.64×10^{-4}
	$\Upsilon_3(1^3G_3)\gamma$	0.946	2.29×10^{-3}
	$h_{b3}(1^1F_3)\gamma$	9.12×10^{-6}	2.20×10^{-8}
	BB	41.4 MeV	~ 100
$\chi_{b3}(2^3F_3)$	Total	41.4 MeV	100
	gg	0.167	3.08×10^{-2}
	$\Upsilon_2(1^3D_2)\gamma$	1.83	0.337
	$\Upsilon_3(1^3D_3)\gamma$	0.145	2.67×10^{-2}
	$\Upsilon_2(2^3D_2)\gamma$	15.4	2.84
	$\Upsilon_3(2^3D_3)\gamma$	1.80	0.331
	$\Upsilon_3(1^3G_3)\gamma$	0.0664	1.22×10^{-2}
	$\Upsilon_4(1^3G_4)\gamma$	0.957	0.176
	$h_{b3}(1^1F_3)\gamma$	9.40×10^{-5}	1.73×10^{-5}
	BB^*	0.524 MeV	96.5
$\chi_{b4}(2^3F_4)$	Total	0.543 MeV	100
	gg	0.126	1.22×10^{-2}
	$\Upsilon_3(1^3D_3)\gamma$	1.85	0.180
	$\Upsilon_3(2^3D_3)\gamma$	16.9	1.64
	$\Upsilon_3(1^3G_3)\gamma$	8.80×10^{-4}	8.54×10^{-5}
	$\Upsilon_4(1^3G_4)\gamma$	0.0535	5.19×10^{-3}
	$\Upsilon_5(1^3G_5)\gamma$	1.05	0.102
	$h_{b3}(1^1F_3)\gamma$	3.90×10^{-4}	3.79×10^{-5}
	BB	1.01 MeV	98.1
	BB^*	6.93×10^{-4} MeV	6.73×10^{-2}
Total	Total	1.03 MeV	100

E. F -wave states

In the following, we will focus on the higher F -wave bottomonia, i.e., $2F$, $3F$, and $4F$ bottomonia. The theoretical mass values of F -wave bottomonia are presented in Table III. Their average mass values are the same as those of the spin-singlet states of 10609, 10812, and 10988 MeV with radial quantum number $n = 2, 3, 4$, respectively. From Fig. 2, it is also easily to find that the mass values of these particles are close to the S -wave bottomonium states corresponding to radial quantum number $n = 4, 5, 6$, respectively.

TABLE XXXIV: Partial widths and branching ratios of the OZI-allowed strong decay, annihilation decay, and radiative transition and the total widths for 3^1F_3 and 3^3F_2 bottomonium states. The width results are in units of keV.

state	channels	Width	$\mathcal{B}(\%)$
$h_{b3}(3^1F_3)$	$\eta_{b2}(1^1D_2)\gamma$	0.530	5.14×10^{-4}
	$\eta_{b2}(2^1D_2)\gamma$	2.20	2.13×10^{-3}
	$\eta_{b2}(3^1D_2)\gamma$	14.2	1.38×10^{-2}
	$\eta_{b4}(2^1G_4)\gamma$	1.59	1.54×10^{-3}
	$\chi_{b2}(2^3F_2)\gamma$	3.41×10^{-4}	3.30×10^{-7}
	$\chi_{b3}(2^3F_3)\gamma$	1.14×10^{-4}	1.10×10^{-7}
	BB^*	52.7 MeV	51.0
	B^*B^*	49.2 MeV	47.6
	$B_sB_s^*$	1.35 MeV	1.31
	Total	103.2 MeV	100
$\chi_{b2}(3^3F_2)$	gg	3.17	2.20×10^{-3}
	$\Upsilon_1(1^3D_1)\gamma$	0.540	3.75×10^{-4}
	$\Upsilon_2(1^3D_2)\gamma$	0.0468	3.25×10^{-5}
	$\Upsilon_3(1^3D_3)\gamma$	4.52×10^{-4}	3.14×10^{-7}
	$\Upsilon_1(2^3D_1)\gamma$	2.14	1.49×10^{-3}
	$\Upsilon_2(2^3D_2)\gamma$	0.260	1.80×10^{-4}
	$\Upsilon_3(2^3D_3)\gamma$	0.00462	3.21×10^{-6}
	$\Upsilon_1(3^3D_1)\gamma$	12.3	8.54×10^{-3}
	$\Upsilon_2(3^3D_2)\gamma$	2.12	1.47×10^{-3}
	$\Upsilon_3(3^3D_3)\gamma$	0.0569	3.95×10^{-5}
	$\Upsilon_3(2^3G_3)\gamma$	1.53	1.06×10^{-3}
	$h_{b3}(1^1F_3)\gamma$	3.47×10^{-5}	2.41×10^{-8}
	BB	28.5 MeV	19.8
	BB^*	32.5 MeV	22.5
	B^*B^*	81.1 MeV	56.3
	B_sB_s	0.898 MeV	0.623
	$B_sB_s^*$	1.08 MeV	0.753
	Total	144.1 MeV	100

TABLE XXXV: Partial widths and branching ratios of OZI-allowed strong decay, annihilation decay, and radiative transition and the total widths for 3^3F_3 and 3^3F_4 bottomonium states. The width results are in units of keV.

state	channels	Width	$\mathcal{B}(\%)$
$\chi_{b3}(3^3F_3)$	gg	0.270	2.32×10^{-4}
	$\Upsilon_2(1^3D_2)\gamma$	0.494	4.24×10^{-4}
	$\Upsilon_3(1^3D_3)\gamma$	0.0289	2.48×10^{-5}
	$\Upsilon_2(2^3D_2)\gamma$	2.01	1.72×10^{-3}
	$\Upsilon_3(2^3D_3)\gamma$	0.169	1.45×10^{-4}
	$\Upsilon_2(3^3D_2)\gamma$	12.5	1.07×10^{-2}
	$\Upsilon_3(3^3D_3)\gamma$	1.48	1.27×10^{-3}
	$\Upsilon_3(2^3G_3)\gamma$	0.105	9.01×10^{-5}
	$\Upsilon_4(2^3G_4)\gamma$	1.49	1.28×10^{-3}
	$h_{b3}(2^1F_3)\gamma$	7.35×10^{-5}	6.30×10^{-8}
	BB^*	60.6 MeV	51.9
	B^*B^*	54.3 MeV	46.5
	$B_sB_s^*$	1.78 MeV	1.5
	Total	116.6 MeV	100
$\chi_{b4}(3^3F_4)$	gg	0.210	3.13×10^{-4}
	$\Upsilon_3(1^3D_3)\gamma$	0.487	7.27×10^{-4}
	$\Upsilon_3(2^3D_3)\gamma$	2.05	3.06×10^{-3}
	$\Upsilon_3(3^3D_3)\gamma$	13.9	2.07×10^{-2}
	$\Upsilon_3(2^3G_3)\gamma$	0.00141	2.10×10^{-6}
	$\Upsilon_4(2^3G_4)\gamma$	0.0848	1.27×10^{-4}
	$\Upsilon_5(2^3G_5)\gamma$	1.64	2.45×10^{-3}
	$h_{b3}(1^1F_3)\gamma$	3.17×10^{-4}	4.73×10^{-7}
	BB	0.426 MeV	0.636
	BB^*	14.3 MeV	21.3
	B^*B^*	51.9 MeV	77.5
	B_sB_s	0.365 MeV	0.545
	$B_sB_s^*$	0.0605 MeV	9.03×10^{-2}
	Total	67.0 MeV	100

results of $2F$ and $3F$ bottomonia, which are also studied by Ref. [26] in the framework of the GI model. By analyzing and comparing our calculation with the GI model [26], we conclude

1. The radiative transitions of F -wave states also have a rule very similar to P -wave and D -wave bottomonia, which can be seen by comparing the predictions of the modified GI model and GI model. That is, our partial widths of radiative decays are smaller than those of the GI model on the whole except for the radiative processes $2F \rightarrow 1D$ and $3F \rightarrow 2D$.
2. $2F$ bottomonia are states near the threshold, and their

In Tables XXXIII-XXXV, we present the numerical decay

TABLE XXXVI: Partial widths and branching ratios of OZI-allowed strong decay, annihilation decay, and radiative transition and the total widths for 4^1F_3 and 4^3F_2 bottomonium states. The width results are in units of keV.

state	channels	Width	$\mathcal{B}(\%)$
$h_{b3}(4^1F_3)$	$\eta_{b2}(1^1D_2)\gamma$	0.238	3.51×10^{-4}
	$\eta_{b2}(2^1D_2)\gamma$	0.701	1.03×10^{-3}
	$\eta_{b2}(3^1D_2)\gamma$	2.09	3.08×10^{-3}
	$\eta_{b2}(4^1D_2)\gamma$	12.2	1.80×10^{-2}
	$\eta_{b4}(3^1G_4)\gamma$	2.00	2.95×10^{-3}
	$\chi_{b2}(2^3F_2)\gamma$	3.67×10^{-4}	5.41×10^{-7}
	$\chi_{b3}(2^3F_3)\gamma$	9.41×10^{-5}	1.39×10^{-7}
	$\chi_{b3}(2^3F_4)\gamma$	5.96×10^{-6}	8.79×10^{-9}
	BB^*	29.3 MeV	43.2
	$BB(1^3P_0)$	0.0617 MeV	9.10×10^{-2}
	B^*B^*	37.6 MeV	55.5
	$B_sB_s^*$	0.235 MeV	0.346
	$B_s^*B_s^*$	0.548 MeV	0.808
	Total	67.8 MeV	100
$\chi_{b2}(4^3F_2)$	$\Upsilon_1(1^3D_1)\gamma$	0.283	3.62×10^{-4}
	$\Upsilon_2(1^3D_2)\gamma$	0.0183	2.34×10^{-5}
	$\Upsilon_3(1^3D_3)\gamma$	7.59×10^{-5}	9.71×10^{-8}
	$\Upsilon_1(2^3D_1)\gamma$	0.708	9.05×10^{-4}
	$\Upsilon_2(2^3D_2)\gamma$	0.0675	8.63×10^{-5}
	$\Upsilon_3(2^3D_3)\gamma$	7.79×10^{-4}	9.96×10^{-7}
	$\Upsilon_1(3^3D_1)\gamma$	1.99	2.54×10^{-3}
	$\Upsilon_2(3^3D_2)\gamma$	0.253	3.24×10^{-4}
	$\Upsilon_3(3^3D_3)\gamma$	0.00471	6.02×10^{-6}
	$\Upsilon_1(4^3D_1)\gamma$	10.4	1.33×10^{-2}
	$\Upsilon_2(4^3D_2)\gamma$	1.81	2.31×10^{-3}
	$\Upsilon_3(4^3D_3)\gamma$	0.0490	6.27×10^{-5}
	$\Upsilon_3(3^3G_3)\gamma$	1.82	2.33×10^{-3}
	$h_{b3}(1^1F_3)\gamma$	4.94×10^{-5}	6.32×10^{-8}
	BB	13.7 MeV	17.5
	BB^*	24.7 MeV	31.6
	B^*B^*	39.3 MeV	50.2
	B_sB_s	0.0849 MeV	0.109
	$B_sB_s^*$	0.0947 MeV	0.121
	$B_s^*B_s^*$	0.373 MeV	0.477
	Total	78.2 MeV	100

TABLE XXXVII: Partial widths and branching ratios of OZI-allowed strong decay, annihilation decay, and radiative transition and the total widths for 4^3F_3 and 4^3F_4 bottomonium states. The width results are in units of keV.

state	channels	Width	$\mathcal{B}(\%)$
$\chi_{b3}(4^3F_3)$	$\Upsilon_2(1^3D_2)\gamma$	0.232	3.28×10^{-4}
	$\Upsilon_3(1^3D_3)\gamma$	0.00934	1.32×10^{-5}
	$\Upsilon_2(2^3D_2)\gamma$	0.649	9.17×10^{-4}
	$\Upsilon_3(2^3D_3)\gamma$	0.0417	5.89×10^{-5}
	$\Upsilon_2(3^3D_2)\gamma$	1.90	2.68×10^{-3}
	$\Upsilon_3(3^3D_3)\gamma$	0.166	2.34×10^{-4}
	$\Upsilon_2(4^3D_2)\gamma$	10.8	1.53×10^{-2}
	$\Upsilon_3(4^3D_3)\gamma$	1.29	1.82×10^{-3}
	$\Upsilon_3(3^3G_3)\gamma$	0.127	1.79×10^{-4}
	$\Upsilon_4(3^3G_4)\gamma$	1.88	2.66×10^{-3}
	$h_{b3}(3^1F_3)\gamma$	6.49×10^{-5}	9.17×10^{-8}
	BB^*	36.9 MeV	52.1
	$BB(1^3P_0)$	1.11×10^{-4} MeV	1.57×10^{-4}
	B^*B^*	33.3 MeV	47.0
	$B_sB_s^*$	0.214 MeV	0.303
	$B_s^*B_s^*$	0.400 MeV	0.566
	Total	70.8 MeV	100
$\chi_{b4}(4^3F_4)$	$\Upsilon_3(1^3D_3)\gamma$	0.202	3.34×10^{-4}
	$\Upsilon_3(2^3D_3)\gamma$	0.637	1.05×10^{-3}
	$\Upsilon_3(3^3D_3)\gamma$	1.94	3.21×10^{-3}
	$\Upsilon_3(4^3D_3)\gamma$	11.8	1.95×10^{-2}
	$\Upsilon_3(3^3G_3)\gamma$	0.00166	2.74×10^{-6}
	$\Upsilon_4(3^3G_4)\gamma$	0.103	1.70×10^{-4}
	$\Upsilon_5(3^3G_5)\gamma$	1.89	3.12×10^{-3}
	$h_{b3}(2^1F_3)\gamma$	3.65×10^{-4}	6.03×10^{-7}
	BB	0.00769 MeV	1.27×10^{-2}
	BB^*	3.33 MeV	5.5
	B^*B^*	55.7 MeV	92.1
	B_sB_s	0.272 MeV	0.449
	$B_sB_s^*$	0.192 MeV	0.317
	$B_s^*B_s^*$	0.960 MeV	1.59
	Total	60.5 MeV	100

corresponding open-bottom channels are either BB or BB^* , whose partial widths of the GI model are much larger than our predictions. We predict that the total widths of $h_{b3}(2F)$ and $\chi_{b3}(2F)$ states are 0.413 and 0.543 MeV, respectively, which are about one-30th times the results of the GI model. The total widths of the other two particles $\chi_{b2}(2F)$ and $\chi_{b4}(2F)$ are calcu-

lated as 41.4 and 1.03 MeV, respectively. This result is about 2 to 3 times smaller than those of the GI model. From the above results, it can be easily noticed that the $\chi_{b2}(2F)$ is a relatively broad state but the other $2F$ states are all narrow states, which means that it is not difficult to distinguish the spin-triplet with $J = 2$ of $2F$ bottomonia from the experiment. Some important radiative decay modes of these narrow states may also have large contributions to the total width. Hence, the processes $h_{b3}(2F) \rightarrow \eta_{b2}(2D)\gamma$, $\chi_{b3}(2F) \rightarrow \Upsilon_2(2D)\gamma$, and $\chi_{b4}(2F) \rightarrow \Upsilon_3(2D)$ are possibly one of promising ways to detect these narrow $2F$ bottomonia.

3. Different from the decay behaviors of $2F$ bottomonia, the total widths of $h_{b3}(3F)$ and $\chi_{bJ}(3F)$ with $J = 2, 3, 4$ states are estimated to be 103.2, 144.1, 116.6, and 67.0 MeV, respectively, from the modified GI model. It is apparent that $3F$ bottomonia are broad on the whole, which is consistent with the GI model. The dominant decay modes of four $3F$ bottomonia are B^*B^* and BB^* and their contributions to the total width reach 80 % to 98 %. The decay mode BB should also be important for the $\chi_{b2}(3^3F_2)$ state, where our branching ratio of BB is 19.8 % while the GI model gives only 7.85 %. Finally, for the $\chi_{b4}(3^3F_4)$ state we need to emphasize that the mode BB^* is important and $B_sB_s^*$ is negligible because of the predicted branching ratios of 21.3 % and 9.03×10^{-4} , respectively. However, the prediction of GI model is completely inconsistent with our result, which is to be identified in future experiments.

The numerical results of $4F$ bottomonia decays are shown in Tables XXXVI and XXXVII and the predicted total widths of $4F$ states are located at near 70 MeV. In their open-bottom decay channels, the contributions of bottom-strange mesons to the total widths are all small, among which the largest is not more than 3 %. The dominant decay modes of $h_{b3}(4F)$ and $\chi_{bJ}(4F)$ with $J = 2, 3$ are B^*B^* and BB^* , whose sum of branching ratios is more than 80 %. Only the mode B^*B^* with branching ratio 92.1 % governs the $\chi_{b4}(4^3F_4)$ state. The BB channel is also important for the $\chi_{b2}(4^3F_2)$ state but is negligible for the $\chi_{b4}(4^3F_4)$ state on account of the branching ratios 17.5 % and 1.27×10^{-4} , respectively.

F. G-wave states

G-wave bottomonia are typical high spin states, which are difficult to be experimentally found in recent years. However, we still give our predictions of decay behaviors for the higher G-wave bottomonia with radial quantum number up to 3, which has an extra calculation of $3G$ bottomonium state compared to Ref. [26]. The hyperfine mass splittings among the spin-singlet and spin-triplet states of $2G$ and $3G$ are quite small and the average mass values of $2G$ and $3G$ bottomonia in Table III are 10747 and 10929 MeV, respectively, which are close to those of $4P$ and $5P$ bottomonia, respectively. The decay information on partial widths of several decay types and total widths of $2G$ and $3G$ bottomonia are shown in Tables

TABLE XXXVIII: Partial widths and branching ratios of the OZI-allowed strong decay, and radiative transition and the total widths for the $2G$ bottomonium states. The width results are in units of keV.

state	channels	Width	$\mathcal{B}(\%)$
$\eta_{b4}(2^1G_4)$	$h_{b3}(1^1F_3)\gamma$	1.44	1.01×10^{-3}
	$h_{b3}(2^1F_3)\gamma$	17.1	1.19×10^{-2}
	$\Upsilon_3(1^3G_3)\gamma$	1.70×10^{-4}	1.19×10^{-7}
	$\Upsilon_4(1^3G_4)\gamma$	6.57×10^{-5}	4.59×10^{-8}
	$\Upsilon_5(1^3G_5)\gamma$	5.19×10^{-6}	3.63×10^{-9}
	BB^*	77.3 MeV	54.0
	B^*B^*	65.8 MeV	46.0
	Total	143.1 MeV	100
$\Upsilon_3(2^3G_3)$	$\chi_{b2}(1^3F_2)\gamma$	1.43	1.29×10^{-3}
	$\chi_{b3}(1^3F_3)\gamma$	0.0874	7.89×10^{-5}
	$\chi_{b4}(1^3F_4)\gamma$	9.33×10^{-4}	8.42×10^{-7}
	$\chi_{b2}(2^3F_2)\gamma$	16.0	1.44×10^{-2}
	$\chi_{b3}(2^3F_3)\gamma$	1.33	1.20×10^{-3}
	$\chi_{b4}(2^3F_4)\gamma$	0.0203	1.83×10^{-5}
	$\eta_{b4}(1^1G_4)\gamma$	7.15×10^{-7}	6.45×10^{-10}
	BB	19.4 MeV	17.5
	BB^*	56.4 MeV	50.9
	B^*B^*	35.0 MeV	31.6
	B_sB_s	0.00886 MeV	8.00×10^{-3}
	Total	110.8 MeV	100
$\Upsilon_4(2^3G_4)$	$\chi_{b3}(1^3F_3)\gamma$	1.37	9.82×10^{-4}
	$\chi_{b4}(1^3F_4)\gamma$	0.0651	4.67×10^{-5}
	$\chi_{b3}(2^3F_3)\gamma$	16.0	1.15×10^{-2}
	$\chi_{b4}(2^3F_4)\gamma$	1.03	7.38×10^{-4}
	$\eta_{b4}(1^1G_4)\gamma$	5.62×10^{-5}	4.03×10^{-8}
	BB^*	87.3 MeV	62.5
	B^*B^*	52.3 MeV	37.5
	Total	139.5 MeV	100
$\Upsilon_5(2^3G_5)$	$\chi_{b4}(1^3F_4)\gamma$	1.37	8.59×10^{-4}
	$\chi_{b4}(2^3F_4)\gamma$	16.6	1.04×10^{-2}
	$\eta_{b4}(1^1G_4)\gamma$	1.87×10^{-4}	1.17×10^{-7}
	BB	15.7 MeV	9.87
	BB^*	21.3 MeV	13.4
	B^*B^*	122 MeV	76.8
	B_sB_s	1.50×10^{-5} MeV	9.38×10^{-6}
	Total	159.4 MeV	100

TABLE XXXIX: Partial widths and branching ratios of the OZI-allowed strong decay, and radiative transition and the total widths for 3^1G_4 and 3^3G_3 bottomonium states. The width results are in units of keV.

state	channels	Width	$\mathcal{B}(\%)$
$\eta_{b4}(3^1G_4)$	$h_{b3}(1^1F_3)\gamma$	0.317	5.95×10^{-4}
	$h_{b3}(2^1F_3)\gamma$	1.74	3.26×10^{-3}
	$h_{b3}(3^1F_3)\gamma$	14.2	2.66×10^{-2}
	$\Upsilon_3(2^3G_3)\gamma$	1.74×10^{-4}	3.26×10^{-7}
	$\Upsilon_4(2^3G_4)\gamma$	7.11×10^{-5}	1.33×10^{-7}
	$\Upsilon_5(2^3G_5)\gamma$	8.31×10^{-6}	1.56×10^{-8}
	BB^*	21.7 MeV	40.6
	B^*B^*	29.5 MeV	55.3
	$B_sB_s^*$	0.973 MeV	1.82
	$B_s^*B_s^*$	1.18 MeV	2.21
	Total	53.3 MeV	100
$\Upsilon_3(3^3G_3)$	$\chi_{b2}(1^3F_2)\gamma$	0.328	8.24×10^{-4}
	$\chi_{b3}(1^3F_3)\gamma$	0.0152	3.82×10^{-5}
	$\chi_{b4}(1^3F_4)\gamma$	1.02×10^{-4}	2.56×10^{-7}
	$\chi_{b2}(2^3F_2)\gamma$	1.75	4.40×10^{-3}
	$\chi_{b3}(2^3F_3)\gamma$	0.111	2.79×10^{-4}
	$\chi_{b4}(2^3F_4)\gamma$	0.00126	3.17×10^{-6}
	$\chi_{b2}(3^3F_2)\gamma$	13.5	3.39×10^{-2}
	$\chi_{b3}(3^3F_3)\gamma$	1.14	2.86×10^{-3}
	$\chi_{b4}(3^3F_4)\gamma$	0.0173	4.35×10^{-5}
	$\eta_{b4}(1^1G_4)\gamma$	2.18×10^{-6}	5.48×10^{-9}
	BB	4.88 MeV	12.2
	BB^*	20.1 MeV	50.4
	B^*B^*	13.2 MeV	33.3
	B_sB_s	0.336 MeV	0.844
	$B_sB_s^*$	0.00500 MeV	1.26×10^{-2}
	$B_s^*B_s^*$	1.27 MeV	3.20
	Total	39.8 MeV	100

XXXVIII-XL. For the radiative transition of $2G$ states, we obtain the behaviors similar to P, D, F -wave states. Hence, we no longer explain it here. Furthermore, the total widths of $2G$ bottomonia are estimated to be about $110 \sim 160$ MeV, which means that they are all broad states although these values are significantly small relative to those of the GI model. Since the mass values of $2G$ bottomonia do not reach the threshold line of P -wave bottom mesons and the largest partial width of B_sB_s is about 10^{-3} orders of magnitude, the main decay modes of $2G$ states are BB, BB^* and B^*B^* . The mode BB^* is dominant for the $\Upsilon_3(2^3G_3)$ and $\Upsilon_4(2^3G_4)$ with branching ratios 50.9 % and 62.5 %, respectively. The mode B^*B^* with a branching ra-

TABLE XL: Partial widths and branching ratios of OZI-allowed strong decay and, radiative transition and the total widths for 3^3G_4 and 3^3G_5 bottomonium states. The width results are in units of keV.

state	channels	Width	$\mathcal{B}(\%)$
$\Upsilon_4(3^3G_4)$	$\chi_{b3}(1^3F_3)\gamma$	0.304	6.03×10^{-4}
	$\chi_{b4}(1^3F_4)\gamma$	0.0108	2.14×10^{-5}
	$\chi_{b3}(2^3F_3)\gamma$	1.66	3.29×10^{-3}
	$\chi_{b4}(2^3F_4)\gamma$	0.0821	1.63×10^{-4}
	$\chi_{b3}(3^3F_3)\gamma$	13.3	2.64×10^{-2}
	$\chi_{b4}(3^3F_4)\gamma$	0.852	1.69×10^{-3}
	$\eta_{b4}(2^1G_4)\gamma$	5.91×10^{-5}	1.17×10^{-7}
	BB^*	26.1 MeV	51.7
	B^*B^*	22.4 MeV	44.5
	$B_sB_s^*$	0.780 MeV	1.55
	$B_s^*B_s^*$	1.11 MeV	2.21
	Total	50.4 MeV	100
$\Upsilon_5(3^3G_5)$	$\chi_{b4}(1^3F_4)\gamma$	0.299	4.43×10^{-4}
	$\chi_{b4}(2^3F_4)\gamma$	1.67	2.47×10^{-3}
	$\chi_{b4}(3^3F_4)\gamma$	14.1	2.09×10^{-2}
	$\eta_{b4}(2^1G_4)\gamma$	1.90×10^{-4}	2.81×10^{-7}
	BB	5.16 MeV	7.65
	BB^*	3.02 MeV	4.47
	B^*B^*	56.5 MeV	83.7
	B_sB_s	0.306 MeV	0.453
	$B_sB_s^*$	0.950 MeV	1.41
	$B_s^*B_s^*$	1.56 MeV	2.31
	Total	67.5 MeV	100

tio 76.8 % is critical for the $\Upsilon_5(2^3G_5)$. Finally, the modes BB^* and B^*B^* have the same importance for the $\eta_{b4}(2^1G_4)$ state.

Similarly, the $3G$ bottomonium states cannot decay into P -wave bottom mesons on account of mass values. In Tables **XXXIX** and **XL**, the predicted total widths of $\eta_{b4}(3G)$ and $\Upsilon_J(3G)$ with $J = 3, 4, 5$ states are 53.3, 39.8, 50.4, and 67.5 MeV, respectively. All the contributions of bottom-strange mesons to the total widths of $3G$ states occupy about 4 %. In addition, the strong decay behaviors of channels BB, BB^* , and B^*B^* of $3G$ bottomonia are almost exactly the same as the case of $2G$ bottomonia, which also indicates that the dominant decay modes of each $2G$ bottomonium state and corresponding radially excited $3G$ state are similar to each other.

V. SUMMARY

As we all know, the screening effect usually plays a very important role for highly excited mesons. It affects mass values, wave functions of mesons and hence, estimates of cor-

responding decay behaviors. Motivated by the recent studies of bottomonium properties in the framework of the Godfrey-Isgur relativized quark model [26], we have performed the most comprehensive study on the properties of bottomonium family by using the modified Godfrey-Isgur model with a screening effect. We have also studied radiative transition, annihilation decay, hadronic transition, and OZI-allowed two-body strong decay of $b\bar{b}$ states. Our calculated numerical results have indicated that our predictions for the properties of higher bottomonia are quite different from the conclusion of GI model. Hence, we also expect that this work could provide some valuable results to the future research of bottomonium in experiment.

Our work in this paper can be divided into two parts, study of mass spectrum and study of decay behaviors of bottomonium states. Furthermore, we have focused our main attention on the prediction and analysis of higher bottomonia due to significant reflection of the screening effect. Firstly, we have taken advantage of the measured mass of 18 observed bottomonium states in Table II to fit eight undetermined parameters of the modified GI model in Table I. The screening parameter μ has been given by 0.07426 GeV for the bottomonium system. In addition, our theoretical mass values have been greatly improved compared to those of the GI model. At the same time, our results have been well matched with experimental results. Based on the above preparation, the predicted mass spectrum of bottomonium states has been given in Table III. It is interesting to note that the mass values of $\Upsilon(7S)$ and $\Upsilon(8S)$ are predicted as 11157 and 11296 MeV, respectively, which are higher than the measured mass of $\Upsilon(11020)$ only by 154 and 293 MeV, respectively.

Classified in L , the decay properties of bottomonium states have been separately discussed in accordance with mass values above and below the open-bottom threshold. We have found that a screening effect is weak for the decay behaviors of the most bottomonium states below the threshold, whose estimates are similar to those of the GI model. For the higher bottomonium states above the threshold, the screening effect has become important and we have obtained fairly inconsistent conclusion on characteristic decay behaviors of bottomonium mesons between the GI model with and without screening effects. Here, we have provided results to check the validity of our model in future experiments.

In the following years, exploration for higher bottomonium states will become a major topic in the future LHCb and forthcoming Belle II experiments. Until then, highly excited states still missing at present are likely to be found. Moreover, some hidden experimental information of observed $b\bar{b}$ states can be further perfected. In this work, we have provided abundant theoretical information for these higher bottomonia, which is helpful for piloting experiments to search for these missing bottomonia.

Acknowledgments

This paper appears in arXiv just on 2018 Chinese New Year's Eve. With it, we want to celebrate Chinese New Year.

Good luck and great success in the coming new year! This project is partly supported by the National Natural Science Foundation of China under Grant Nos. 11222547, 11175073, and 11647301. Xiang Liu is also supported in part by the National Program for Support of Top-notch Young Professionals and the Fundamental Research Funds for the Central Universities.

Appendix A: Theoretical models of decay behaviors

In this Appendix, we give all the formulas necessary for calculating radiative transitions, annihilation decays, hadronic transitions, and two-body OZI-allowed strong decays.

1. Radiative transitions

The radiative transitions of a heavy quarkonium are important in the sense that radiative decays not only are main decay channels of some particles below the open-flavor threshold, but help us better understand the inner structure of a quarkonium, i.e., wave functions and interactions of $Q\bar{Q}$. For the E1 transition process, $n^{2S+1}L_J \rightarrow n'^{2S'+1}L'_{J'} + \gamma$ of charmonium, the partial width is given by [52],

$$\Gamma_{E1} = \frac{4}{3} \alpha e_b^2 \omega^3 \delta_{L,L'+1} C_{if} |\langle \psi_f | r | \psi_i \rangle|^2 \quad (A1)$$

with

$$C_{if} = \max(L, L') (2J' + 1) \begin{Bmatrix} L' & J' & S \\ J & L & 1 \end{Bmatrix}^2 \quad (A2)$$

where the e_b is a bottom quark charge in units of $|e|$ and α is a fine-structure constant, ω is an emitted photon energy and $\langle \psi_f | r | \psi_i \rangle$ is the transition matrix element which has the integral form $\int_0^\infty R_{n'L'}(r) r R_{nL}(r) r^2 dr$. Here the radial wave function $R_{nL}(r)$ is obtained from the modified GI model using parameters listed in Table I, and they are the same in the calculation of M1 radiative transitions.

The partial width of the M1 radiative transition with the spin flip from the initial state $n^{2S+1}L_J$ to the final state $n'^{2S'+1}L_{J'}$ can be written as [53]

$$\Gamma_{M1} = \frac{4\alpha e_b^2 \omega^3}{3m_b^2} \delta_{S,S'+1} \frac{2J'+1}{2L+1} \left| \left\langle \psi_f \left| j_0 \left(\frac{\omega r}{2} \right) \right| \psi_i \right\rangle \right|^2 \quad (A3)$$

with

$$\left\langle \psi_f \left| j_0 \left(\frac{\omega r}{2} \right) \right| \psi_i \right\rangle = \int_0^\infty R_{n'L'}(r) j_0 \left(\frac{\omega r}{2} \right) R_{nL}(r) r^2 dr \quad (A4)$$

where m_b is the mass of a bottom quark, $j_0(\frac{\omega r}{2})$ is the spherical Bessel function and other parameters have been defined above. The results of radiative transition will be discussed in Secs. III and IV.

2. Annihilation decays

The annihilation decay of a heavy quarkonium is important especially for those low excited states below the open-flavor threshold, where the annihilation decay to gluons is dominant. Furthermore, the decay mode is generally available in experiments, in which a vector meson 3S_1 or 3D_1 generates lepton pairs, i.e., e^+e^- , $\mu^+\mu^-$, and $\tau^+\tau^-$. The measured branching ratios of lepton-pair decays can also be used to judge whether experimental XYZ exotic states are treated as conventional mesons or not because this ratio is usually very small for the multi-quark states [54]. It is important to study the annihilation decays of bottomonium states into gluons, light quarks, leptons, and photons in this paper, and the general formula for annihilation decays of a heavy quarkonium will be extensively studied by using perturbative QCD methods [55–67]. The most important feature of annihilation decays is that the probability of annihilation is related to the zero point of the meson wave function or its n -th order derivative where n corresponds to the orbital angular momentum of a meson, i.e., $n = L$. For the lepton pair annihilation decay of 3S_1 or 3D_1 bottomonium state, this process occurs via a virtual photon in the tree level, and their width expression with the first-order QCD radiative corrections can be found in Ref. [61, 67]. The formulas for annihilation processes $n^3S_1 \rightarrow ggg$, $n^3S_1 \rightarrow \gamma\gamma\gamma$ and $n^3S_1 \rightarrow gg\gamma$ and the annihilation mode of P -wave state including QCD radiative corrections are given in Ref. [61]. The general expressions for the decays into two gluons and two photon of spin singlet state with an arbitrary total angular momentum are given in Ref. [62]. Finally, for the bottomonium states with the higher angular momentum, the authors of Ref. [63, 64] have given complete expressions for the annihilation decay width to three gluons for D -wave spin-triplet states. In Refs. [65, 66], the annihilation decay of F -wave spin-triplet states into two gluons was also studied. Fortunately, the authors of Ref. [26] have summarized all these lowest-order annihilation decay formulas with the first order QCD corrections of a heavy quarkonium from S -wave to G -wave states. Hence, we do not specifically list these formulas here. It is worth noticing that according to the formula of Ref. [61] and our model input, we recalculate each coefficient of first order radiative corrections for the processes $\chi_{b0}(nP) \rightarrow gg$ and $\chi_{b2}(nP) \rightarrow gg$ and we also add the radiative correction terms for $\chi_{b0}(5P, 6P)$ and $\chi_{b2}(5P, 6P)$ states in this work. We find that the coefficient $C(nP)$ in the radiative correction term $C(nP)\alpha_s/\pi$ of the above processes are modified only for the radial excited states, $\chi_{b0}(3P)$ and $\chi_{b2}(2, 3, 4P)$. The corresponding constants $C(nP)$'s are 10.4, 0.89, 1.59 and 2.10, respectively. The radiative corrections for $\chi_{b0}(5, 6P)$ and $\chi_{b2}(5, 6P)$ are also estimated to be 10.6, 10.7, 2.50 and 2.85, respectively. Finally, we need to emphasize that some of parameters in the annihilation decay calculations are given by $m_b=5.027$ GeV, $\alpha_s(b\bar{b})=0.18$ and $\alpha = 1/137$.

3. hadronic transitions

The hadronic transition of a heavy quarkonium usually refers to the release of a light hadron when the $Q\bar{Q}$ state moves to a lower energy level, which is very critical in the search for some bottomonium particles below open-bottom thresholds. In this work, the hadronic transitions of bottomonia will be studied in the framework of the QCD multipole expansion method, in which the hadronic transition is described as first emitting one gluon from a heavy quark to form the intermediate hybrid state with a color octet $Q\bar{Q}$ pair and then recombine themselves into a light hadron with another emitted gluon via the hadronization process. Since the mass difference of a heavy quarkonium between before and after the transition is usually small, the wavelengths of emitted gluons are generally far larger than the radius of the heavy quarkonium. Similar to electromagnetic radiation, gluon field can be treated in the multipole expansion form in this situation, which was first proposed in Ref. [68]. Next, we briefly introduce the QCD multipole expansion method and more details can be found in the review article Ref. [69].

The quark and gluon fields are assumed to be $\psi(x)$ and $A_\mu^a(x)$, respectively and are transformed as

$$\begin{aligned}\Psi(\mathbf{x}, t) &= U^{-1}(\mathbf{x}, t)\psi(x), \\ \frac{\lambda_a}{2}A_\mu^{a'}(\mathbf{x}, t) &= U^{-1}(\mathbf{x}, t)\frac{\lambda_a}{2}A_\mu^a(x)U(\mathbf{x}, t) \\ &\quad - \frac{i}{g_s}U^{-1}(\mathbf{x}, t)\partial_\mu U(\mathbf{x}, t)\end{aligned}\quad (A5)$$

by the introduction of an operator $U(\mathbf{x}, t)$ defined as

$$U(\mathbf{x}, t) = P \exp \left[ig_s \int_{\mathbf{x}} \frac{\lambda_a}{2} \mathbf{A}^a(\mathbf{x}', t) d\mathbf{x}' \right], \quad (A6)$$

where P is the path-ordering operator and \mathbf{x} is the mass center of a quarkonium. In fact, this transformation indicates that $\Psi(\mathbf{x}, t)$ dressed by gluons plays a role of a constituent quark in the effective Lagrangian of system which can be obtained in Ref. [70]. As mentioned above, the process of launching gluons of heavy quarkonium can be treated by the multipole expansion method where in the zero position, the emitted transformed gluon field $A'_\mu(\mathbf{x}, t)$ can be expanded as

$$\begin{aligned}A'_0(\mathbf{x}, t) &= A'_0(0, t) - \mathbf{x} \cdot \mathbf{E}(0, t) + \cdots, \\ \mathbf{A}'(\mathbf{x}, t) &= -\frac{1}{2}\mathbf{x} \times \mathbf{B}(0, t) + \cdots\end{aligned}\quad (A7)$$

on the basis of effective Lagrangian, the corresponding Hamiltonian can be derived as the follow form [70]

$$H_{QCD}^{eff} = H_{QCD}^{(0)} + H_{QCD}^{(1)} + H_{QCD}^{(2)}, \quad (A8)$$

where the $H_{QCD}^{(0)}$ is part of kinetic and potential energy of heavy quarkonium field which is not the simply Hamiltonian of free field but already contains relatively strong interaction, and the $H_{QCD}^{(1)}$ and $H_{QCD}^{(2)}$ are usually seen as a perturbation which are consist with the interactions of color charge, color-electric dipole moment and color-magnetic dipole moment

as well as higher order multipole momentum of quarkonium field respectively. The general formula of S-matrix element in the QCD multipole expansion is given in Ref.[71]. Here, we only focus on the spin-nonflip $\pi\pi$ transitions which were dominated by double electric-dipole (E1-E1) transitions since other transitions including spin-flip $\pi\pi$ processes where E1-M1 transition is main and spin-nonflip η decays which are contributed by E1-M2 and M1-M1 transitions are usually suppressed compared with the E1-E1 transitions. Starting from the general formula of S-matrix, the amplitude of spin-nonflip $\pi\pi$ transitions can be written as [70–72]

$$\mathcal{M}_{E1E1} = i \frac{g_E^2}{6} \langle \Phi_F h | \bar{\mathbf{x}} \cdot \mathbf{E} \frac{1}{E_I - H_{QCD}^{(0)} - iD_0} \bar{\mathbf{x}} \cdot \mathbf{E} | \Phi_I \rangle, \quad (\text{A9})$$

where $|\Phi_I\rangle$ and $\langle \Phi_F h |$ are initial quarkonium and final quarkonium and light hadron, respectively. $\bar{\mathbf{x}}$ is the separation of heavy quark and anti-quark and $(D_0)_{bc} = \delta_{bc} \partial_0 - g_s f_{abc} A_0^a$. After inserting a complete set of intermediate states, this transition amplitude can be divided into two parts which are a heavy quark MGE (multipole gluon emission) factor and an H (hadronization) factor, respectively and the concrete form is given by [72]

$$\mathcal{M}_{E1E1} = i \frac{g_E^2}{6} \sum_{KL} \frac{\langle \Phi_F | \bar{\mathbf{x}}_k | KL \rangle \langle KL | \bar{\mathbf{x}}_l | \Phi_I \rangle}{E_I - E_{KL}} \langle \pi\pi | E_k^a E_l^a | 0 \rangle. \quad (\text{A10})$$

As for the MGE factor which has two electric dipole factors, the initial state $|\Phi_I\rangle$ first transforms to the intermediate vibrational state $\langle KL |$ formed by the color-octet quarkonium and gluon called as a hybrid state. Since this three-body bound state cannot be solved by the QCD, we use the quark confining string (QCS) model [73–75] as a viable approach to calculate the intermediate hybrid, which will be mentioned later. The part of an MGE factor can be calculated by applying the eigenvalue and wave function of an intermediate hybrid, initial and final quarkonium states. The H factor $\langle \pi\pi | E_k^a E_l^a | 0 \rangle$ clearly reflects the process of two emitted gluons transforming to the light hadrons after hadronization. This H factor is highly nonperturbative due to the low scale of energy. Hence, this matrix element can not be also directly obtained by the QCD, however, a phenomenological approximation can be given by using the partially conserved axial-vector current and soft pion theorem [72, 76]. Based on the above treatments, the final transition rate is given by [72]

$$\begin{aligned} \Gamma(\phi_I \rightarrow \phi_F + \pi\pi) &= \delta_{l_I l_F} \delta_{J_I J_F} \left(G |C_1|^2 - \frac{2}{3} H |C_2|^2 \right) |\mathcal{A}_1|^2 \\ &\quad + (2l_I + 1)(2l_F + 1)(2J_F + 1) \\ &\quad \times \sum_k (2k + 1) \left[1 + (-1)^k \right] \left\{ \begin{matrix} s & l_F & J_F \\ k & J_I & l_I \end{matrix} \right\}^2 \\ &\quad \times H |C_2|^2 |\mathcal{A}_2|^2 \end{aligned} \quad (\text{A11})$$

with

$$\mathcal{A}_1 = \sum_L (2L + 1) \begin{pmatrix} l_I & 1 & L \\ 0 & 0 & 0 \end{pmatrix} \begin{pmatrix} L & 1 & l_I \\ 0 & 0 & 0 \end{pmatrix} f_{IF}^{L11}, \quad (\text{A12})$$

$$\mathcal{A}_2 = \sum_L (2L + 1) \begin{pmatrix} l_F & 1 & L \\ 0 & 0 & 0 \end{pmatrix} \begin{pmatrix} L & 1 & l_I \\ 0 & 0 & 0 \end{pmatrix} \left\{ \begin{matrix} l_I & L & 1 \\ 1 & k & l_F \end{matrix} \right\} f_{IF}^{L11}, \quad (\text{A13})$$

where C_1 and C_2 are parameters which are determined by the processes of $\Upsilon(2S) \rightarrow \Upsilon(1S)\pi\pi$ and $\Upsilon(1D) \rightarrow \Upsilon(1S)\pi\pi$, respectively. The symbols $l_I(l_F)$, $J_I(J_F)$ are the orbital and total angular momentum of initial (final) state, respectively and the spin s does not change after the reaction. The f_{IF}^{L11} has the following structure

$$\begin{aligned} f_{IF}^{L11} &= \sum_K \frac{1}{M_I - M_{KL}} \int dr r^{2+P_F} R_F(r) R_{KL}(r) \\ &\quad \times \int dr' r'^{2+P_I} R_{KL}(r') R_I(r'), \end{aligned} \quad (\text{A14})$$

where M_{KL} and $R_{KL}(r)$ are the mass and radial wave function of the intermediate state, respectively. The phase-space factors G and H are written as

$$\begin{aligned} G &= \frac{3}{4} \frac{M_F}{M_I} \pi^3 \int dM_{\pi\pi}^2 K \left(1 - \frac{4m_\pi^2}{M_{\pi\pi}^2} \right)^{1/2} (M_{\pi\pi}^2 - 2m_\pi^2)^2, \quad (\text{A15}) \\ H &= \frac{1}{20} \frac{M_F}{M_I} \pi^3 \int dM_{\pi\pi}^2 K \left(1 - \frac{4m_\pi^2}{M_{\pi\pi}^2} \right)^{1/2} \left[(M_{\pi\pi}^2 - 4m_\pi^2)^2 \right. \\ &\quad \times \left(1 + \frac{2}{3} \frac{K^2}{M_{\pi\pi}^2} \right) + \frac{8K^4}{15M_{\pi\pi}^4} (M_{\pi\pi}^4 + 2m_\pi^2 M_{\pi\pi}^2 + 6m_\pi^4) \left. \right], \end{aligned} \quad (\text{A16})$$

with K given by

$$K = \frac{\sqrt{[(M_I + M_F)^2 - M_{\pi\pi}^2][(M_I - M_F)^2 - M_{\pi\pi}^2]}}{2M_I}. \quad (\text{A17})$$

The intermediate hybrid states can be described by the quark confining string (QCS) model [73–75], in which we consider that the quark and anti-quark are connected by an appropriate color electric flux tube or string. If the string is in the ground state, the system of a quark-antiquark pair is a meson where the string corresponds to the strong confinement interaction. The vibration of the string means a new state with gluon excitation effects, which is composed of the excited gluon field and quark-antiquark pair, i.e., the so-called hybrid state. For this vibrational mode, assuming both ends of a string are fixed because of too heavy quark masses, then the effective vibrational potential can be given by [74]

$$V_n(r) = \sigma(r) r \left(1 - \frac{2n\pi}{2n\pi + \sigma(r)[(r - 2d)^2 + 4d^2]} \right)^{-\frac{1}{2}} \quad (\text{A18})$$

with

$$d = \frac{1}{4} \sigma(r) r^2 \frac{\alpha_n}{2m_b + \sigma(r) r \alpha_n}, \quad (\text{A19})$$

where d is the correction of finite heavy quark mass and n indicates the excitation level. The α_n related to the shape of

the vibrational string [74] is taken as $\sqrt{1.5}$, which is consistent with Ref. [27] and is insensitive to our mass spectrum of hybrid states.

The potential of a hybrid meson can be expressed as [75]

$$V_{hyb}(r) = V_G(r) + V_S(r) + [V_n(r) - \sigma(r)r], \quad (\text{A20})$$

where $V_G(r)$ is one-gluon exchange potential and $V_S(r)$ is a color confining potential. It is easy to see that the above potential becomes a general $Q\bar{Q}$ interaction when $n = 0$ for the vibrational potential V_n . For theoretical self-consistency, forms of $V_G(r)$ and $V_S(r)$ are taken from our modified GI model and due to a screening effect, the effective string tension $\sigma(r)$ is not a constant but rather a function of a distance r of Q and \bar{Q} . The specific expressions of potentials $V_G(r)$ and $V_S(r)$ can be written as

$$\begin{aligned} V_G(r) &= -\frac{4\alpha_s(r)}{3r}, \\ V_S(r) &= \sigma(r)r + c \end{aligned} \quad (\text{A21})$$

with

$$\begin{aligned} \alpha_s(r) &= \sum_k \alpha_k \frac{2}{\sqrt{\pi}} \int_0^{\gamma_k r} e^{-x^2} dx, \\ \sigma(r) &= b(1 - e^{-\mu r})/(\mu r). \end{aligned} \quad (\text{A22})$$

Solving the Schrödinger equation for a hybrid meson, one obtains the mass spectrum and corresponding wave function of a hybrid state, which are used to calculate the width of hadronic transition by Eq. (A11). Nevertheless, we have to emphasize that the QCD multipole expansion is dependent on the inputs and has its own error due to theoretical uncertainties. Hence, we should regard the calculated width of hadronic transition as rough estimates rather than precise results. In addition, considering that there may be a more complex mechanism of hadronic transition for highly excited states, we focus on the hadronic transition of the bottomonium states only below open-bottom threshold in this work. The numerical results of hadronic decay will be discussed in Secs. III and it should be noted that the GI's results of hadronic transition Ref. [26] are derived from the reduced matrix elements, which are obtained by measured transition rates rather than direct calculations. Here, we adopt the direct QCD multipole-expansion method to calculate a partial width of hadronic transition of bottomonium states and it is also useful to make a comparison with the results of Ref. [26].

4. Two-body OZI-allowed strong decays

Quark-Pair Creation (QPC) model is applicable to the calculation of OZI allowed hadron strong decays. This model is proposed by the Micu [77] at the earliest in 1968 and it has been further developed by the Orsay Group [78–81] which is one of the most popular phenomenological method to deal with the OZI allowed strong decays and has been greatly used in the calculation of strong decay. The model assumes that a

created quark-antiquark pair $q\bar{q}$ from the vacuum is a 3P_0 state which has spin-parity $J^{PC} = 0^{++}$, so the model also known as 3P_0 model. In the following, we will briefly introduce this model. For the OZI allowed strong decay process $A \rightarrow B + C$, the transition operators \mathcal{T} can be expressed as

$$\begin{aligned} \mathcal{T} &= -3\gamma \sum_m \langle 1m; 1-m | 00 \rangle \int d\mathbf{p}_3 d\mathbf{p}_4 \delta^3(\mathbf{p}_3 + \mathbf{p}_4) \\ &\times \mathcal{Y}_{1m} \left(\frac{\mathbf{p}_3 - \mathbf{p}_4}{2} \right) \chi_{1,-m}^{34} \phi_0^{34} \omega_0^{34} b_{3i}^\dagger(\mathbf{p}_3) d_{4j}^\dagger(\mathbf{p}_4). \end{aligned} \quad (\text{A23})$$

where $\mathcal{Y}_{lm}(\mathbf{p}) = p^l Y_{lm}(\theta_p, \phi_p)$ is a solid spherical harmonic function and $b_3^\dagger(d_4^\dagger)$ is quark (antiquark) creation operator, $\phi_0^{34} = (u\bar{u} + d\bar{d} + s\bar{s})/\sqrt{3}$ and ω_0^{34} are SU(3) flavor and color wave function of vacuum quark pair respectively, and the dimensionless parameter γ describes the strength of creating a quark-antiquark pair from the vacuum. γ value for $s\bar{s}$ pair creation is generally more than a factor of $1/\sqrt{3}$ compared to that of $u\bar{u}/d\bar{d}$ pair creation. The reason of the existence of factor $1/\sqrt{3}$ is in order to show the SU(3) symmetry breaking [48, 78–82]. the parameter γ for bottomonium system can be determined by fitting experimental with of $\Upsilon(4S)$, $\Upsilon(10860)$ and $\Upsilon(11020)$ state whose related results are listed in Table V. The transition matrix of decay process can be written as

$$\langle BC | \mathcal{T} | A \rangle = \delta^3(\mathbf{P}_B + \mathbf{P}_C) \mathcal{M}^{M_{JA} M_{JB} M_{Jc}} \quad (\text{A24})$$

where \mathbf{P}_B and \mathbf{P}_C are the momenta of final meson B and C in the center frame of initial meson A respectively and $\mathcal{M}^{M_{JA} M_{JB} M_{Jc}}$ is the decay amplitude. The mock state $|D\rangle$ where D is an arbitrary state including initial state A and final state B, C [83] has the form

$$\begin{aligned} &|D(n^{2S+1} L_{JM_J})(\mathbf{P}_D)\rangle \\ &= \sqrt{2E} \sum_{M_S, M_L} \langle LM_L; S M_S | J M_J \rangle \chi_{S, M_S}^D \\ &\times \phi^D \omega^D \int d\mathbf{p}_1 d\mathbf{p}_2 \delta^3(\mathbf{P}_D - \mathbf{p}_1 - \mathbf{p}_2) \\ &\times \Psi_{nLM_L}^D(\mathbf{p}_1, \mathbf{p}_2) |q_1(\mathbf{p}_1) \bar{q}_2(\mathbf{p}_2)\rangle, \end{aligned} \quad (\text{A25})$$

where the front factor E is particle energy and $\Psi_{nLM_L}^D(\mathbf{p}_1, \mathbf{p}_2)$, χ^D , ϕ^D and ω^D donate spatial, spin, flavor and color wave function of meson D respectively, $\langle LM_L; S M_S | J M_J \rangle$ is Clebsch-Gordan coefficients. This work uses exact spatial wave function of bottomonium obtained by modified GI model with parameter listed in Table I and the theoretical masses and numerical wave functions of bottom and bottom-strange meson are from the calculation of Ref. [84], and it is worth noting that the principle of mass input for involved bottom and bottom-strange meson is completely same with bottomonium states and their special results are shown in Table IV where two 1^+ bottom meson $B(1P_1)$ and $B(1P'_1)$ are the mixture of 3P_1 and 1P_1 state, here, mixing angle θ_{1P} is adopted as $-\arcsin(\sqrt{2/3}) = -54.7^\circ$ in the heavy quark limit [85–87]. Combined Eqs. (A23)-(A24) and Eq. (A25), the decay amplitude $\mathcal{M}^{M_{JA} M_{JB} M_{Jc}}$ can be derived.

For the convenience of experimental measurement the decay amplitudes could be related to the helicity partial wave

amplitudes by Jacob-Wick formula [88]

$$\mathcal{M}^{JL}(\mathbf{P}) = \frac{\sqrt{2L+1}}{2J_A+1} \sum_{M_{J_B} M_{J_C}} \langle L0; JM_{J_A} | J_A M_{J_A} \rangle \times \langle J_B M_{J_B}; J_C M_{J_C} | J_A M_{J_A} \rangle \mathcal{M}^{M_{J_A} M_{J_B} M_{J_C}} \quad (\text{A26})$$

where J and L are the total and orbital angular momenta between final state B and C respectively and $\mathbf{P} = \mathbf{P}_B$. Finally, the partial width of the $A \rightarrow BC$ can be written as

$$\Gamma_{A \rightarrow BC} = \pi^2 \frac{|\mathbf{P}_B|}{m_A^2} \sum_{J,L} |\mathcal{M}^{JL}(\mathbf{P})|^2, \quad (\text{A27})$$

where m_A is the mass of the initial state A . In addition, in the calculations of strong decay, the constituent quark mass of bottom, up/down and strange quark are taken as 5.027, 0.22 and 0.419 GeV, respectively.

-
- [1] J. J. Aubert *et al.* [E598 Collaboration], Experimental Observation of a Heavy Particle J, *Phys. Rev. Lett.* **33**, 1404 (1974).
- [2] J. E. Augustin *et al.* [SLAC-SP-017 Collaboration], Discovery of a Narrow Resonance in $e^+ e^-$ Annihilation, *Phys. Rev. Lett.* **33**, 1406 (1974) [Adv. Exp. Phys. **5**, 141 (1976)].
- [3] S. W. Herb *et al.*, Observation of a Dimuon Resonance at 9.5-GeV in 400-GeV Proton-Nucleus Collisions, *Phys. Rev. Lett.* **39**, 252 (1977).
- [4] W. R. Innes *et al.*, Observation of structure in the Υ region, *Phys. Rev. Lett.* **39**, 1240 (1977) Erratum: [*Phys. Rev. Lett.* **39**, 1640 (1977)].
- [5] N. Brambilla *et al.*, Heavy quarkonium: progress, puzzles, and opportunities, *Eur. Phys. J. C* **71**, 1534 (2011).
- [6] D. Besson *et al.* [CLEO Collaboration], Observation of New Structure in the $e^+ e^-$ Annihilation Cross-Section Above B anti-B Threshold, *Phys. Rev. Lett.* **54**, 381 (1985).
- [7] D. M. J. Lovelock *et al.*, Masses, Widths, And Leptonic Widths Of The Higher Upsilon Resonances, *Phys. Rev. Lett.* **54**, 377 (1985).
- [8] C. Klopfenstein *et al.*, Observation of the Lowest P -Wave $b\bar{b}$ Bound States, *Phys. Rev. Lett.* **51**, 160 (1983).
- [9] F. Pauss *et al.*, Observation of χ_b Production in the Exclusive Reaction $\Upsilon' \rightarrow \gamma\chi_b \rightarrow \gamma\gamma\Upsilon \rightarrow \gamma\gamma(e^+e^- \text{ or } \mu^+\mu^-)$, *Phys. Lett.* **130B**, 439 (1983).
- [10] K. Han *et al.*, Observation Of P Wave B Anti-b Bound States, *Phys. Rev. Lett.* **49**, 1612 (1982).
- [11] G. Eigen *et al.*, Evidence For χ'_b Production In The Exclusive Reaction $\Upsilon'' \rightarrow \gamma\chi'_b \rightarrow (\gamma\gamma\Upsilon' \text{ or } \gamma\gamma\Upsilon)$, *Phys. Rev. Lett.* **49**, 1616 (1982).
- [12] B. Aubert *et al.* [BaBar Collaboration], Observation of the bottomonium ground state in the decay $\Upsilon(3S) \rightarrow \gamma\eta_b$, *Phys. Rev. Lett.* **101**, 071801 (2008) Erratum: [*Phys. Rev. Lett.* **102**, 029901 (2009)].
- [13] J. P. Lees *et al.* [BaBar Collaboration], Study of radiative bottomonium transitions using converted photons, *Phys. Rev. D* **84**, 072002 (2011).
- [14] G. Bonvicini *et al.* [CLEO Collaboration], Measurement of the $\eta_b(1S)$ mass and the branching fraction for $\Upsilon(3S) \rightarrow \gamma\eta_b(1S)$, *Phys. Rev. D* **81**, 031104 (2010).
- [15] S. Dobbs, Z. Metreveli, K. K. Seth, A. Tomaradze and T. Xiao, Observation of $\eta_b(2S)$ in $\Upsilon(2S) \rightarrow \gamma\eta_b(2S)$, $\eta_b(2S) \rightarrow \text{hadrons}$, And Confirmation of $\eta_b(1S)$, *Phys. Rev. Lett.* **109**, 082001 (2012).
- [16] R. Mizuk *et al.* [Belle Collaboration], Evidence for the $\eta_b(2S)$ and observation of $h_b(1P) \rightarrow \eta_b(1S)\gamma$ and $h_b(2P) \rightarrow \eta_b(1S)\gamma$, *Phys. Rev. Lett.* **109**, 232002 (2012).
- [17] G. Aad *et al.* [ATLAS Collaboration], Observation of a new χ_b state in radiative transitions to $\Upsilon(1S)$ and $\Upsilon(2S)$ at ATLAS, *Phys. Rev. Lett.* **108**, 152001 (2012).
- [18] V. M. Abazov *et al.* [D0 Collaboration], Observation of a narrow mass state decaying into $\Upsilon(1S) + \gamma$ in $p\bar{p}$ collisions at $\sqrt{s} = 1.96$ TeV, *Phys. Rev. D* **86**, 031103 (2012).
- [19] J. P. Lees *et al.* [BaBar Collaboration], Evidence for the $h_b(1P)$ meson in the decay $\Upsilon(3S) \rightarrow \pi^0 h_b(1P)$, *Phys. Rev. D* **84**, 091101 (2011).
- [20] I. Adachi *et al.* [Belle Collaboration], First observation of the P -wave spin-singlet bottomonium states $h_b(1P)$ and $h_b(2P)$, *Phys. Rev. Lett.* **108**, 032001 (2012).
- [21] G. Bonvicini *et al.* [CLEO Collaboration], First observation of a $\Upsilon(1D)$ state, *Phys. Rev. D* **70**, 032001 (2004).
- [22] P. del Amo Sanchez *et al.* [BaBar Collaboration], Observation of the $\Upsilon(1^3D_J)$ Bottomonium State through Decays to $\pi^+\pi^-\Upsilon(1S)$, *Phys. Rev. D* **82**, 111102 (2010).
- [23] N. Brambilla *et al.* [Quarkonium Working Group], Heavy quarkonium physics, hep-ph/0412158.
- [24] R. Lewis and R. M. Woloshyn, Higher angular momentum states of bottomonium in lattice NRQCD, *Phys. Rev. D* **85**, 114509 (2012).
- [25] R. J. Dowdall *et al.* [HPQCD Collaboration], Bottomonium hyperfine splittings from lattice non-relativistic QCD including radiative and relativistic corrections, *Phys. Rev. D* **89**, no. 3, 031502 (2014) Erratum: [*Phys. Rev. D* **92**, 039904 (2015)].
- [26] S. Godfrey and K. Moats, Bottomonium Mesons and Strategies for their Observation, *Phys. Rev. D* **92**, no. 5, 054034 (2015).
- [27] J. Segovia, P. G. Ortega, D. R. Entem and F. Fernandez, Bottomonium spectrum revisited, *Phys. Rev. D* **93**, no. 7, 074027 (2016).
- [28] B. Q. Li and K. T. Chao, Bottomonium Spectrum with Screened Potential, *Commun. Theor. Phys.* **52**, 653 (2009).
- [29] W. J. Deng, H. Liu, L. C. Gui and X. H. Zhong, Spectrum and electromagnetic transitions of bottomonium, *Phys. Rev. D* **95**, no. 7, 074002 (2017).
- [30] D. Ebert, R. N. Faustov and V. O. Galkin, Properties of heavy quarkonia and B_c mesons in the relativistic quark model, *Phys. Rev. D* **67**, 014027 (2003).
- [31] J. Ferretti and E. Santopinto, Higher mass bottomonia, *Phys. Rev. D* **90**, no. 9, 094022 (2014).
- [32] Y. Li, P. Maris, X. Zhao and J. P. Vary, Heavy Quarkonium in a Holographic Basis, *Phys. Lett. B* **758**, 118 (2016).
- [33] J. Vijande, F. Fernandez and A. Valcarce, Constituent quark

- model study of the meson spectra, *J. Phys. G* **31**, 481 (2005).
- [34] S. N. Gupta, S. F. Radford and W. W. Repko, Semirelativistic Potential Model for Heavy Quarkonia, *Phys. Rev. D* **34**, 201 (1986).
- [35] J. L. Richardson, The Heavy Quark Potential and the Υ , J/ψ Systems, *Phys. Lett.* **82B**, 272 (1979).
- [36] W. Buchmuller and S. H. H. Tye, Quarkonia and Quantum Chromodynamics, *Phys. Rev. D* **24**, 132 (1981).
- [37] A. Martin, A FIT of Upsilon and Charmonium Spectra, *Phys. Lett.* **93B**, 338 (1980).
- [38] S. F. Radford and W. W. Repko, Potential model calculations and predictions for heavy quarkonium, *Phys. Rev. D* **75**, 074031 (2007).
- [39] L. Motyka and K. Zalewski, Mass spectra and leptonic decay widths of heavy quarkonia, *Eur. Phys. J. C* **4**, 107 (1998).
- [40] P. Gonzalez, A. Valcarce, H. Garcilazo and J. Vijande, Heavy meson description with a screened potential, *Phys. Rev. D* **68**, 034007 (2003).
- [41] Y. B. Ding, K. T. Chao and D. H. Qin, Possible effects of color screening and large string tension in heavy quarkonium spectra, *Phys. Rev. D* **51**, 5064 (1995).
- [42] M. Beyer, U. Bohn, M. G. Huber, B. C. Metsch and J. Resag, Relativistic effects and the constituent quark model of heavy quarkonia, *Z. Phys. C* **55**, 307 (1992).
- [43] Y. B. Ding, K. T. Chao and D. H. Qin, Screened Q anti-Q potential and spectrum of heavy quarkonium, *Chin. Phys. Lett.* **10**, 460 (1993).
- [44] T. Wei-Zhao, C. Lu, Y. You-Chang and C. Hong, Bottomonium states versus recent experimental observations in the QCD-inspired potential model, *Chin. Phys. C* **37**, 083101 (2013).
- [45] P. Gonzalez, Generalized screened potential model, *J. Phys. G* **41**, 095001 (2014).
- [46] S. Godfrey and N. Isgur, Mesons in a Relativized Quark Model with Chromodynamics, *Phys. Rev. D* **32**, 189 (1985).
- [47] Q. T. Song, D. Y. Chen, X. Liu and T. Matsuki, Charmed-strange mesons revisited: mass spectra and strong decays, *Phys. Rev. D* **91**, 054031 (2015).
- [48] Q. T. Song, D. Y. Chen, X. Liu and T. Matsuki, Higher radial and orbital excitations in the charmed meson family, *Phys. Rev. D* **92**, no. 7, 074011 (2015).
- [49] K. D. Born, E. Laermann, N. Pirch, T. F. Walsh and P. M. Zerwas, Hadron Properties in Lattice QCD With Dynamical Fermions, *Phys. Rev. D* **40**, 1653 (1989).
- [50] B. Q. Li and K. T. Chao, Higher Charmonia and X,Y,Z states with Screened Potential, *Phys. Rev. D* **79**, 094004 (2009).
- [51] C. Patrignani *et al.* [Particle Data Group], Review of Particle Physics, *Chin. Phys. C* **40**, no. 10, 100001 (2016).
- [52] W. Kwong and J. L. Rosner, D -Wave Quarkonium Levels of the Υ Family, *Phys. Rev. D* **38**, 279 (1988).
- [53] V. A. Novikov, L. B. Okun, M. A. Shifman, A. I. Vainshtein, M. B. Voloshin and V. I. Zakharov, Charmonium and Gluons: Basic Experimental Facts and Theoretical Introduction, *Phys. Rept.* **41**, 1 (1978).
- [54] A. M. Badalian, B. L. Ioffe and A. V. Smilga, Four Quark States In The Heavy Quark System, *Nucl. Phys. B* **281**, 85 (1987).
- [55] T. Appelquist and H. D. Politzer, Orthocharmonium and e^+e^- Annihilation, *Phys. Rev. Lett.* **34**, 43 (1975).
- [56] A. De Rujula and S. L. Glashow, Is Bound Charm Found?, *Phys. Rev. Lett.* **34**, 46 (1975).
- [57] M. S. Chanowitz, Comment on the Decay of ψ (3.1) Into Even G - Parity States, *Phys. Rev. D* **12**, 918 (1975).
- [58] R. Barbieri, R. Gatto and R. Kogerler, Calculation of the Annihilation Rate of P Wave Quark - anti-Quark Bound States, *Phys. Lett.* **60B**, 183 (1976).
- [59] R. Barbieri, R. Gatto and E. Remiddi, Singular Binding Dependence in the Hadronic Widths of 1^{++} and 1^{+-} Heavy Quark anti-Quark Bound States, *Phys. Lett.* **61B**, 465 (1976).
- [60] R. Barbieri, E. d'Emilio, G. Curci and E. Remiddi, Strong Radiative Corrections to Annihilations of Quarkonia in QCD, *Nucl. Phys. B* **154**, 535 (1979).
- [61] W. Kwong, P. B. Mackenzie, R. Rosenfeld and J. L. Rosner, Quarkonium Annihilation Rates, *Phys. Rev. D* **37**, 3210 (1988).
- [62] E. S. Ackleh and T. Barnes, Two photon widths of singlet positronium and quarkonium with arbitrary total angular momentum, *Phys. Rev. D* **45**, 232 (1992).
- [63] G. Belanger and P. Moxhay, Three-Gluon Annihilation of D -Wave Quarkonium, *Phys. Lett. B* **199**, 575 (1987).
- [64] L. Bergstrom and P. Ernstrom, Decays of D -wave quarkonium states into ggg and γgg , *Phys. Lett. B* **267**, 111 (1991).
- [65] E. S. Ackleh, T. Barnes and F. E. Close, Two photon helicity selection rules and widths for positronium and quarkonium states with arbitrary angular momenta, *Phys. Rev. D* **46**, 2257 (1992).
- [66] R. W. Robinett and L. Weinkauff, Covariant formalism for F -wave quarkonium production and annihilation: Application to $^3F_J \rightarrow gg$ decays, *Phys. Rev. D* **46**, 3832 (1992).
- [67] A. Bradley and A. Khare, QCD Correction to the Leptonic Decay Rate of D -Wave Vector Mesons, *Z. Phys. C* **8**, 131 (1981).
- [68] K. Gottfried, Hadronic Transitions Between Quark - anti-Quark Bound States, *Phys. Rev. Lett.* **40**, 598 (1978).
- [69] Y. P. Kuang, QCD multipole expansion and hadronic transitions in heavy quarkonium systems, *Front. Phys. China* **1**, 19 (2006).
- [70] T. M. Yan, Hadronic Transitions Between Heavy Quark States in Quantum Chromodynamics, *Phys. Rev. D* **22**, 1652 (1980).
- [71] Y. P. Kuang, Y. P. Yi and B. Fu, Multipole Expansion in Quantum Chromodynamics and the Radiative Decays $J/\psi \rightarrow \gamma + \eta$ and $J/\psi \rightarrow \gamma + \pi^0$, *Phys. Rev. D* **42**, 2300 (1990).
- [72] Y. P. Kuang and T. M. Yan, Predictions for Hadronic Transitions in the $b\bar{b}$ System, *Phys. Rev. D* **24**, 2874 (1981).
- [73] S. H. H. Tye, A Quark-Binding String, *Phys. Rev. D* **13**, 3416 (1976).
- [74] R. Giles and S. H. H. Tye, The Application of the Quark-Confining String to the ψ Spectroscopy, *Phys. Rev. D* **16**, 1079 (1977).
- [75] W. Buchmuller and S. H. H. Tye, Vibrational States in the Υ Spectroscopy, *Phys. Rev. Lett.* **44**, 850 (1980).
- [76] L. S. Brown and R. N. Cahn, Chiral Symmetry and $\psi' \rightarrow \psi \pi \pi$ Decay, *Phys. Rev. Lett.* **35**, 1 (1975).
- [77] L. Micu, Decay rates of meson resonances in a quark model, *Nucl. Phys. B* **10**, 521 (1969).
- [78] A. Le Yaouanc, L. Oliver, O. Pene and J. C. Raynal, Naive quark pair creation model of strong interaction vertices, *Phys. Rev. D* **8**, 2223 (1973).
- [79] A. Le Yaouanc, L. Oliver, O. Pene and J.-C. Raynal, Naive quark pair creation model and baryon decays, *Phys. Rev. D* **9**, 1415 (1974).
- [80] A. Le Yaouanc, L. Oliver, O. Pene and J. C. Raynal, Resonant Partial Wave Amplitudes in $\pi N \rightarrow \pi \pi N$ According to the Naive Quark Pair Creation Model, *Phys. Rev. D* **11**, 1272 (1975).
- [81] A. Le Yaouanc, L. Oliver, O. Pene and J.-C. Raynal, Strong Decays of ψ'' (4.028) as a Radial Excitation of Charmonium, *Phys. Lett.* **71B**, 397 (1977).
- [82] A. Le Yaouanc, L. Oliver, O. Pene and J. C. Raynal, Why Is ψ''' (4.414) SO Narrow?, *Phys. Lett.* **72B**, 57 (1977).
- [83] C. Hayne and N. Isgur, Beyond the Wave Function at the Origin: Some Momentum Dependent Effects in the Nonrelativistic Quark Model, *Phys. Rev. D* **25**, 1944 (1982).
- [84] Y. Sun, Q. T. Song, D. Y. Chen, X. Liu and

- S. L. Zhu, Higher bottom and bottom-strange mesons, *Phys. Rev. D* **89**, no. 5, 054026 (2014).
- [85] S. Godfrey and R. Kokoski, The Properties of P -Wave Mesons with One Heavy Quark, *Phys. Rev. D* **43**, 1679 (1991).
- [86] T. Matsuki, T. Morii and K. Seo, Mixing angle between 3P_1 and 1P_1 in HQET, *Prog. Theor. Phys.* **124**, 285 (2010).
- [87] T. Barnes, N. Black and P. R. Page, Strong decays of strange quarkonia, *Phys. Rev. D* **68**, 054014 (2003).
- [88] M. Jacob and G. C. Wick, On the general theory of collisions for particles with spin, *Annals Phys.* **7**, 404 (1959) [*Annals Phys.* **281**, 774 (2000)].
- [89] S. Meinel, Bottomonium spectrum at order v^6 from domain-wall lattice QCD: Precise results for hyperfine splittings, *Phys. Rev. D* **82**, 114502 (2010).
- [90] J. P. Lees *et al.* [BaBar Collaboration], Study of di-pion bottomonium transitions and search for the $h_b(1P)$ state, *Phys. Rev. D* **84**, 011104 (2011).
- [91] M. Kornicer *et al.* [CLEO Collaboration], Measurements of branching fractions for electromagnetic transitions involving the $\chi_{bJ}(1P)$ states, *Phys. Rev. D* **83**, 054003 (2011).
- [92] U. Tamponi *et al.* [Belle Collaboration], First observation of the hadronic transition $\Upsilon(4S) \rightarrow \eta h_b(1P)$ and new measurement of the $h_b(1P)$ and $\eta_b(1S)$ parameters, *Phys. Rev. Lett.* **115**, no. 14, 142001 (2015).
- [93] B. Aubert *et al.* [BaBar Collaboration], A measurement of the total width, the electronic width, and the mass of the $\Upsilon(10580)$ resonance, *Phys. Rev. D* **72**, 032005 (2005).
- [94] K.-F. Chen *et al.* [Belle Collaboration], Observation of an enhancement in $e^+e^- \rightarrow \Upsilon(1S)\pi^+\pi^-$, $\Upsilon(2S)\pi^+\pi^-$, and $\Upsilon(3S)\pi^+\pi^-$ production around $\sqrt{s} = 10.89$ GeV at Belle, *Phys. Rev. D* **82**, 091106 (2010).
- [95] D. Santel *et al.* [Belle Collaboration], Measurements of the $\Upsilon(10860)$ and $\Upsilon(11020)$ resonances via $\sigma(e^+e^- \rightarrow \Upsilon(nS)\pi^+\pi^-)$, *Phys. Rev. D* **93**, no. 1, 011101 (2016).
- [96] A. Abdesselam *et al.* [Belle Collaboration], Energy scan of the $e^+e^- \rightarrow h_b(nP)\pi^+\pi^-$ ($n = 1, 2$) cross sections and evidence for $\Upsilon(11020)$ decays into charged bottomonium-like states, *Phys. Rev. Lett.* **117**, no. 14, 142001 (2016).
- [97] B. Aubert *et al.* [BaBar Collaboration], Measurement of the $e^+e^- \rightarrow b\bar{b}$ cross section between $\sqrt{s} = 10.54$ -GeV and 11.20-GeV, *Phys. Rev. Lett.* **102**, 012001 (2009).
- [98] J. M. Torres-Rincon and F. J. Llanes-Estrada, Heavy Quark Fluorescence, *Phys. Rev. Lett.* **105**, 022003 (2010).